Macrophage depletion enhances gut dysbiosis and severity in sepsis mouse model

Miss Pratsanee Hiengrach

จุฬาลงกรณ์มหาวิทยาลัย
CHULALONGKORN UNIVERSITY

A Dissertation Submitted in Partial Fulfillment of the Requirements

for the Degree of Doctor of Philosophy in Medical Microbiology (Interdisciplinary Program)

Medical Microbiology,Interdisciplinary Program

GRADUATE SCHOOL

Chulalongkorn University

Academic Year 2022

การลดลงของแมคโครฟาจต่อการเสียสมดุลของเชื้อจุลชีพในลำไส้และภาวะการติดเชื้อในกระแส
โลหิตในโมเดลหนูทดลองติดเชื้อในกระแสโลหิต

น.ส.ปรัศนีย์ เฮียงราช

Thesis Title   Macrophage depletion enhances gut dysbiosis and severity
                         in sepsis mouse model
By   Miss Pratsanee Hiengrach
Field of Study   Medical Microbiology (Interdisciplinary Program)
Thesis Advisor   Associate Professor ASADA LEELAHAVANICHKUL, M.D.,
                         Ph.D.
Thesis Co Advisor   Associate Professor ARIYA CHINDAMPORN, Ph.D.

Accepted by the GRADUATE SCHOOL, Chulalongkorn University in Partial
Fulfillment of the Requirement for the Doctor of Philosophy

--- Dean of the GRADUATE SCHOOL
(Assistant Professor YOOTTHANA CHUPPUNNARAT, Ph.D.)

DISSERTATION COMMITTEE
--- Chairman
(Wiwat Chancharoenthana, M.D., Ph.D.)
--- Thesis Advisor
(Associate Professor ASADA LEELAHAVANICHKUL, M.D.,
Ph.D.)
--- Thesis Co-Advisor
(Associate Professor ARIYA CHINDAMPORN, Ph.D.)
--- Examiner
(Associate Professor KANITHA PATARAKUL, M.D., Ph.D.)
--- Examiner
(Associate Professor PATCHAREE RITPRAJAK, D.D.S., Ph.D.)
--- Examiner
(Associate Professor RANGSIMA REANTRAGOON, M.D.,
Ph.D.)

ปรัศนีย์ เฮียงราช : การลดลงของแมคโครฟาจต่อการเสียสมดุลของเชื้อจุลชีพในลำไส้และภาวะการติดเชื้อใน
กระแสโลหิตในโมเดลหนูทดลองติดเชื้อในกระแสโลหิต. (Macrophage depletion enhances gut dysbiosis
and severity in sepsis mouse model) อ.ที่ปรึกษาหลัก : รศ. ดร. นพ.อัษฎาศ์ ลีฬหวนิชกุล, อ.ที่ปรึกษาร่วม :
รศ. ดร.อริยา จินดามพร

       เม็ดเลือดขาวชนิดแมคโครฟาจเป็นเซลล์ที่มีหน้าที่สำคัญในการตอบสนองต่อความเสียหายของเนื้อเยื่อหรือการติด
เชื้อต่าง ๆ แม้ว่าในปัจจุบันการยับยั้งการทำงานของเซลล์แมคโครฟาจได้มีการนำมาใช้ประโยชน์ในการรักษาโรคที่เกี่ยวข้องกับ
กระดูก อาทิเช่น โรคกระดูกพรุน, ภาวะกระดูกละลาย หรือภาวะการณ์ลดการเจริญเติบโตของเซลล์มะเร็ง แต่การยับยั้งการ
ทำงานของเม็ดเลือดขาวชนิดนี้อาจส่งผลให้เกิดความผิดปกติต่อการตอบสนองของระบบภูมิคุ้มกันในระยะรุนแรงได้ โดยเฉพาะ
การยับยั้งการทำงานของเซลล์แมคโครฟาจในระบบทางเดินอาหาร ดังนั้นหากมีการยับยั้งการทำงานของเซลล์ชนิดนี้อาจมี
ผลข้างเคียงทำให้ไม่สามารถควบคุมสมดุลเชื้อจุลชีพในระบบทางเดินอาหารนำไปสู่ความรุนแรงของภาวะการติดเชื้อในกระแส
โลหิตมากยิ่งขึ้น ในงานวิจัยนี้ได้ให้สาร Clodronate-liposome เพื่อลดจำนวนเซลล์เม็ดเลือดขาวชนิดแมคโครฟาจ อีกทั้ง
เหนี่ยวนำภาวะติดเชื้อในกระแสโลหิตโดยวิธี cecal ligation and puncture (CLP) ในโมเดลหนูทดลอง ผลการทดลองพบว่าหนู
ทดลองที่มีการลดลงของเซลล์เม็ดเลือดขาวชนิดแมคโครฟาจเกิดการเปลี่ยนแปลงของเชื้อจุลชีพในระบบทางเดินอาหาร มีการ
เพิ่มขึ้นของเชื้อราในไฟลัม Ascomycota คือ *Candida pintolopesii* และพบเชื้อแบคทีเรียก่อโรค ได้แก่ *Klebsiella
pneumoniae, Acinetobacter radioresistens* และ *Enterococcus faecalis* ทำให้ลำไส้เกิดความเสียหายและเกิดการ
แพร่กระจายของเชื้อเข้าสู่ระบบไหลเวียนโลหิต นอกจากนี้ยังพบการตอบสนองทางภูมิคุ้มกันโดยการหลั่งสารไซโตไคน์ มีการ
อักเสบและความเสียหายของตับและไตสูงขึ้นอย่างมีนัยสำคัญทางสถิติอันเป็นสาเหตุให้ความรุนแรงของภาวะการติดเชื้อใน
กระแสโลหิตเพิ่มขึ้น และเพื่อศึกษาบทบาทความสัมพันธ์ของเชื้อราในการเหนี่ยวนำการเพิ่มจำนวนของแบคทีเรียที่แยกได้จาก
หนูทดลองมีผลทำให้ความรุนแรงของภาวะการติดเชื้อในกระแสโลหิตมากขึ้น ซึ่งนำไปสู่การทดลองที่ใช้ heat-kill lysate ของเชื้อ
C. pintolopesii, C. albicans ATCC90028, *C. albicans* ที่แยกได้จากเลือดของผู้ป่วยติดเชื้อในกระแสโลหิต และ
ส่วนประกอบของเซลล์เชื้อราชนิด (1 → 3)-β-D-glucan (BG) จึงถูกนำมาเลี้ยงร่วมกับเชื้อแบคทีเรียแยกได้จากโลหิตหนู
ทดลอง ผลการทดลองพบว่า *Candida* yeast cells และ BG มีผลเพิ่มการเจริญเติบโตของเชื้อแบคทีเรียได้อย่างมีนัยสำคัญทาง
สถิติเปรียบเทียบกับกลุ่มควบคุม นอกจากนี้เชื้อราและเชื้อแบคทีเรียที่แยกจากโลหิตของหนูทดลองยังมีผลเสริมการตอบสนอง
ทางภูมิคุ้มกันโดยการหลั่งสารไซโตไคน์ของ enterocytes ชนิด Caco-2 เพิ่มขึ้นอย่างมีนัยสำคัญทางสถิติ การทดลองนี้จึงสรุป
ได้ว่าการลดลงของเซลล์เม็ดเลือดขาวชนิดแมคโครฟาจเปลี่ยนแปลงเชื้อจุลชีพในระบบทางเดินอาหารโดยการเพิ่มขึ้นของเชื้อรา
จึงเป็นผลให้สนับสนุนแบคทีเรียเพิ่มจำนวนมากยิ่งขึ้น ทำให้เกิดความเสียหายของลำไส้และเชื้อจุลชีพเข้าสู่กระแสโลหิต ทำ
ให้มีการตอบสนองทางภูมิคุ้มกันและความเสียหายของอวัยวะภายในนำไปสู่ความรุนแรงของภาวะติดเชื้อในกระแสโลหิต ดังนั้น
การตรวจสอบการเปลี่ยนแปลงของเชื้อจุลชีพโดยเฉพาะเชื้อราในระหว่างที่ผู้ป่วยรับการรักษาโดยใช้สารลดจำนวนเซลล์เม็ด
เลือดขาวชนิดแมคโคฟาจจึงเป็นสิ่งที่จำเป็นอย่างยิ่ง

สาขาวิชา	จุลชีววิทยาทางการแพทย์ (สหสาขาวิชา)	ลายมือชื่อนิสิต ....
ปีการศึกษา	2565	ลายมือชื่อ อ.ที่ปรึกษาหลัก ....
		ลายมือชื่อ อ.ที่ปรึกษาร่วม ....

6381002820 : MAJOR MEDICAL MICROBIOLOGY (INTERDISCIPLINARY PROGRAM)

KEYWORD: Macrophage, Clodronate-liposome, Gut dysbiosis, Sepsis

Pratsanee Hiengrach : Macrophage depletion enhances gut dysbiosis and severity in sepsis mouse model. Advisor: Assoc. Prof. ASADA LEELAHAVANICHKUL, M.D., Ph.D. Co-advisor: Assoc. Prof. ARIYA CHINDAMPORN, Ph.D.

Macrophage is vital players in the responsiveness of the innate immune system against injury or infection. Although macrophage depletion is well-known for some emerging therapies, such as osteoporosis, osteopenia, and decreasing tumor-associated macrophages in melanoma, dysfunction of macrophages leads to an inability of an appropriate immune response and implicated in various disease processes, especially intestinal macrophages that play a key role in the gut immune system and the regulation of gastrointestinal physiology. To obtain an understanding of the role of sepsis-associated macrophages, clodronate was used for the dysfunction of mouse macrophages with and without cecal ligation and puncture (CLP) sepsis. Macrophage depletion significantly increased fecal Ascomycota, with a slight growth of bacterial microbiota which might be enhanced gut-barrier damage as *Candida pintolopesii*, *Klebsiella pneumoniae*, *Acinetobacter radioresistens,* and *Enterococcus faecalis* that were identified from mouse blood. In addition, increased mortality, cytokine overproduction, organ damage (liver and kidney), gut leakage (FITC-dextran), imbalance of fecal fungi and pathogenic bacteria, as well as fungemia and bacteremia in sepsis with macrophage-depleted animals was more severe than sepsis in control mice (fungemia and bacteremia). To determine the interaction between fungal molecules and bacterial abundance, each heat-kill lysate of *C. pintolopesii*, *C. albicans* ATCC90028, *C. albicans* (isolated from human blood), and purified (1→3)-β-D-Glucan (BG), a major component of the fungal cell wall was co-cultured with each pathogenic bacterium, including *K. pneumoniae, E. faecalis, and A. radioresistens*, indicating that the enhanced growth of bacteria that were isolated from the blood implying a direct enhancer to some bacterial species. Furthermore, the additive effect of heat-kill lysate *Candida* yeast cells or their components together with heat-kill lysate of isolated bacteria on enterocytes (Caco-2) also supported an influence of gut fungi in worsening sepsis. In conclusion, macrophage depletion enhanced fecal *Candida* and fecal pathogenic bacteria overgrowth, intestinal barrier damage, and gut translocation of bacteria and fungi that additively worsened sepsis severity. These findings suggested that fecal fungus could spontaneously elevate in response to macrophage-depleted therapy, increasing the severity of sepsis.

Field of Study:	Medical Microbiology (Interdisciplinary Program)	Student's Signature	
Academic Year:	2022	Advisor's Signature	
		Co-advisor's Signature	

ACKNOWLEDGEMENTS

TABLE OF CONTENTS

LIST OF TABLES

จุฬาลงกรณ์มหาวิทยาลัย

CHULALONGKORN UNIVERSITY

LIST OF FIGURES

จุฬาลงกรณ์มหาวิทยาลัย

CHULALONGKORN UNIVERSITY

LIST OF ABBREVIATIONS

°C	Degree Celsius
µL	Microliter (a unit of capacity)
1X PBS	1X Phosphate-buffered saline
A. radioresistens	*Acinetobacter radioresistens*
ALT	Alanine transaminase
ASVs	Amplicon sequence variants
AMPs	Anti-microbial proteins
ANT	Adenine nucleotide translocator
AGM	Aorta-gonad-mesonephros
APCs	Antigens presenting cells
Arg1	Arginase1
B. fragilis	*Bacteroides fragilis*
BG	(1, 3)-beta-D-glucan
BP	Bisphosphonate
C. albicans	*Candida albicans*
Caco-2 cell line	Colorectal adenocarcinoma cells
CFU	Colony forming unit
Clod	Clodronate (Macrophage-depleted)
Clod-CLP	Sepsis with macrophage-depleted
CLP	Cecal ligation and puncture
CSF1	Colony-stimulating factor1
CRC	Colorectal cancer
DAMPs	Damage-associated molecular patterns
DCs	Dendritic cells

DMEM	Dulbecco's Modified Eagle Medium
E. faecalis	*Enterococcus faecalis*
ELISA	Enzyme-linked immunosorbent assay
E. coli	*Escherichia coli*
F. prausnitzii	*Faecalibacterium prausnitzii*
FBS	Fetal bovine serum
FITC-dextran	Fluorescein Isothiocyanate-Dextran
g	Gram (a unit of capacity)
GF	Germ-free
GI tract	Gastrointestinal tract
GCSF	Granulocyte colony-stimulating factor
GM-CSF	Granulocyte-macrophage colony-stimulating factor
HSC	Hematopoietic stem cells
i.p. injection	Intraperitoneal injection
i.v. injection	Intravenous injection
IBD	Inflammatory bowel disease
IBS	Irritable bowel syndrome
IECs	Intestinal epithelial cells
IFN-γ	Interferon-gamma
IL-1, IL-1α, and IL-1β	Interleukin-1, Interleukin-1alpha, and Interleukin-1beta
IL-10	Interleukin-10
IL-13	Interleukin-13
IL-4	Interleukin-4
IL-6	Interleukin-6

IL-7	Interleukin-7
IL-8 or CXCL8	Interleukin-8 or C-X-C ligand
K. pneumoniae	*Klebsiella pneumoniae*
kDa	Kilo-Dalton
Lipo	Liposome control
Lipo-CLP	Sepsis without macrophage-depleted
LPS	Lipopolysaccharide
M	Mole
M1	Macrophage M1
M2	Macrophage M2
M-CSF	Macrophage colony-stimulating factor
MLN	Mesenteric lymph nodes
mL	Milliliter (a unit of capacity)
MOI	Multiplicity of infection
MW	Molecular weight
NK cell	Natural killer cell
NO	Nitric oxide
OA	Osteoarthritis
PAMPs	Pathogen-associated molecular patterns
PenG/Strep	Penicillin G/Streptomycin
pg/mL	Picograms per milliliter (a unit of capacity)
PRRs	Pathogen recognition receptors
Treg	Regulatory T cells
R. gnavus	*Ruminococcus gnavus*
s.c. administration	Subcutaneous administration
SDA	Sabouraud Dextose Agar

SDB	Sabouraud Dextose Broth
SCr	Serum creatinine
S. aureus	*Staphylococcus aureus*
S. pneumoniae	*Streptococcus pneumoniae*
Th1	T helper type 1
Th17	T helper type 17
Th2	T helper type 2
TGF-β	Transforming growth factor beta
TJs	Tight junctions
TLRs	Toll-like receptors
TME	Tumor microenvironment
TNF-α	Tumor necrosis factor-alpha
TSA	Tryptic Soy Agar
TSB	Tryptic Soy Broth

CHAPTER I

INTRODUCTION

Gut dysbiosis is the imbalance of microorganisms that live in the gastrointestinal (GI) tract, leading to inflammatory diseases and metabolic dysfunctions (1). Generally, gut microbes or gut flora always communicate with other microorganisms of the ecological system and host acting in a symbiotic relationship, which plays a vital role in the maturity of the intestinal immune system. Not only Gram-negative bacteria are the most common pathogen causing gut dysbiosis (2, 3), but also fungus is one of the pathogens that significantly enhanced gut dysbiosis or gut microbe imbalance, and sepsis severity in the cecal ligation and puncture (CLP) mouse model through fungal molecules, activating immune cell responses and leading to cytokine storm (more immune cell responses) (4). In addition, broad-spectrum antibiotic administrations also significantly induced sepsis severity by enhancing higher liver damage, gut dysbiosis, and increasing pathogenic bacteria in mice gut (5).

Macrophages originate from blood monocytes that leave the circulation to differentiate in different tissues, and they are specialized cells for the detection, phagocytosis, and responsibility to harmful organisms at the infectious site (6). In terms of sepsis-associated pathophysiology, macrophage performs polymerized phenotypes that are broadly separated into two categories, including classical (pro-inflammatory, M1) and alternative (anti-inflammatory, M2), as well as a regulatory phenotype and subtype of this broad categorization (7, 8). To achieve their functionally distinct roles of macrophage, clodronate-liposome (dichloromethylenebisphosphonate) acted as a key role for macrophage depletion by inhibiting adenine nucleotide translocator (ANT), which is the ADP/ATP translocase enzyme, an important translocate enzyme in mitochondria, leading to loss of cell energy and death by a suicidal apoptosis

mechanism. To date, macrophage-depleted drug is used to decrease osteoclast activity in human bone-related diseases and musculoskeletal conditions, such as osteoarthritis (OA), bone pain from skeletal metastases in breast cancer, and bone edema syndrome (9, 10). The previous report demonstrated that depletion of macrophages in an animal model is usually performed with a clodronate-liposome (11) due to without any side effects in mice. Similarly, the mouse model shows macrophage depletion be achieved approximately 80-90% within 24 – 48 h after a single dose of intravenous (i.v.) or intraperitoneal (i.p.) injection (12), and also enhances the depletion of both M1 and M2 macrophages in various organs, such as liver, kidney, intestine, bone marrow, and colon (13). The depletion of M1 macrophages reduced the infiltration of activated T cells and inflammation which could be evaluated as a potential therapeutic approach for inflammatory diseases (14), whereas M2 macrophage depletion affected to kidney injury was more severe and renal function was impaired by increasing pro-inflammatory cytokines and decreasing anti-inflammatory cytokines (7). The most common adverse effects were mild gastrointestinal disturbances, such as nausea, vomiting, diarrhea, tiredness, confusion, and irritability (15). Although the benefits of macrophage depletion by clodronate-liposome administration can improve inflammatory diseases and tumors, together with adverse effects in humans were published (16), the relationship between the role of macrophage depletion and gut microbe patterns in sepsis severity is still a mystery. The purpose of this study was to demonstrate that macrophage depletion may cause adverse effects in animal with uncontrollable gut microbes, leading to changes in gut microbiome patterns and gut translocation results in sepsis severity. In addition, CLP can induce polymicrobial abdominal sepsis on clodronate-liposome administration C57BL/6 mice was used to investigate the impacts of macrophage depletion on sepsis severity and gut dysbiosis.

CHAPTER II
OBJECTIVES

Research question

Does macrophage depletion enhance gut dysbiosis and worsens sepsis severity in the cecal ligation and puncture (CLP) mouse model?

Hypothesis

Macrophage depletion enhances gut dysbiosis and worsens sepsis severity in cecal ligation and puncture (CLP) mouse models via increased gut fungi and pathogenic bacteria.

Objectives

1. To investigate macrophage depletion enhances gut dysbiosis and sepsis severity in the cecal ligation and puncture (CLP) sepsis mouse model.
2. To investigate the interaction between pathogenic microorganisms and sepsis severity in the cecal ligation and puncture (CLP) mouse model.

Conceptual framework
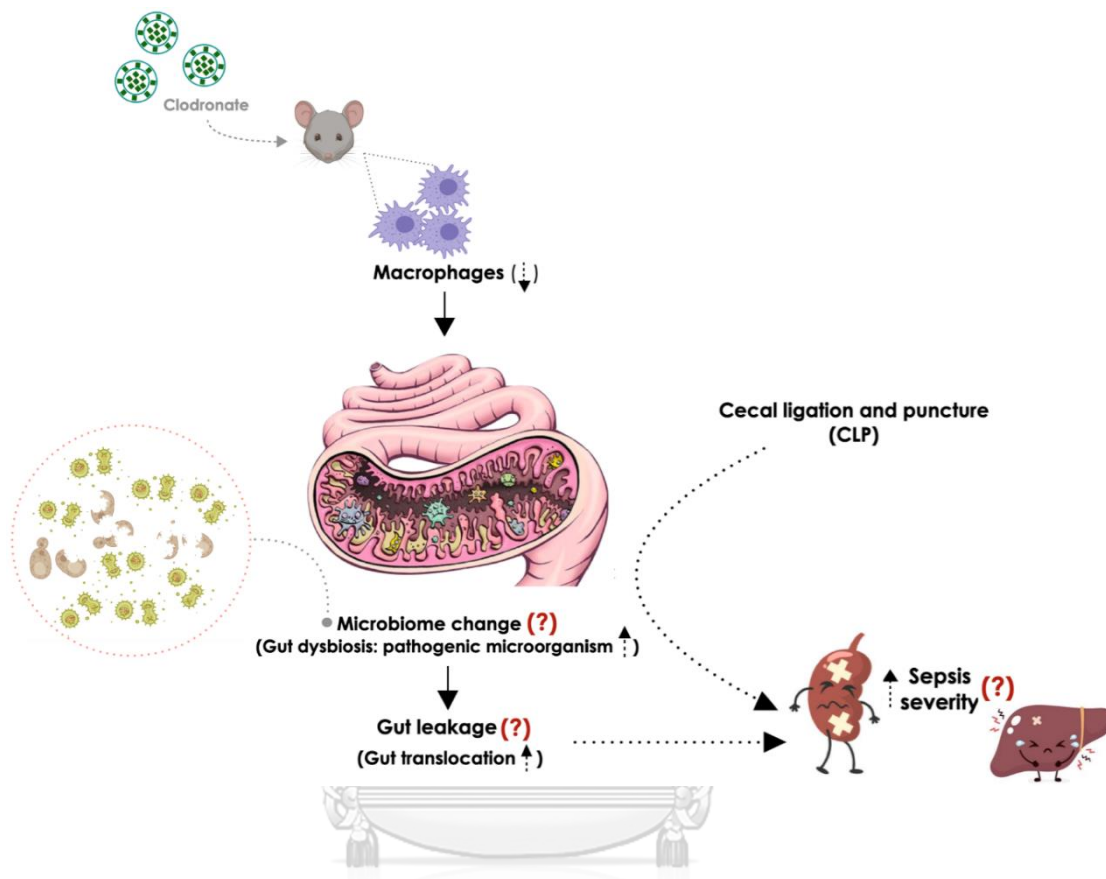
Workflow
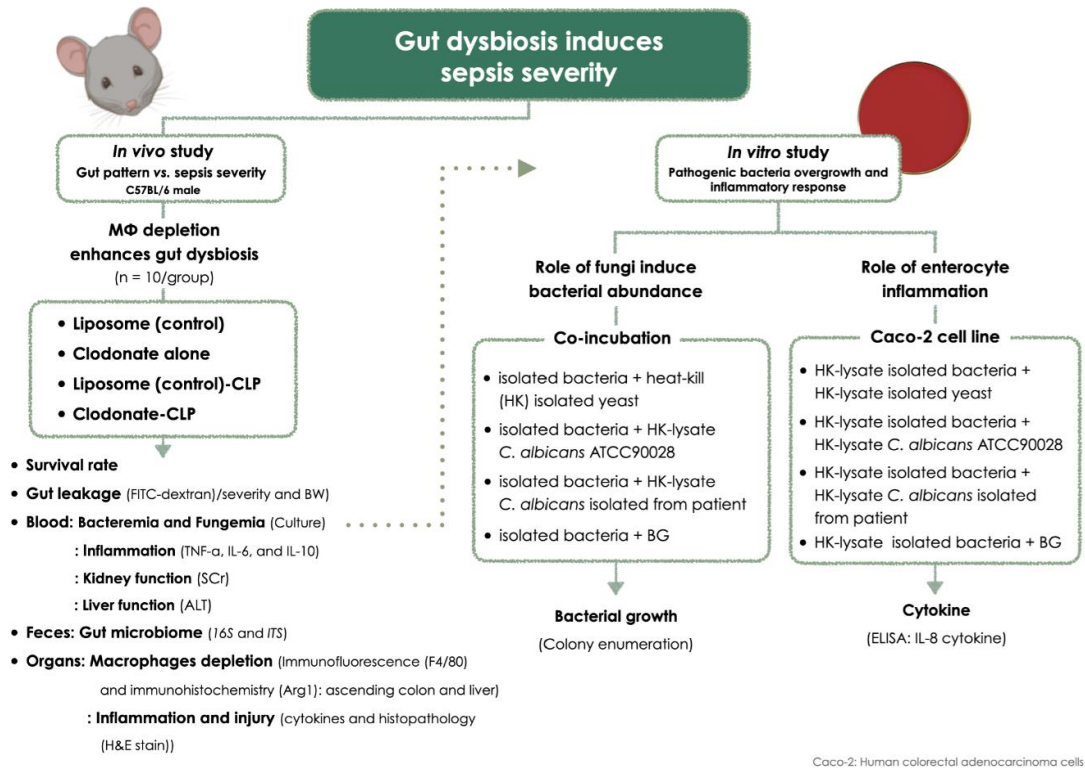
CHAPTER III

LITERATURE REVIEWS

1. Macrophages

Macrophages are dynamic cells that play an important role in the induction and resolution of inflammation, and they were originally described in 1883 by Élie Metchnikoff. Macrophages are developed in bone marrow as monocytes, which are the major groups of white blood cells of the human immune system that circulate in the bloodstream. The generation of macrophages depends on the hematopoietic growth factor receptor CSF1R (M-CSFR), such as ligands of CSF1R and colony-stimulating factor 1 (CSF1)/macrophage colony-stimulating factor (M-CSF). While hematopoietic cytokines, such as granulocyte-macrophage colony-stimulating factor (GM-CSF) and granulocyte colony-stimulating factor (G-CSF), encourage the proliferation and differentiation of granulocyte progenitor cells (Figure 1) (17). The unique phenotypes of macrophages are the migration toward tissues or settle down in the tissue, called specialized macrophages (18), including i) mesangial cells (kidney), ii) alveolar macrophages (lung), iii) microglial cells (brain), iv) Langerhans cells (skin), v) histiocyte (tissue), vi) Kupffer cells (liver), vii) follicular DCs (lymph nodes), and viii) intestinal macrophages, all of which represent the largest population of tissue macrophages in most adult tissues (19).
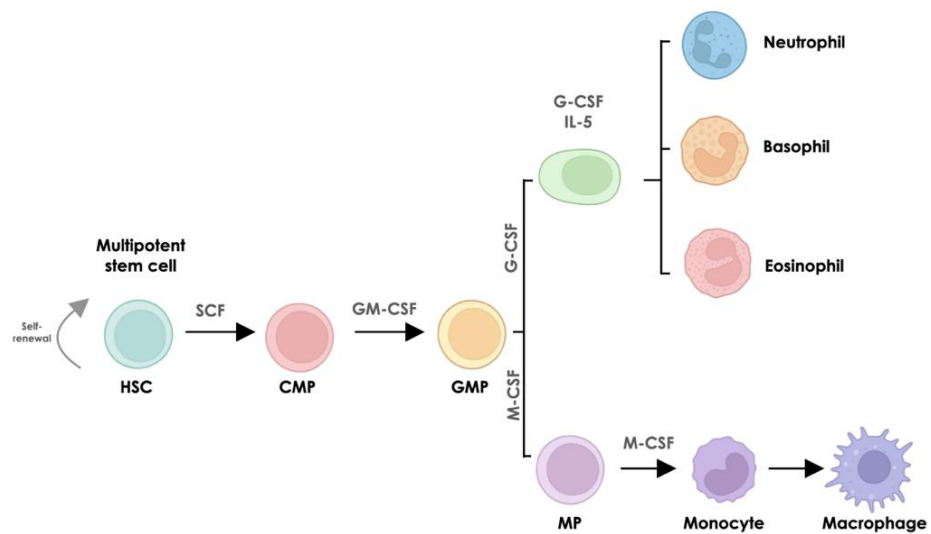
Figure 1 Scheme of the origin and develop of macrophages

The characteristic of macrophage development was generated by BioRender (https://app.biorender.com/) on October 8[th.], 2022 with a minor modification from Kely Campos Navegantes, et al., J Transl Med, 2017.

1.1 Macrophage functions and polarizations

Macrophages are also known as one of the professional antigen-presenting cells (APCs) (20) that respond to infection and accumulate damaged, and dead cells. The general functions of macrophages in the innate immune system, such as opsonic recognition, production of pro- and anti-inflammatory cytokines, the releasing of G-CSF and GM-CSF, excessive release of toxic species (nitric oxide (NO) and superoxide), antigen processing, and presentation (21, 22). For activating the adaptive immune system, macrophages play many functions, like the secretion of hydrolytic enzymes, inducing neovascularization and contributing to angiogenesis and lymphangiogenesis, modulating osteoclastogenesis, and inducing Th1 cells differentiation, controlling the effector of T-cell homeostasis, promoting the T-cell priming, and also may induce Th17 cell differentiation (23-25). Normally, monocytes and macrophages

support the regulation of the immune system, which might result in autoimmunity. Depending on the surroundings, these cells can dynamically polarize between pro- and anti-inflammatory cytokines, acting with various physiological functions (26). Then, macrophages can divide depending on their functions, including helping eliminate foreign substances by engulfing foreign materials and initiating an immune response (promote tissue inflammation and activated macrophages) that are called the classically activated macrophages or "M1 macrophages". In contrast, macrophages can switch their phenotypes for regulators of the wound healing process, tissue repair, and immunoregulation called "M2 macrophages" (Figure 2) (7).

1.1.1   M1 macrophage (pro-inflammatory)

M1 macrophages are involved in autoimmune disorders and anti-tumor immunity (27, 28). Their function is an intermediate innate immunity against a variety of bacteria, fungi, protozoa, and viruses. Commonly, macrophages are stimulated to the M1 subset by lipopolysaccharides (LPS), a component of several bacterial products, and inflammatory cytokines, such as interferon (IFN). Due to the secretion of cytokines, such as tumor necrosis factor-α (TNF-α), interleukin-6 (IL-6), interleukin-12 (IL-12), and interleukin-23 (IL-23) and chemokines (Chemokine (C-C motif) ligand 5 (CCL5), chemokine (C-X-C motif) ligand (CXCL) 9, CXCL10, and CXCL5), M1 macrophages strongly promote the recruitment of Th1 and NK cells leading to inflammations. It has also been demonstrated that M1 macrophages increase the expression of the protein suppressor of cytokine signaling 3 (SOCS3) intracellularly, which raises the production of reactive oxygen intermediates and nitrogen, as well as the expression of major histocompatibility complex (MHC) class II

molecules and costimulatory molecules (29, 30). According to that theory, M1 macrophages not only support Th1 immune responses but also contribute to tissue damage and tumoricidal action. As a result, an over-activation may result in tissue damage, as the case with several inflammations, autoimmune, and chronic diseases, such as Crohn's disease, rheumatoid arthritis, diabetes, autoimmune hepatitis, and multiple sclerosis (31-33). The common cell surface markers used to identify human and mouse M1 macrophages, such as CD4/80, CD80, CD86, CD64, CD16, and CD32 as markers. In addition, the expression of nitric oxide synthase (iNOS) in M1 macrophages can also serve as a phenotypic marker (34).

1.1.2   M2 macrophage (anti-inflammatory)

M2 macrophages play a role in the control of the immune system, tissue remodeling, the eradication of parasites, the promotion of tumors, and the development of autoimmune disorders. Normally, M2 macrophages express surface markers as CD163 and CD206, which are major markers for the identification, followed by CD68, arginase1 (Arg1), and DECTIN-1 (34). Three distinct subpopulations of the M2 macrophages occurred, including the macrophages M2a, M2b, and M2c macrophages, depending on their functional and biochemical aspects (35, 36). In short, the M2a macrophage is activated by interleukin-4 (IL-4) and/or interleukin-13 (IL-13) through the binding of these cytokines to their receptors and activates the signal transducer and activator of the transcription-6 (STAT-6) signaling pathway. It upregulates the histone demethylase jumonji domain-containing protein-3 (JMJD3), by inducing expression of the M2 gene and inhibits the M1 gene during tissue repair and anti-inflammatory response (37, 38). Additionally,

Mrc1, resistin-like a (Retnla, Fizz1), and chitinase 3-like 3 (Chi3l3, Ym1) expression are upregulated by M2a macrophages indicating that these expressions are specific indicators of M2a macrophages (38). Moreover, M2a also induces the invasion of eosinophils, basophils, Th2 cells, and regulatory T-cells by secreting C-C Motif Chemokine Ligand (CCL) 24, CCL17, CCL1, and CCR1 at the site of inflammation (39). The M2b are polarized by combined immune complexes that contain toll-like receptors (TLRs) and/or interleukin-1 (IL-1) receptor agonists and release large amounts of pro-inflammatory cytokines, such as IL-1, interleukin-1 (IL-6), and TNF (28, 40). Finally, M2c is induced by transforming growth factor (TGF)-β, glucocorticoids, or interleukin-10 (IL-10). Which, IL-10 is produced by dendritic cells, B cells, cytotoxic T-cells, T-cells, natural killer (NK) cells, mast cells, neutrophils, eosinophils, monocytes, and macrophages. The activation mediated by IL-10 acts through a transmembrane receptor complex composed of interleukin-10 receptors1 and 2 (IL-10R1 and IL-10R2). Then, the IL-10/IL-10R1 interaction leads to a change in the cytokine conformations causing its dimerization with IL-10R2 and Jak1/STAT3 signaling pathways (41).
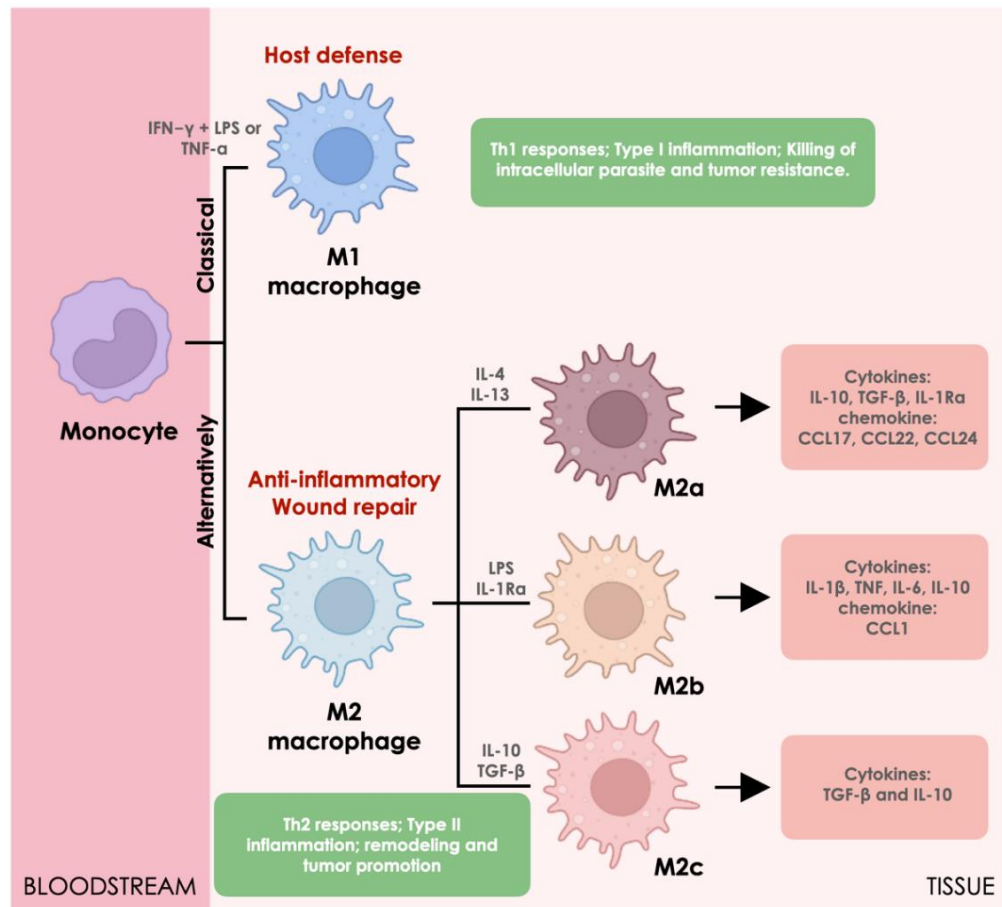
Figure 2 Schematic diagram of the polarization and activation of macrophages

The schematic diagram of the polarization and activation of macrophages. (Modified from; Kely Campos Navegantes, *et al.*, J Transl Med, 2017). This picture was generated by BioRender (https://app.biorender.com/) on October 8[th.], 2022.

2. Clodronate-liposome

Clodronate is a synthetic chemical in terms of non-nitrogenous bisphosphonate (BP) medication that is encapsulated into "liposome" vesicles, which has the property to inhibit osteoclast activity (Figure 3) and was developed in the late 1960s (42). Encapsulated bisphosphonate is used in clinical treatment to prevent or inhibit the development of bone metastases and for the treatment of inflammatory diseases, such

as rheumatoid arthritis and osteoarthritis (43). The pharmacodynamic properties of clodronate have already been discussed in both *in vitro* research and *in vivo* animal models that are associated with bone metastases-inducing cancer, parathyroid hormone, or other factors (15). To date, clodronate is still commonly used in a variety of human bone-related diseases, for example, osteoporosis, osteopenia, osteolytic lesions, hypercalcemia, and use in bone pain associated with skeletal metastases in patients with breast cancer and multiple myeloma (44). Moreover, clodronate has been used to treat musculoskeletal conditions, for instance, osteoarthritis (OA) and bone edema syndrome (9, 10). Clodronate-liposome is a suitable structure for phagocyte-targeted therapies providing advantages, such as low immunogenicity, biocompatibility, cell specificity, and drug protection and stability (45). Although clodronate-liposome can be depleted of mononuclear phagocytic cells, including bone marrow progenitors, blood monocytes, and tissue macrophages, macrophage dysfunction can lead to an inability to an appropriate immune response and implicated in various disease processes.
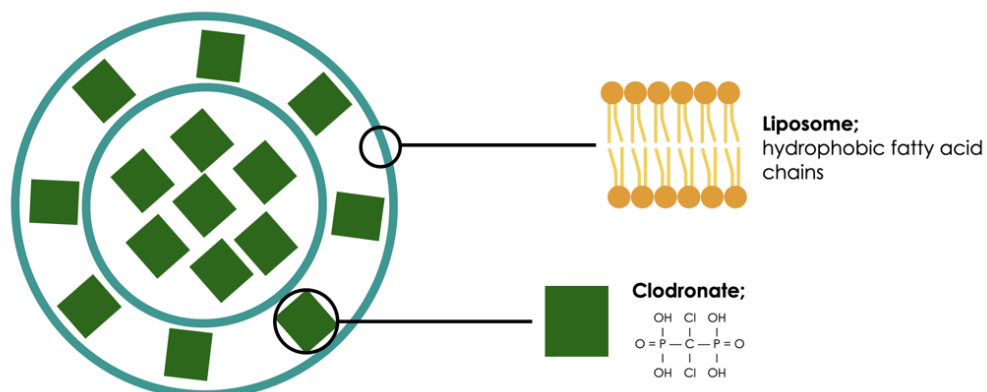
Figure 3 Structure of clodronate-liposome

Clodronate-liposome is composed of concentric phospholipid bilayers together with hydrophilic molecules clodronate (green squares; see also structural formula) is encapsulated during the formation of the liposome. This picture was generated by BioRender (https://app.biorender.com/) on January $7^{th.}$, 2023.

2.1 The mechanism of clodronate-liposome to depleted macrophage

Macrophage function is inhibited by clodronate-liposome using its phagocytosis. After macrophages engulf the clodronate-liposome (Figure 4A-B), the phagolysosome is fused with a lysozyme (Figure 4C), the enzyme-digested phospholipid bilayers of the liposome vesicle and released clodronate into the cytosol, respectively (Figure 4D). In addition, clodronate in the cytosol inhibits ADP/ATP translocase enzyme, called "liposome-mediated macrophage suicide" (46) in mitochondria leading to cell death by apoptosis (Figure 4E). Besides macrophage phagocytosis, size (small; 85 nm in diameter) and charge (negatively) of liposome vesicle are important factors for a specific target in the mononuclear phagocytic system (MPS) (47, 48).
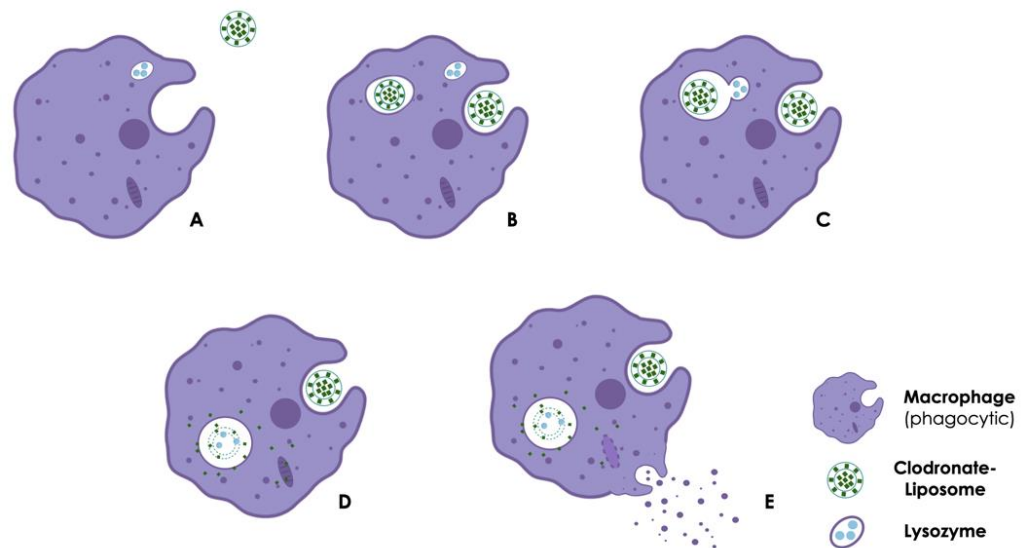
Figure 4 The mechanism of clodronate-liposome depletes macrophages

Clodronate-liposome induces macrophage apoptosis (A-E), phagolysosome releasing the clodronate into the cytosol (D) and inducing cells apoptosis (E) via inhibiting ADP/ ATP translocase disrupts the electron transport chain in mitochondria (cellular ATP loss) , 80-90% after a single intravenous or intraperitoneal administration. (Modified from; Encapsula NanoSciences LLC, http://www.clodrosome.com/other-info/mechanism-of-depletion/). The picture was generated by BioRender (https://app.biorender.com/) on March 5th, 2022.

2.1.1   Effects of clodronate-liposome-depleted macrophage

Although clodronate is useful as a specific tool in clinical for the prevention or inhibition of the development of bone metastases and for the therapy of inflammatory diseases, it has been reported some severe side effects for a long period and in high doses used, such as osteonecrosis of the jaw (ONJ) (reducing angiogenesis and bone remodeling) (49), bone fracture, decreases kidney and liver functions, joint or muscle pain that can be severe, hypocalcemia, and conjunctivitis (eye infections) (50). The most

common adverse effects reported were mild gastrointestinal (GI) disturbances, such as nausea, vomiting, diarrhea, tiredness, confusion, and irritability (15). Moreover, the depletion of macrophages can cause fibrosis and impair muscle regeneration via increased expressions of inflammatory cytokines, chemokines, and oxidative stress during the healing stage (51). As well-known that macrophage impacts microorganisms in the human body, especially in the GI tract. The previous study reported only the benefit of clodronate-liposome-treatment changed the gut microbiota, a higher concentration of Firmicutes, a phylum with known anti-tumorigenic properties in the colon cancer (52). However, the adverse effect of macrophage depletion impacts gut pathogenic microorganisms and inflammatory diseases remain unpublished.

In terms of animal model, clodronate-liposome is able to deplete macrophages up to 80-90% after a single intravenous (i.v.) or intraperitoneal (i.p.) administration (12), which can deplete macrophages in both M1 and M2 macrophage polarization in the mouse model (13). A previous study implies macrophage depletion from clodronate-liposome is also associated with decreased bone turnover and oral osseous wound healing in the mouse model (53). Although the benefits of macrophage depletion by clodronate-liposome administration can improve inflammatory diseases and tumors, together with adverse effects in humans were published (16), the role of macrophage depletion link between gut microbe patterns in sepsis severity is still unexplored.

3. Gut dysbiosis

3.1 Definition of gut dysbiosis

Gut microbiome is an equivalence of microorganisms, including bacteria, viruses, fungi, protozoa, and archaea that live in the gastrointestinal (GI) tract approximately $10^{13} - 10^{14}$ organisms (1). The major gut microbiota phyla are composed of Bacteroidetes (65%), Firmicutes (16%), Actinobacteria (9%), Proteobacteria (5%), and other phyla (5%) (54, 55). Generally, gut microbes or gut flora always communicate with other microorganisms of the ecological system acting in a symbiotic relationship, which plays a vital role in the maturity of the intestinal immune system. Conversely, an abnormal host immune defense and reduction in the diversity of gut microbes may be caused inflammatory diseases and metabolic dysfunctions (56), called "gut dysbiosis" (Figure 5). Gut dysbiosis means the imbalance of microorganisms that live in the GI tract, leading to inflammatory diseases and metabolic dysfunctions (1). Not only a loss of beneficial microbiota, but also an increase in harmful microorganisms are characteristics of dysbiosis (pathobionts) (57), affecting the ratio of potentially harmful to beneficial commensal microorganisms is more important for the development of diseases. A recent report suggests the increase of pathogenic bacteria in the gut, such as *Escherichia coli* (*E. coli*), *Klebsiella* spp., *Proteus* spp., *Enterobacter* spp., *Shigella* spp., *Salmonella* spp., and *Serratia* spp. are commonly mentioned in gut dysbiosis (Table 1).
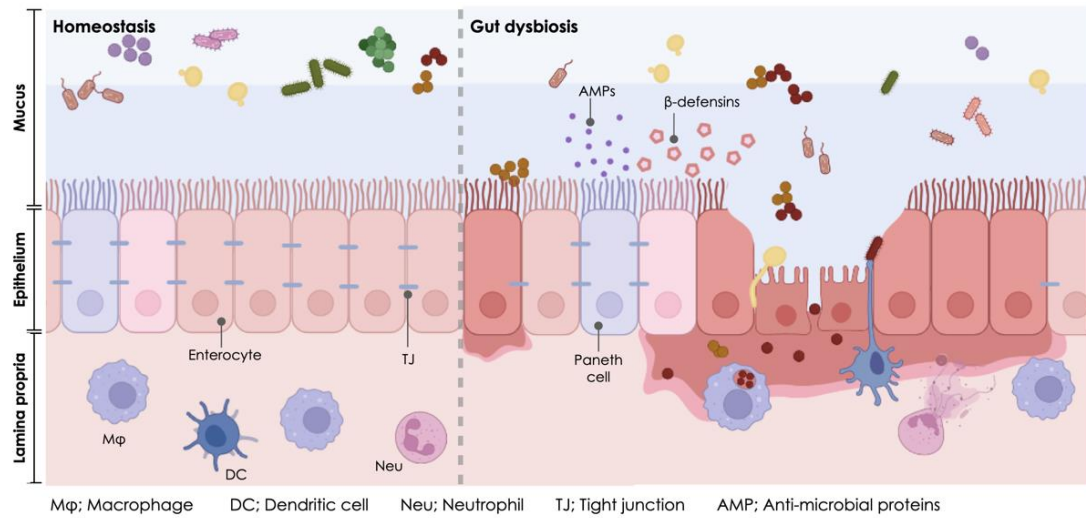
Figure 5 Scheme of the relationship between the gut microbiome and gut dysbiosis

The relationship between the gut microbiome and gut dysbiosis was generated by BioRender (https://app.biorender.com/) on January 8th, 2023 using the publication of Jenelle Marcelle Safadi, *et al*., Molecular Psychiatry, 2022 (58) as the template.

Table 1 Gastrointestinal pathogens are associated with various diseases

Species	Associated diseases (increased)	Inversely associated (decreased)	References
Bacteroides fragilis	Diarrhea	-	(59)
Clostridium difficile	Diarrhea	-	(60)
Salmonella enterica	Irritable bowel syndrome (IBS), Diarrhea	-	(61), (62)
Clostridium spp.	Diarrhea	-	(63)
Escherichia/Shigella	Crohn's disease, IBS	-	(64)
Salmonella spp.	Diarrhea	-	(65)
Campylobacter spp.	IBS, Diarrhea	-	(66)
Akkermansia muciniphila	Type II Diabetes	Obesity, ulcerative colitis, Crohn's disease	(67), (68)
Lactobacillus spp.	Obesity	Obesity, Type II Diabetes, IBS, Diarrhea	(69), (70)
Bifidobacterium spp.	-	Constipation, Crohn's disease, IBS	(71)

3.2 Gut dysbiosis-associated diseases

Previous studies describe that gut dysbiosis is an important cause of intestinal barrier breakdown, bacterial translocation or gut translocations, and gut dysbiosis is also a well-known factor that contributes to the emergence of several immune-mediated diseases, such as inflammatory bowel disease (IBD) (72), type 1 diabetes and obesity (73), and colorectal cancer (CRC) (74). Briefly, the presence of potentially pro-inflammatory bacteria, such as *Bacteroides* spp. and *Ruminococcus gnavus* (*R. gnavus*), are linked to IBD, while the presence of anti-inflammatory species, such as *Faecalibacterium prausnitzii* (*F. prausnitzii*), predominates in healthy individuals. The populations of pathogenic bacteria can be used to determine the potential association between intestinal dysbiosis and certain human diseases as shown in Table 1 (75). In addition, microbes or their molecules that enter into intestinal epithelium cells (IECs) are called "gut translocation or bacteria translocation", which defines microbes in the intestinal lumen, both live and dead microbes, and microbial products, such as exotoxins, endotoxins, and cell wall fragments. It penetrate through the gastrointestinal mucosa to the lamina propria, local mesenteric lymph nodes (MLN), internal organs, and mostly sterile tissues (76). In research involving animal models, a lower ratio between Firmicutes/ Bacteroidetes and fewer *Bacteroides* species has been related to obesity (77). Furthermore, gut dysbiosis is commonly related to the gut barrier function that the causing of "gut translocation" and enhances inflammatory cell activations.

Commonly, the causes of gut translocation are associated with many factors including i) intestinal mucosa changes permeability (increased mucosa permeability), the tight junctions (TJs) in the gut epithelial wall break down, allowing substances from the lumen to translocate into the bloodstream, and

other organs, ii) decreased host immune system and lower immune cells are present, which are easy for opportunistic infection of nosocomial pathogens, and iii) intestinal bacteria overgrowth (imbalance), a serious condition affecting the small intestine. It happens when the number of bacteria in the small intestine increases from approximately 10^5 CFU/mL to around 10^8 CFU/mL (78) which results from many situations, such as surgery, antibiotic treatments, and illness (Figure 6) (79).
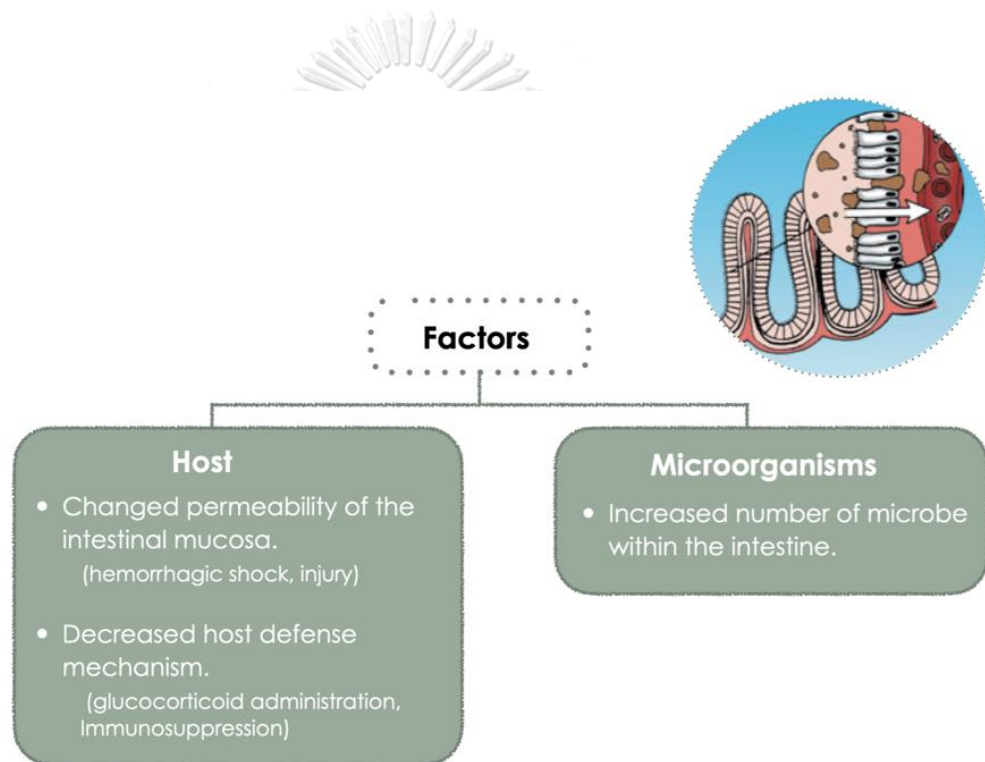
Figure 6 Gut translocation factors

Factors associated with gut dysbiosis induce gut translocation that is slightly modified from Vaishnavi C., *et al*., Indian J Med Microbiol, 2013 (79). The schematic was generated by Keynote on January 4th, 2022.

3.3 Pathophysiology of gut dysbiosis

Gut microorganisms live in the intestinal lumen and control the invasion of pathogenic bacteria through microbe-to-microbe interactions and the immune systems (80). Once, gut dysbiosis, IECs are damaged and epithelial TJs lose functions, the microbes have been invaded through the enterocytes. Gut pathogens activate innate immune cells, for example, IECs secrete IL-8 cytokine, goblet cells secret mucus, and Paneth cells secret antimicrobial proteins (AMPs), such as alpha-defensin, lysozyme, and phospholipase A2 (81). In the lamina propria, macrophages and dendritic cells are the essential innate immune cells, which play an important role in controlling an infection via phagocytosis activity, professional antigen-presenting cells (APCs), cytokines and chemokines production (both pro- and anti-inflammatory cytokines), and anti-microbial action. APCs have engulfed and digested pathogens, and present and secrete cytokines and chemokines to recruit and activate other immune cells at the site of infection, including T and B cells. Subsequently, the innate immune malfunction can impact uncontrol gut microbiota, leading to gut translocation from various virulence factors, for example, *E. coli* (EHEC phenotype) secret espF to induce mitochondrial death, tight junction disruption, immune evasion, and host IECs death (82), as well as gut fungus, such as *C. albicans* secrete candidalysin, fungus peptide toxin, which destroys host cells (83), causing of inflammatory immune cell responses, and inflammatory diseases, especially IBD and sepsis, respectively (Figure 7) (84).
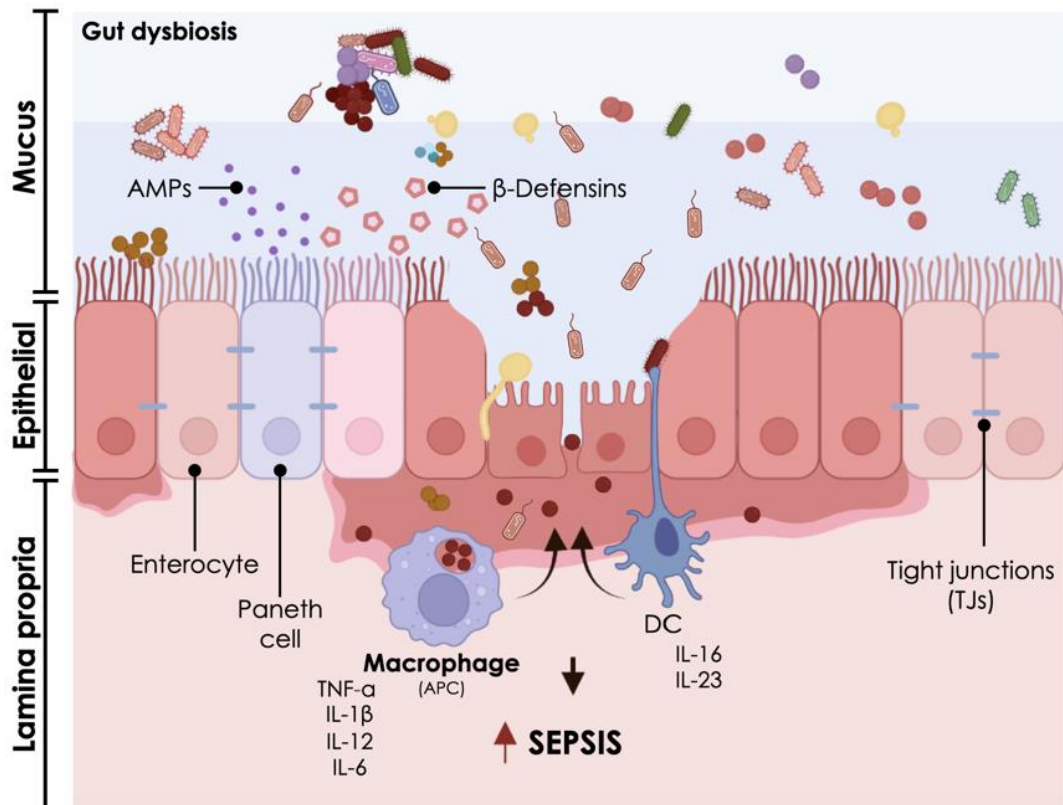
Figure 7 Gut dysbiosis enhances sepsis mechanism

Gut dysbiosis induces sepsis severity was generated using BioRender (https://app.biorender.com/) on November 29th, 2022 with a minor modification of Mehmet Coskun, Front Med (Lausanne), 2014 (84).

3.4 Mechanisms of pathogenic molecules activate immune cells

3.4.1 LPS activates the immune system through Toll-like receptor 4 (TLR4)

In order to mediate both short-term and long-term host defense, the innate immune system uses specialized proteins known as pattern recognition receptors to detect pathogens (PRRs) causing the activation of intracellular signal transduction networks that encourage inflammatory gene production (85). One of the best-studied PRRs is Toll-like receptor 4 (TLR4),

a receptor for bacterial lipopolysaccharide (LPS) that is a crucial component of Gram-negative bacteria, such as *E. coli*, *Salmonella* spp., *Porphyromonas* spp., and *Helicobacter* spp. leading to a certain pattern of cytokine release to control inflammation (86). The chemical structure of LPS can be categorized into three parts, including i) lipid A moiety (the most conserved), ii) oligosaccharide chain, and iii) polysaccharide chain is well-known as an 'O-antigen' (87). Once gut dysbiosis and gut translocation, LPS in the extracellular space is sensed by the plasma-membrane located TLR4–co-receptor MD2 complex in conjunction with co-receptor CD14, which specifically recognizes the lipid A structure of LPS (88). Afterward, TLR4 ligates and transduces the signal via the adapters MyD88 and TIR-domain-containing adapter-inducing interferon-β (TRIF) genes activated nuclear Factor kappa-light-chain-enhancer of activated B cells (NF-κB), and IFN regulatory factor 3 (IRF3)-mediated transcription of genes encoding molecules of cytokines and chemokines (Figure 8). Therefore, excessive activation of TLR4 with LPS and the consequent cytokine storm was thought to underlie endotoxic shock or sepsis.

3.4.2 Fungal (1→3)-β-D-Glucan (BG) induces an immune response and inflammation

The current report suggests that invasive fungal infections are a major cause of sepsis in severely sick patients, associated with significant morbidity and mortality (89). β-D-Glucan (BG) is a component of β-1,3-D-glucopolysaccharides that is widely distributed in cell wall components of the plant, algae, fungi, and some bacteria, that are not synthesized by mammals (90). The association between structure and activity for BGs is

clearly established, such as (1→4)-**β**-D-Glucan, oat-derived BGs function as effective dietary fibers that improve metabolic health parameters, including dyslipidemia and insulin resistance (91), while (1→3)-**β**-D-Glucan was isolated from yeast-derived-glucans have an immunomodulatory impact that targets the innate immune responses, depending on a variety of sources and structures (92). BGs are recognized by the C-type lectin receptor, especially Dectin-1 which activates immune functions as follows,

i) Phagocytosis; Dectin-1-mediated phagocytosis depends on immunoreceptor tyrosine-based activation motif (ITAM) phosphorylation and the activation of the Src family of protein tyrosine kinases (SFKs). The previous study suggests the mutation of Dectin-1 ITAM tyrosine (membrane-proximal tyrosine) reduced phagocytosis of zymosan (93), and Src inhibitors prevented Dectin-1-mediated phagocytosis (94). Then, the Dectin-1 phagosome is activated by BG which acts as a scaffold for the construction of the downstream signaling complex.

ii) Oxidative burst or oxidative stresses; the phagocyte oxidase complex, which is in charge of generating reactive oxygen species (ROS) after fungi are detected and internalized. Stimulation of macrophages, DCs, and neutrophils with BG particles induces an oxidative burst. Dectin-1-induced ROS generation is caused by ITAM signaling, including Src and spleen tyrosine kinase (Syk) activation (95).

iii) Regulation of transcription, Dectin-1 triggers innate immunological responses by activating NF-**K**B pathways, mitogen-activated protein kinase (MAPK) signaling, and nuclear factor of activated T cells (NFAT) transcription factors through the caspase recruitment domain-containing protein 9

(CARD9) and drives pro-inflammatory cytokine and chemokine productions (96) (Figure 8).

In addition, LPS and *Candida*-BG are major microbial origin molecules as canonical cell wall components of Gram-negative bacteria and fungi, the most and second-most abundant gut microbes, respectively (97). These pathogen molecules do not trigger systemic immune responses when the gut barrier is functioning normally; however, when the gut barrier is damaged (leaky gut or gut leakage), it is possible for these molecules to move from the gut into the blood circulation (gut translocation) (97). During gut barrier damage, BG in serum is correlated with glucans in gut contents, as the oral administration of viable or heat-killed *Candida* yeast cells enhances serum BG. This is similar to increased endotoxemia (serum LPS) from Gram-negative bacteria in gut contents (98). Moreover, gut translocation of LPS together with BG had a synergistic effect that worsens sepsis severity in mouse models (99). Because Dectin-1 and TLR-4 simultaneous activation by BG, together with endotoxin, leads to enhanced macrophage cytokine responses (100).
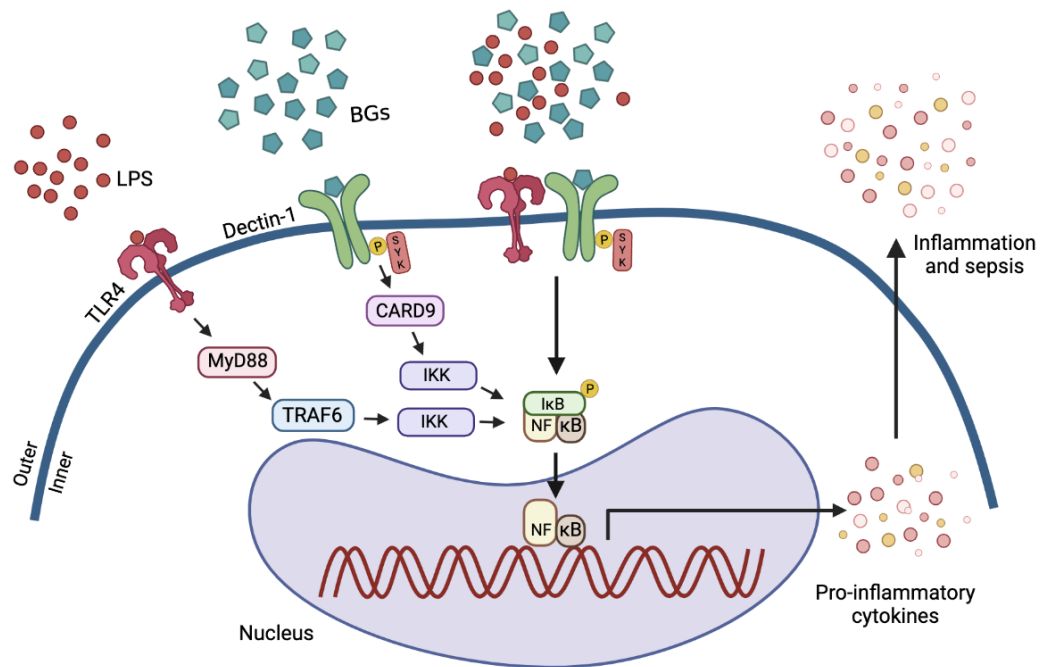
Figure 8 Scheme of the BG and/or LPS induce immune cell responses

The picture demonstrates the possible additional pro-inflammatory impact of lipopolysaccharides (LPS) and $(1\rightarrow3)$-β-D-glucan (BGs), through the synergistic effect of both Toll-like receptor-4 (TLR-4) and Dectin-1, the pattern recognition receptors for LPS and BGs, respectively, which was created by BioRender (https://app.biorender.com/) on December 17th, 2022 using a previous report of Hiengrach P., *et al*., International Journal of Molecular Sciences, 2022) (101) as the template. Syk; Spleen tyrosine kinase, IKK; an inhibitor of nuclear factor kappa-B kinase, and NF-**K**B; nuclear factor kappa B, MyD88; Myeloid differentiation primary response 88, and CARD-9; Syk-Caspase recruitment domain-containing protein 9.

4. Sepsis

4.1 Definition and etiology of sepsis

Sepsis or septicemia refers to an infection of pathogens involving the bloodstream and is a medical emergency, which the causing of an infection-fighting process that may affect the whole body and a potentially life-threatening disease (2, 102). Recently, sepsis is a global healthcare concern, which is associated with an increased morbidity and mortality rate in all countries, such as in the United States is around 300 cases per 100,000 people. Most studies suggest that the most microbial causing sepsis is Gram-negative bacteria, followed by Gram-positive bacteria, and fungi (103, 104). Indeed, the most common pathogen species in septic patients have been demonstrated as *E. coli* (21.5%), followed by *Klebsiella pneumoniae* (*K. pneumoniae*) (9.0%), *Staphylococcus aureus* (*S. aureus*) (6.5%), and *Streptococcus pneumoniae* (*S. pneumoniae*) (5.0%) (105). Previous studies report that *Candida* spp. is the major cause of fungal sepsis, accounting for 10%-15% of infections in healthcare settings, 5% of all instances of severe sepsis and septic shock, and ranking fourth among bloodstream isolates in the United States (89). In addition, a polymicrobial infection with two or more causative pathogens is also present in approximal 20% of sepsis patients as well. Besides, studies on sepsis and septic shock have demonstrated that delaying antibiotics treatment is linked to negative results (106), such as antimicrobial resistance-related life-threatening consequences, and antibiotics administration that significantly enhances sepsis severity as well. Broad-spectrum antibiotics have been demonstrated to induce gut dysbiosis and increase liver injury in the sepsis mouse model (107). Furthermore, *C. albicans*, the predominant fungal in the human GI tract, administrated in mice is the cause of gut dysbiosis and significantly increased

bacterial sepsis severity, which is linked to the intestinal fungal quantity and/or fungal molecules, possibly through cytokines storm and liver damage (108).

Many types of infections are the most often blamed for sepsis, including pneumonia, abdominal infection, kidney infection, and bloodstream infection. Sepsis is a more common disease in patients who have an underlying disease, such as diabetes, acquired immune deficiency syndromes (AIDs), and cancer, as well as the cancer patients are a weak immune response because they are taking corticosteroids, and patients who expose to invasive devices, for example, catheters, breathing tube, and a major surgery (109). Common signs and symptoms of that disease show fever above 38°C or a body temperature below 36°C, coolness, breathing problems (higher than 20 beats per min), fast heart rate (higher than 90 beats per min), extreme pain or discomfort, confusion or disorientation (110), and upregulated systemic inflammatory response or severe sepsis, which it can develop "septic shock" (111). Severe sepsis is the dramatic drop in blood pressure and high level of lactic acid that leads to multiple organ failures, for instance, kidneys, brain, heart, and liver, which they are might be deadly if left untreated (Figure 9). Sepsis has been divided into 3 stages depending on the progression of the disease as follows,

Stage 1 is the bloodstream is infected, which leads to inflammation throughout the body. The common signs show fever and/or chills, confusion or disorientation, difficulty breathing, fast heart rate, low blood pressure (hypotension), and extreme pain.

Stage 2 severe sepsis refers to the organ function beginning to be impaired by the infection and inflammation. The feature of severe sepsis is organ failure. To be diagnosed with severe sepsis, at least one of the following symptoms must be present, including difficulty breathing, bluish discoloration of the skin,

especially lips, fingers, and toes, chills due to a drop in body temperature, decreased urination, dizziness (weak at the knees), changes in mental ability, extreme weakness (asthenia), low platelet count (thrombocytopenia), abnormal heart functions, and unconsciousness.

Stage 3 septic shock is a severe drop in blood pressure that results from the severe sepsis complication. This may result in a lot of very serious issues, including organ dysfunction, respiratory or heart failure, and stroke which becomes more life-threatening.
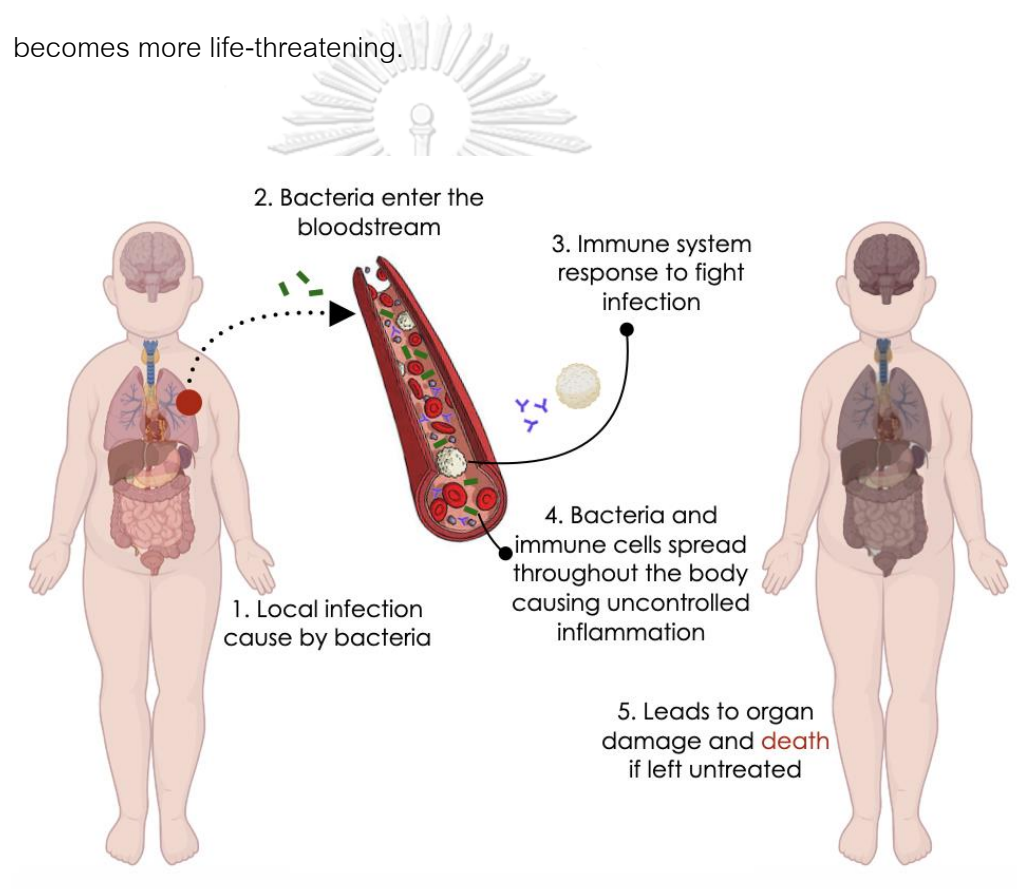

Figure 9 The mechanism of sepsis

Sepsis starts with bacterial infection and immune responses, uncontrol infection and inflammation caused by collateral damage, and death of host cells, which was modified from SickKids staff, Sepsis, 2017 by BioRender (https://app.biorender.com/) on November 15th, 2022.

4.2 Definition and etiology of sepsis

The mechanism starts with a pathogenic infection at the organ and subsequently invaded the bloodstream to activate the innate immune system, such as macrophages, monocytes, neutrophils, and NK cells, which combined with pathogen-associated molecules (PAMPs), such as bacterial endotoxins and BGs using their specific PRRs, meanwhile other specific receptors on monocytes and macrophages, for example, TLRs, C-type lectin receptors, and nucleotide-binding oligomerization or NOD-like receptors, bind to damage-associated molecular patterns (DAMPs) which are the molecules released from damaged cells. Subsequently, these signal transduction pathways affect to transduction and production of pro-inflammatory cytokines, for example IL-1β, IL-6, IL-8, and TNF-α (112), leading to leukocyte proliferation and activation, activation of the complement system, and upregulation of endothelial adhesion molecules and chemokines productions. Many reports suggest that the pathophysiology of sepsis and septic shock involves macrophages, which are outstanding cells and have a potential role at the beginning of the sepsis-induced cascade of inflammatory cytokines. In addition, that cell also produces nitric oxide (NO) in response to these cytokines, which can mediate cytotoxic effects (113-116).

4.3 The impact of macrophages associated sepsis

Macrophages play the most important role in sepsis, which influence immunological homeostasis and inflammatory activities through an imbalance between M1 and M2 macrophages is also another factor that can induce the occurrence and development of sepsis (114). Briefly, pro-inflammatory M1 macrophages, for instance, IFN-γ, TNF-α, IL-1, and NO, infiltrate into the

infectious site, and they can detect products of microorganisms via TLRs and other PRRs that bind specifically to different pathogen components. Then, they produce pro-inflammatory cytokines and chemokines to recruit and activate other immune cells at the site of infection, which leads to inflammatory diseases (sepsis and other inflammatory diseases). In the late stage of sepsis, M2 macrophages play a protective role to prevent septic shock via producing large quantities of anti-inflammatory mediators, such as IL-10, interleukin-11 (IL-11), IL-13, and TGF-β produced for recover or control an inflammation (117, 118). However, severe sepsis may be the important cause of incomplete polarization towards the M2 phenotype. The lack of M2 chemokine expressions in septic monocytes and macrophages, together with the M2 shift in cytokines and marker enzymes, may be connected to immunosuppression with higher secondary infection following sepsis (119).

This study elucidates that macrophage depletion enhances gut microbiota pattern change (gut dysbiosis) and worsens sepsis severity in cecal ligation and puncture mouse models via gut fungi support pathogenic bacteria abundance. Consequently, this study performed CLP to induce polymicrobial abdominal sepsis on clodronate-liposome administration C57BL/6 mice and investigated the effects of macrophage depletion influencing sepsis severity via gut dysbiosis to test this hypothesis.

CHAPTER IV
MATERIALS AND METHODS

1. Animal

The Institutional Animal Care and Use Committee of the Faculty of Medicine, Chulalongkorn University, Bangkok, Thailand followed by the National Institutes of Health's (NIH) animal care and use procedure approved the animal study under the approval number 035/2565. Male C57BL/6 mice aged 8 weeks, weighing 20-25 g, were purchased from Nomura Siam International, Pathumwan, Bangkok, Thailand. Mice were housed in a controlled-temperature environment (24 ± 2°C) with 50% of relative humidity and a 12-h light-dark cycle (light from 7:00 a.m. to 7:00 p.m.). Mice were maintained with a standard diet and water during the experiment.

2. Clodronate induced *in vivo* macrophage depletion and CLP-sepsis model

Liposomes and clodronate-liposomes, concentration 5 mg/mL, (Encapsula NanoSciences LLC, Tennessee, USA) were used for macrophage depletion according to the previous report (13). Animals were randomly divided into four groups (n = 10/group), containing i) mice were intravenously (i.v.) injected with 200 µL/mouse of liposome every two days for one week and acted as the control, ii) mice were i.v. administrated with 200 µL of clodronate-liposome every two days for one week, iii) mice were i.v. injected with 200 µL/mouse of liposome every two days for one week followed by cecal ligation puncture (CLP), and iv) mice were i.v. administrated with 200 µL of clodronate-liposome every two days for one week followed by CLP (Figure 10). In short, the cecum was ligated at 12 mm from cecum tip, then puncture twice with 21G needle, and gently pushed to express a little amount of feces before placed back into abdominal cavity. At 24 h after CLP, all mice were sacrificed by cardiac puncture under isoflurane anesthesia

for sample collection (blood, internal organs, and feces) for evaluation of macrophage depletion-associated biomarkers as follows.
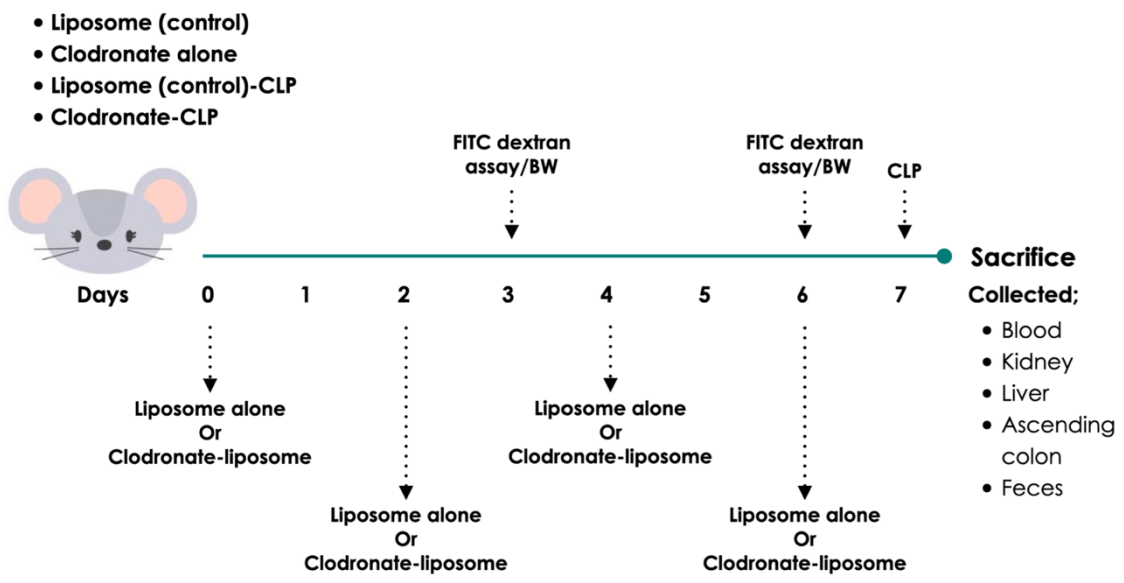
Figure 10 Experimental timeline (*in vivo* study)

Clodronate-liposome administration with and without CLP mouse models.

2.1 Evaluation of macrophage depletion-associated parameters in serum

2.1a) Intestinal permeability

To detect leaky gut, animals were intragastrically administrated with 25 mg/mL of fluorescein isothiocyanate–dextran (FITC-dextran) every three days. After 3 h of oral administration, mouse serums were diluted with an equal amount of sterile 1X phosphate-buffered saline (1X PBS; pH 7.4) and the concentration of FitC-dextran in serum was quantified by fluorospectrometer using an excitation wavelength of 485 nm and an emission wavelength of 528 nm. The concentration of FitC-dextran was serial diluted as the standard.

2.1b) Measurement of pro- and anti-inflammatory cytokines

Enzyme-linked immunosorbent assay (ELISA; Invitrogen, USA) was used for determination the amount of pro-inflammatory cytokines (IL-6 and TNF-α) and anti-inflammatory cytokine (IL-10) in serum. Briefly, a capture antibody was diluted with 1X coating buffer and coated on a 96-well plate at 4°C for overnight. Then, the antibody-coated plate was washed with washing buffer (1X PBS, pH 7.4, containing 0.05% Tween-20) for three times, blocked with 1X ELISA/ELISPOT for 1 h at room temperature, and washed gently with washing buffer, respectively. Subsequently, samples were added to each well of the ELISA plate and incubated at room temperature for 2 h and triply washed with washing buffer. To detect an interesting cytokine, a detection antibody was added to the ELISA plate for 1 h at room temperature and washed with wash buffer for 3 times. Then, the ELISA plate was added with horseradish peroxidase (HRP), incubated at room temperature for 30 min, and triply washed with a washing buffer. To visualize the reaction, 1X tetramethylbenzidine (TMB) substrate was added to detect a cytokine, incubated at room temperature for 15 min in the dark, and added 2N H_2SO_4 was to stop the reaction. Pro- and anti-inflammatory cytokines were quantified by spectrophotometer at a wavelength of excitation at 450 nm and those of emission at 570 nm.

2.1c) Serum creatinine assay

QuantiChrom Creatinine Assay kit (BioAssay, USA) was used for determination the kidney injury according to the manufacturer instruction. In brief, 200 μL of mixed working reagents A and B were immediately added and mixed into each well containing 30 μL of diluted serum in a clear-bottomed 96-well plate. The optical density at the absorbance of 510 nm was quickly determined by spectrophotometer using the standard

creatinine as the baseline. The amount of creatinine in serum should be more than 0.3 mg/dL.

2.1d) Alanine transaminase assay

One of the signals of liver injury is the activity of alanine transaminase (ALT). According to EnzyChrom ALT assay (BioAssay, USA), 20 µL of each sample was added into the working reagent containing 200 µL of assay buffer, 5 µL of co-substrate, 1 µL of lactate dehydrogenase (LDH), and 4 µL of reconstituted NADH. The detected plate was immediately tapped to mix the reaction and incubated at room temperature. The kinetics of alanine transaminase were determined with the rate of NADH consumption by the absorbance at a wavelength of 340 nm after incubation at 5 and at 10 min, respectively. The average normal range of ALT kinetics is 24 U/L.

2.1e) Microorganism enumeration

To examine bacteremia and fungemia in macrophage-depleted mice, 100 µL of blood was directly plated onto blood agar and Sabouraud dextrose agar (SDA; Oxoid, UK) and overnight incubated at 37°C. After incubation, the colonies on each plate were counted and identified species by amplification of *16S rRNA* gene and internal transcribed spacer (ITS) using the BLAST-based tool (https://blast.ncbi.nlm.nih.gov).

2.2 Determination of macrophage depletion-associated parameters in tissue
2.2a) Tissue analysis by Hematoxylin and eosin (H&E) staining

Macrophage-depleted livers, kidneys, and ascending colons were preserved in 10% paraformaldehyde and embedded in paraffin. The samples were sectioned at the thickness of 5 µM and stained with Hematoxylin and eosin (H&E; Sigma-Aldrich, USA) according to the standard protocol. All images were snapped using an inverted

microscope (Olympus, IX81) at 200× magnification in 10 randomly selected areas. Kidney damage scores were determined by immune cell infiltration in scores 0 to 4, including, 0; no damage, 1; 0-25% immune cell infiltration, 2; 25-50% immune cell infiltration, 3; 50-75% immune cell infiltration, and 4; 75-100% immune cell infiltration. Liver damage, inflammation and necrosis were used as the common marker of liver injury, which was reported as the total of the individual scores ranged from 0 (no finding) to 1 (mild), 2 (moderate), and 3 (severe) (120). Ascending colon damage scores were evaluated based on the Geboes Score (GS) (1 2 1). This is a comprehensive grading system that examines erosions or ulcerations, immune cell infiltration, structural alterations, and crypt degradation. The scores ranged from 0-5, including 0 (No abnormality), 1-2 (immune cell infiltrate in the lamina propria), 3 (immune cell infiltrate in the epithelium), 4 (crypt destruction), and 5 (erosion or ulceration/severe).

2.2b) Immunohistochemistry

To determine whether macrophage was completely depleted from internal tissues, F4/80 (ab6640, Abcam, Cambridge, UK) and Arg1 (GeneTex, GTX113131, Irvine, California, USA) were used for macrophage detection by immunohistochemistry staining. All images were visualized by an inverted microscope (Olympus) using two blinded observations at 200× magnification.

2.2c) Immunofluorescence

Internal organs were prepared in Tissue-Tek O.C.T compound (Sakura Finetek, CA, USA), sliced at the thickness of 5 μM, and detected with mouse F4/80 antibody to evaluate the depletion of macrophages. The samples were fixed with cold acetone for 10 min at room temperature, then washed with 1X Tris-Buffered Saline (1X TBS; pH 7.2) buffer containing 0.05% Tween-20 before being permeabilized with 0.1% of Triton X-100

(Sigma Aldrich) for 1 min at room temperature. The fixed samples were blocked a nonspecific binding using 2% bovine serum albumin (BSA; Sigma-Aldrich, USA) in 1X TBS, pH 7.2, for 1 h at room temperature. Then, the samples were incubated at 4°C overnight with primary F4/80 antibody at the dilution of 1:1,000 and triply washed with 1X TBS, pH 7.2, containing 0.05% Tween-20. To visualize the macrophage marker, Alexa Fluor® 488 goat anti-rabbit IgG (ab150077, Abcam, Cambridge, UK) was added onto the tissue slides and incubated at room temperature in the dark for 1 h and washed with 1X TBS, pH 7.2, containing 0.05% Tween-20 for three times to remove any unbound antibodies. Finally, a nuclear cell was stained with 4′,6-diamidino-2-phenylindole (DAPI; Sigma Aldrich) for 10 min at room temperature, washed with wash buffer, and increased fluorophore photostability by prolong antifade mountant (Prolong, Life Technologies, Way Carlsbad, CA 92008, USA), respectively. The fluorescent images were captured using ZEISS LSM 800 Airyscan confocal laser scanning microscope at 63× magnification (Zeiss, Jena, Germany).

2.2d) Cytokine quantification

Kidney and liver were collected to measure the immune responses (multiple organs inflammation), pro- and anti-inflammatory cytokines were determined by ELISA (Invitrogen, USA). All samples were homogenized by sonication under the condition of pulse on for 20 sec, and pulse off for 5 sec, with on ice for 45 sec (Sonics Vibra Cell, VCX 750, Sonics & Materials Inc., Newtown, CT, USA). The lyzed samples were centrifugated and collected for measuring the amount of TNF-α, IL-6, and IL-10 cytokines as mentioned above.

2.3 Evaluation of macrophage depletion-associated parameters in feces

2.3a) DNA extraction and sequencing

To investigate the differentiation of microbiome patterns, 0.3 g of each mouse feces was collected for the gut microbiome analysis following a previous report (122). In brief, mouse feces were homogenized by lysis buffer at 65°C for 3 h, digested using a mechanical bead beater for 20 min with 15 frequency/sec, and the metagenomic DNA was extracted with Phenol: Chloroform method as previously described (123). The purified metagenomic DNA was used as the template for the amplification of the V3-V4 region of the *16S rRNA*-encoding gene and the ITS region. Both the *16S rRNA* and ITS were sequenced by the Illumina Miseq sequencing platform (Illumina, San Diego, CA, USA) using the universal prokaryotic 16S primers, 515F (forward: 5'-GTGCCAGCMGCCGCGGTAA-3' and 806R reverse: 5'-GGACTACHVGGGTWTCTAAT-3'), with the Illumina adapter and Golay barcode sequences for *16S rRNA* gene V4 library construction bacteriome sequencing and the universal eukaryotic primers, ITS1 (forward: 5'-TTCGTAGGTGAACCTGCGG-3' and ITS4 reverse; 5'-TCCTCCGCTTATTGATATGC-3') were used for gut mycobiome identification. The raw sequences and operational taxonomic unit (OTU) of bacteria were classified following Mothur's standard operating platform, whereas the fungal DNA library was sequenced using the Miseq system (Illumina) at Omics Sciences and Bioinformatics Center, Chulalongkorn University. Forward and reverse primers were removed from raw sequences using cutadapt v 1.18. and trimmomatic v 0.39 with the sliding window option to trim individual sequences where the average quality scores less than 15 across 4 base pairs. The amplicon sequence variants (ASVs) were analyzed by the QIIME2 plugin DADA2 pipeline software for the identification of the composition of fungi in fecal samples without unclassified phylum or higher fungal classification. The fungal classification was analyzed using the BLAST-based tool (https://blast.ncbi.nlm.nih.gov)

(122). In addition, the mouse fecal-detected *16S rRNA* and ITS1/4 sequences were deposited in the NCBI database with accession number PRJNA765503.

3. Interaction between fungal molecules and bacteria that induce a bacterial abundance

3.1 Microorganism isolation from murine blood

K. pneumoniae, E. faecalis, and *Acinetobacter radioresistens* (*A. radioresistens*) that were isolated from the blood of the clodronate administrated mice were cultured in Tryptic Soy Broth (TSB; HiMedia, Mumbai, Maharashtra, India) at $37°C$ under aerobic conditions for 24 h, and adjusted the turbidity of $1 × 10^9$ cells/mL to use for functional assays. For fungal isolation, clodronate-liposome blood isolated *C. pintolopesii* was inoculated into Sabouraud dextrose broth (SDB; Oxoid, UK) and incubated at $35°C$ for 18 h. An overnight fungal culture was heat-killed with incubation at $60°C$ for 1 h and lyzed cell using sonication to evaluate the effect of the fungal molecule against bacterial growth.

3.2 *Candida* yeast cells and Beta-glucan affect a bacterial abundance

To access the interaction of a bacterial abundance among fungal molecules from various *Candida*, including i) clodronate-liposome blood-isolated *C. pintolopesii*, ii) *C. albicans* ATCC 90028 (Microbiologics, Saint Cloud, Minnesota, USA), iii) patient-isolated *C. albicans*, and iv) BG powder at 0.1 and 1 mg/mL were used. The quantitation of $1 × 10^9$ cells/mL of blood-isolated bacteria was co-culture with heat-killed lysate *Candida* or BG at the multiplicity of infection (MOI) of 1, 0.1, and 0.01 under aerobic conditions for 24 h before colony enumeration on TSA plates.

4. Responsiveness of Caco-2 cells against bacterial and fungal molecules

4.1 Human colorectal adenocarcinoma (Caco-2) cells

Human colorectal adenocarcinoma (Caco-2) cells (ATCC HTB-37, USA) were cultured in Dulbecco's Modified Eagle Medium (DMEM, Thermo Fisher Scientific, Waltham, Massachusetts, USA) supplemented with 20% heat-inactivated fetal bovine serum (FBS; Gibco, Carlsbad, CA, USA) and 1% PenStrep at 37°C in a 5% CO_2 incubator. More than 80–90% cell confluency that was visualized by the trypan blue exclusion method was seeded into each well of the 12-well plate and rested overnight in completed DMEM containing 20% FBS and 1% PenStrep at 37°C in a 5% CO_2 incubator.

4.2 The role of enterocyte inflammation

To evaluate the responsiveness of colon epithelial cells against fungal molecules with and without bacterial molecules, the concentration of 1×10^6 cells of Caco-2 was incubated with fungal molecules with and without bacterial molecules, such as i) yeast alone at the MOI of 0.1, ii) bacteria alone at the MOI of 0.01, and iii) yeast together with bacteria at the MOI of 0.1 and 0.01, respectively for 24 h at 37°C with 5% CO_2. Beta-glucan (Megazyme, Bray, Ireland) was used as the specific molecules of *Candida*. The supernatant was used for cytokine measurement of IL-8 using ELISA (Invitrogen, USA) according to the manufacturer's protocol as described above.

5. Statistical analysis

Mean ± standard error (SE) was used for data presentation. The differences between groups were examined for statistical significance by one-way analysis of variance (ANOVA) follow by Tukey's analysis or Student's *t*-test for comparisons of multiple groups or 2 groups, respectively. All statistical analyses were performed with

SPSS 11.5 software (SPSS, IL, USA) and Graph Pad Prism version 7.0 software (La Jolla, CA, USA). A p-value of < 0.05 was considered statistically significant.

CHAPTER V
RESULTS

1. Macrophage depletion

Clodronate-liposome administration is well-known as the gold standard for depleting macrophages in mice. To determine macrophages were depleted by clodronate-liposome administration. Ascending colon was detected the F4/80 (M1 macrophage) by immunofluorescence staining. In addition, immunohistochemistry staining was used to examine both F4/80 and Arginase1 (M2 macrophage) marker in ascending colon and liver. Clodronate-liposome (Clod) treated mice were unable to detect macrophage F4/80 cells, indicating that macrophage was completely depleted in ascending colon when compared to the liposome control group (Lipo) (Figure 11A). Similarly, macrophage F4/80 and Arginase1 markers decreased in both ascending colon and liver when compared with liposome control (Figure 12A-C), demonstrating that clodronate-liposome administration has the effect of a reduction of macrophage cells in internal organs, such as ascending colons and liver.
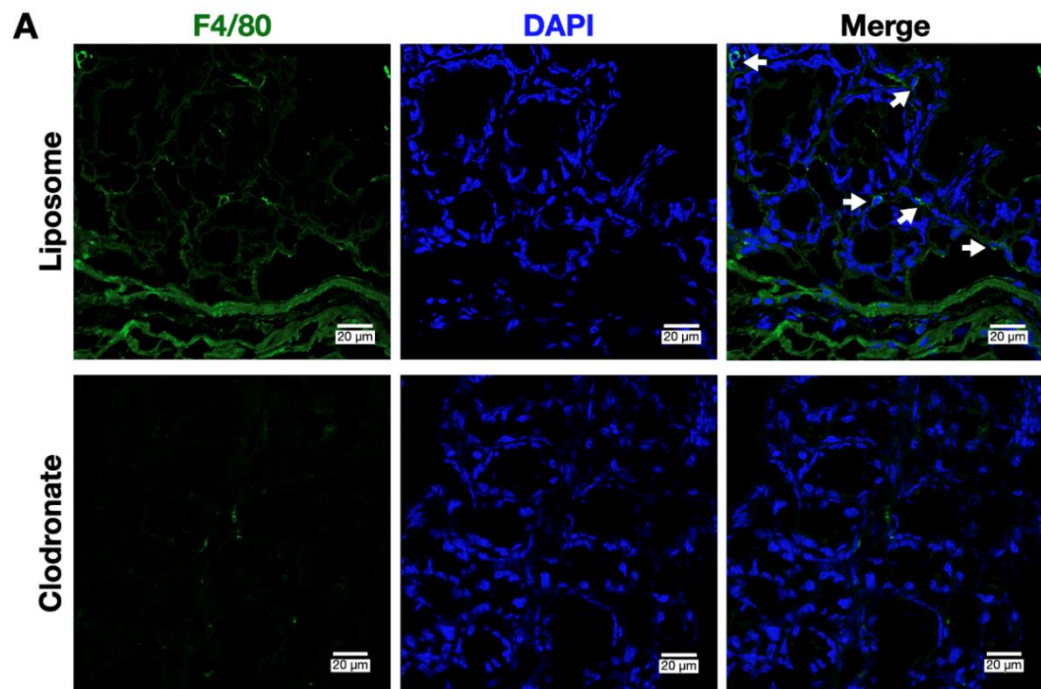
Figure 11 Detection of macrophage depletion in mice

Macrophage depletion was demonstrated by immunofluorescence staining in ascending colon for F4/80 marker (M1 macrophage) (A), (n = 3/group). Lipo; liposome control and Clod; macrophage-depleted control.
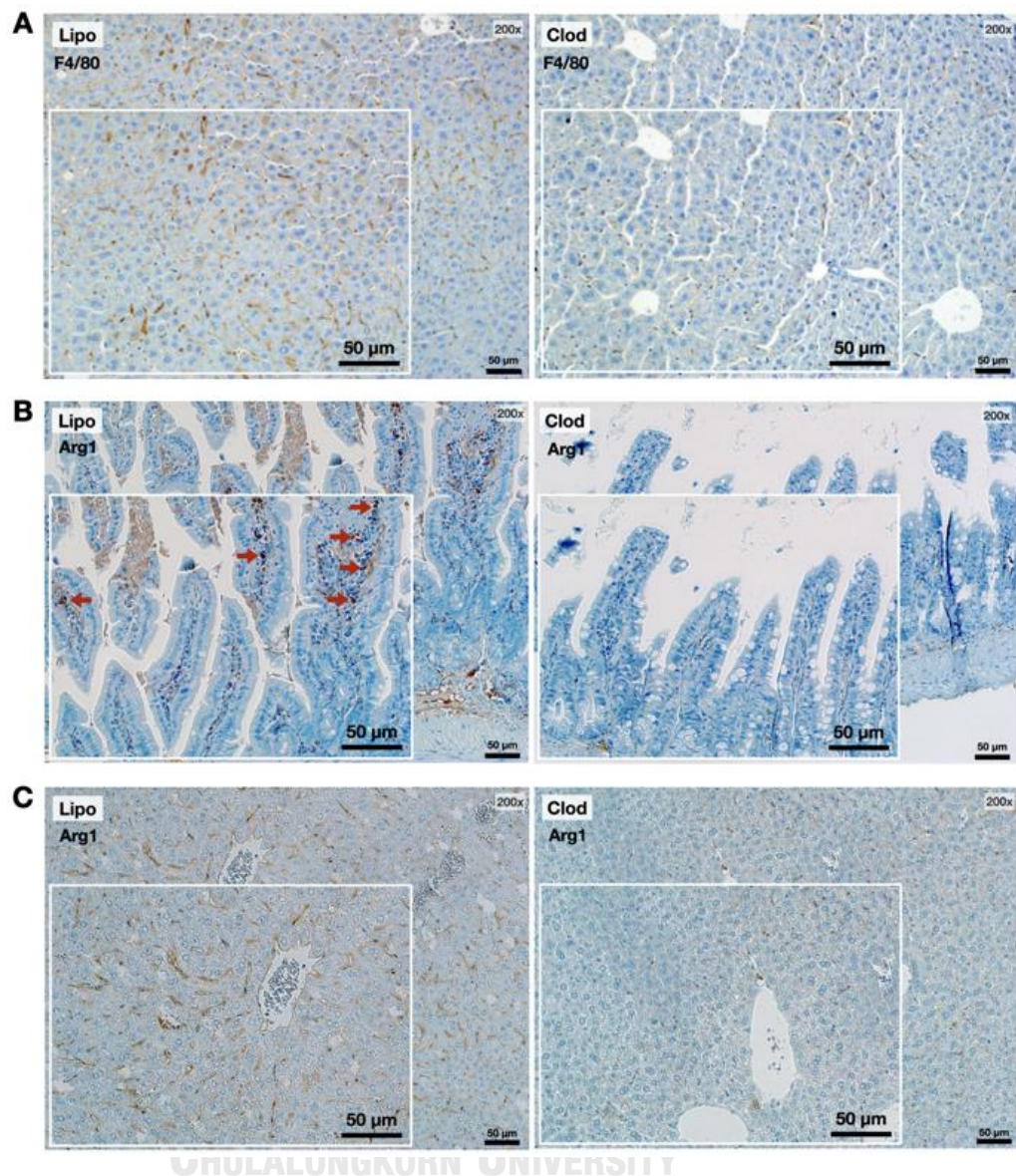
Figure 12 Determination of macrophage depletion

The examination of macrophage depletion was performed by immunohistochemistry staining. The liver was stained for the F4/80 marker (A) and Arginase1 marker (C), whereas the ascending colon was detected for the Arginase1 marker (B), (n = 3/group). Red arrows indicate Arginase1-positive cells in the ascending colon, and the brown color represents F4/80 and/or Arginase1-positive cells. Lipo; liposome control and Clod; macrophage-depleted control.

2. **More severe sepsis-CLP in mice with macrophage depletion, increasing severity and mortality rate**

   To determine the macrophage depletion affects to enhance gut dysbiosis and sepsis severity in CLP mice, the liposome- (Lipo-CLP) and clodronate-liposome mice performed CLP (Clod-CLP) were monitored percent survival and body weight, which are significant indicators for gut dysbiosis. Liposome (Lipo) and clodronate-administrated mice (Clod) were used as the control group. The lowest survival rate was found in sepsis with macrophage-depleted mice (Clod-CLP), followed by sepsis without macrophage-depleted (Lipo-CLP) and macrophage-depleted control (Clod), respectively, in comparison with the liposome control group. In addition, sepsis without macrophage-depleted (Lipo-CLP) and macrophage-depleted control (Clod) have no difference between groups as shown in Figure 12. After administration for 4 days, macrophage-depleted mice were moribund and died at approximately 20%, and more severe after enhanced sepsis as showed 100% of sepsis with macrophage-depleted mice in moribund stage and died on day 8 after the performed experiment (Figure 13A). For detection of body weight, both macrophage-depleted with and without CLP mice slightly decreased within 3 days after administration and significantly decreased on day 6 when compared to liposome administrated with and without CLP mice, while no difference with sepsis without macrophage-depleted mice (Figure 13B).

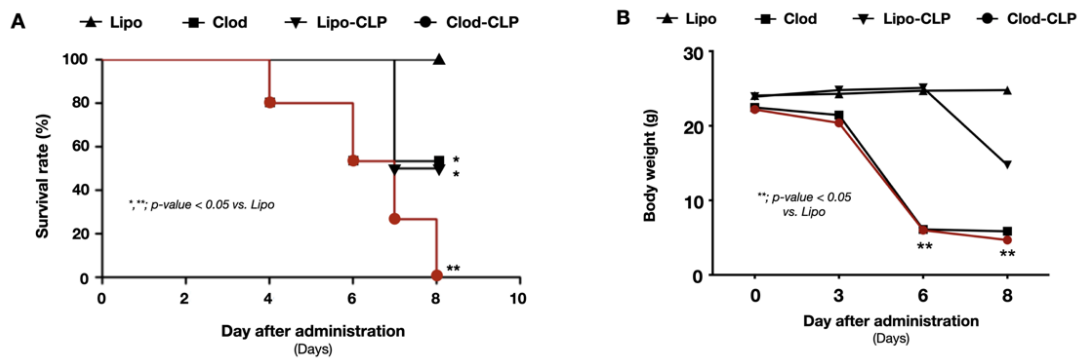**Figure 13** Survival rate and body weight

Survival rate (A) and body weight (B) analysis after macrophage depletion with and without CLP surgery, (n = 10/group). Lipo; liposome control, Clod; clodronate (macrophage-depleted control); Lipo-CLP; sepsis without macrophage-depleted; and Clod-CLP; sepsis with macrophage-depleted (the red line). The data are shown as the mean ± SE, * and **; *p-value < 0.05 vs. Lipo*.

3. **More severe sepsis-CLP in mice with macrophage depletion, an impact of gut permeability defect, and gut translocation**

   a. **Macrophage depletion affects intestinal permeability**

   Determination of gut leakage after macrophage depletion using FitC-dextran assay showed a strong signal of the leaky gut after macrophage depletion for 3 days in the macrophage-depleted group, which was higher than in liposome control without a significant difference (Figure 13A). After 6 days of macrophage depletion, levels of FitC-dextran slightly increased in both experimental groups and significantly higher in the macrophage-depleted group in comparison with the liposome control (Figure 14A). Therefore, macrophage depletion impacts gut leakage, which is possibly one of the important reasons for a moribund stage and death after 3 days of clodronate administration in mice.
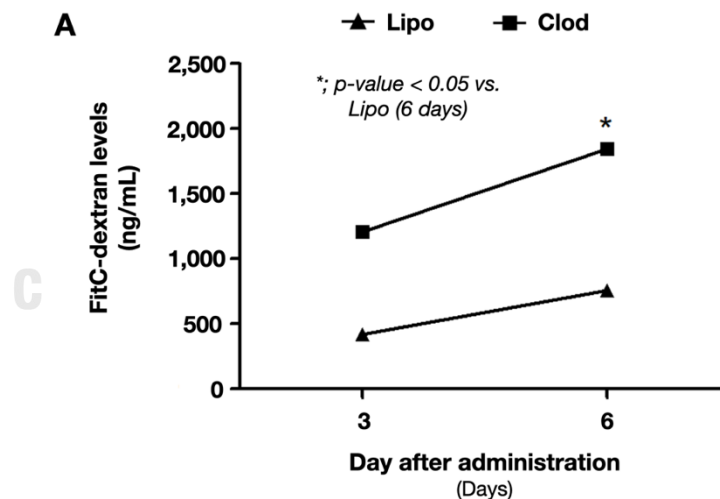
Figure 14 Gut permeability

   Gut permeability using FitC-dextran measurement (A) after macrophage depletion on day 3rd and day 6th in mice, (n = 5/group). The data are shown as the mean ± SE, *; *p-value < 0.05 vs. Lipo* (6 days). Lipo; liposome control, Clod; macrophage-depleted control.

b. Bacteremia and fungemia in macrophage depletion

Evaluation of gut translocation associated with macrophage depletion revealed that bacteremia in the blood of sepsis with macrophage-depleted mice (Clod-CLP) was significantly higher than sepsis without macrophage-depleted (Lipo-CLP) (Figure 15A and B), whereas fungemia in the blood of sepsis without macrophage-depleted mice (Lipo-CLP) did not detect. Bacteremia can detect *K. pneumoniae, E. faecalis, and A. radioresistens*, whereas fungemia performed *C. pintolopesii* that only found in macrophage-depleted mice with and without sepsis (Clod). Consequently, macrophage depletion can enhance uncontrol gut microbes that have effects on the fungal abundance and enhanced microorganisms spread into the bloodstream (Figure 15C and D).
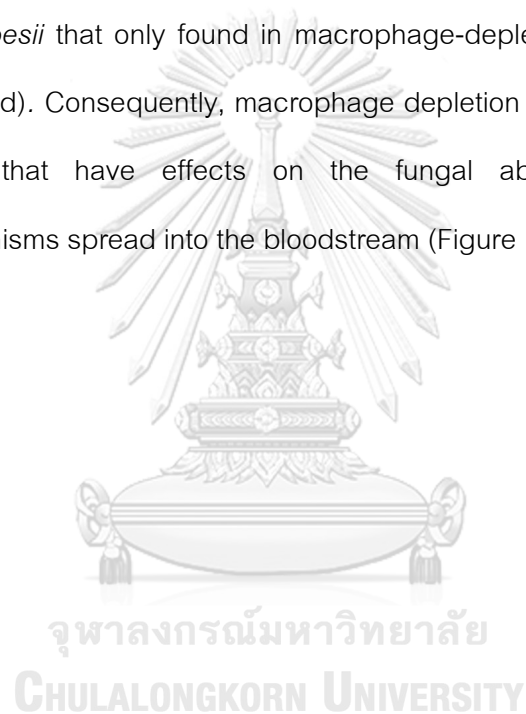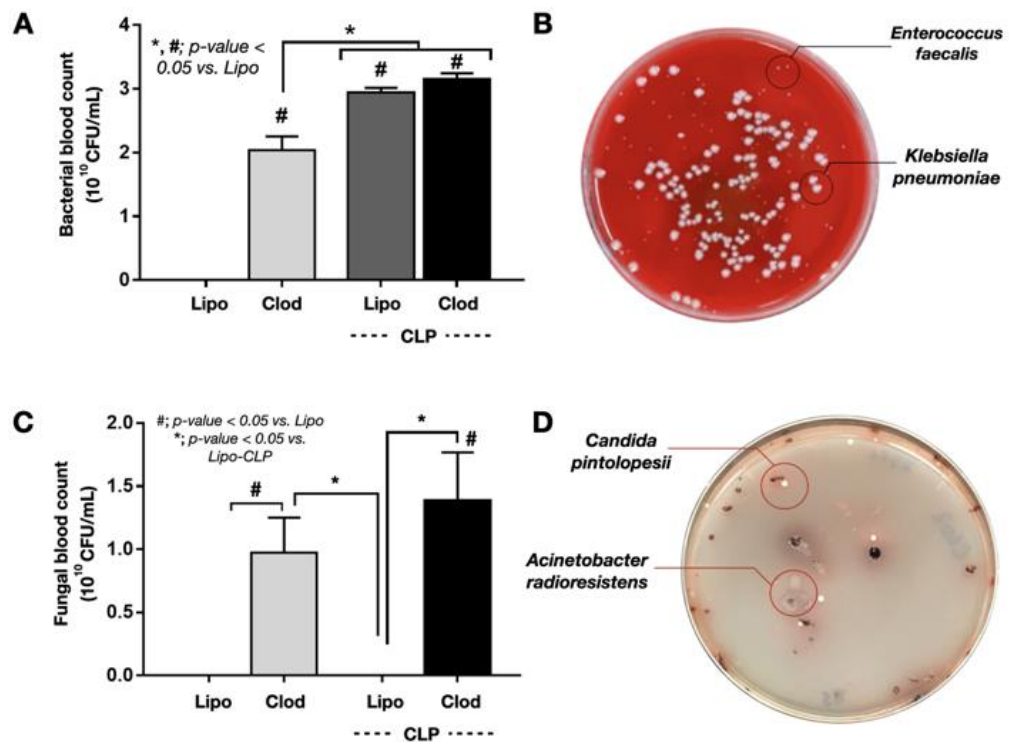
Figure 15 Bacterial and fungal blood count

Gut translocation after macrophage depletion with or without CLP surgery. Bacterial blood count (A), bacterial colonies on Blood agar of Clod group (B), fungal blood count (C), and *C. pintolopesii* colonies on SDA from Clod group (D), (n = 5/group). Lipo; liposome control, Clod; macrophage-depleted control; Lipo-CLP; sepsis without macrophage-depleted; and Clod-CLP; sepsis with macrophage-depleted. The data are shown as the mean ± SE, * and #; *p-value* < *0.05 vs. Lipo or Lipo-CLP.*

c. Enhanced cytokine production in macrophage depletion

The inflammatory responsiveness was examined by analyzing the cytokine production using ELISA after macrophage depletion indicated that pro-inflammatory, TNF-α and IL-6 cytokines, were significantly highest in sepsis with macrophage-depleted mice, followed by sepsis without macrophage-depleted, macrophage-depleted control, and liposome control groups, respectively (Figure 16A and B). For anti-inflammatory cytokines, macrophage-depleted mice with sepsis significantly secreted IL-10 more compared to the others (Figure 16C). In addition, macrophage-depleted control showed a trend to higher than sepsis without macrophage-depleted, but no significant difference.

Figure 16 Measurement of serum cytokine levels

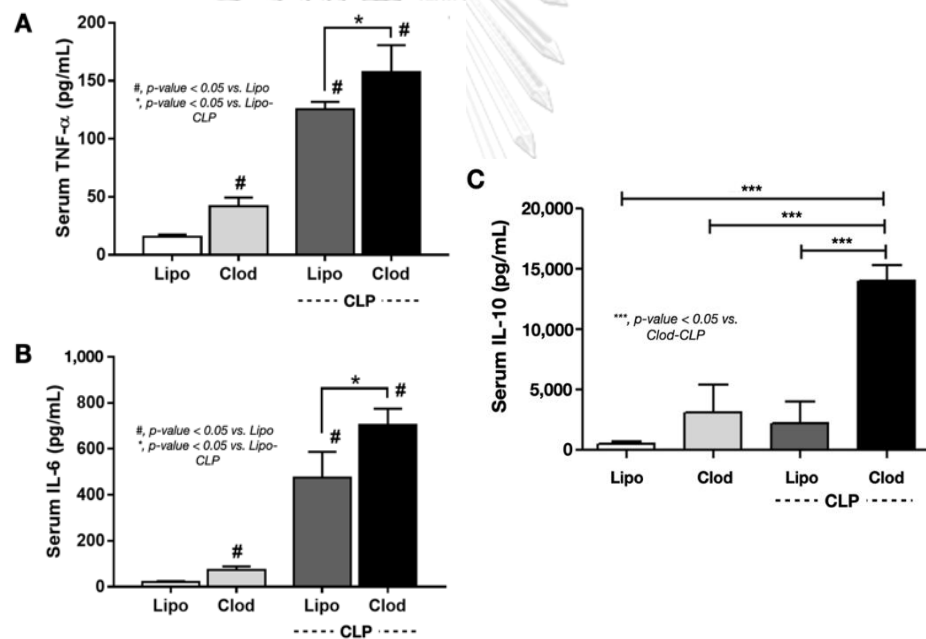Serum TNF-α levels (A), IL-6 levels (B), and IL-10 levels (C), (n = 10/group). Lipo; liposome control, Clod; macrophage-depleted control; Lipo-CLP; sepsis without macrophage-depleted; and Clod-CLP; sepsis with macrophage-depleted. The data are shown as the mean ± SE, #; *p-value < 0.05 vs. Lipo; *; p-value < 0.05 vs. Lipo-CLP, ***; p-value < 0.05 vs. Clod-CLP.*

d. Injury of kidney and liver in macrophage depletion

Serum creatinine (SCr) and serum alanine transaminase (ALT) are the important biomarkers for evaluation of the damage to the kidney and liver, respectively, which found that sepsis with macrophage-depleted mice significantly had the highest of both serum SCr and ALT levels in comparison with other groups (Figure 17A and B). Although sepsis without macrophage-depleted mice presented higher SCr and ALT levels than in the macrophage-depleted control and liposome control groups, a significant difference did not detect. Moreover, macrophage-depleted control and liposome control mice showed no difference between groups. Hence, sepsis with macrophage-depleted mice was associated with more kidney and liver injury, which is the cause of sepsis severity.
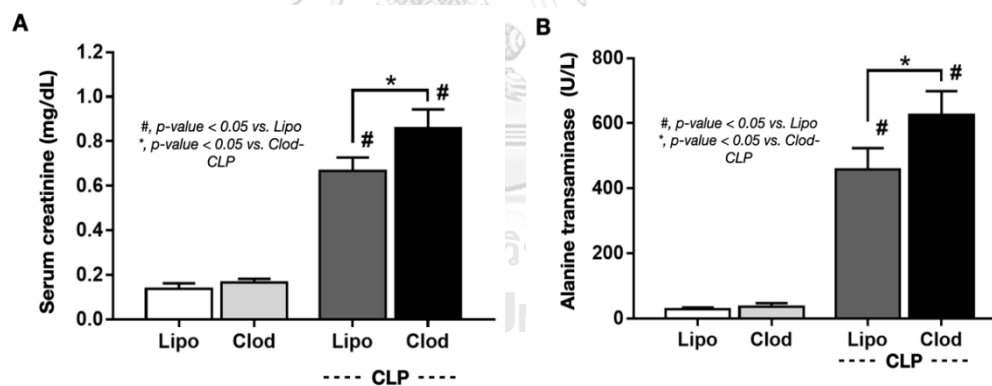
Figure 17 Serum creatinine (SCr) and alanine aminotransferase (ALT)

Quantification of serum SCr (A) and ALT (B). To indicate sepsis severity after macrophage depletion and performed CLP surgery, (n = 10/group). Lipo; liposome control, Clod; macrophage-depleted control; Lipo-CLP; sepsis without macrophage-depleted; and Clod-CLP; sepsis with macrophage-depleted. The data are shown as the mean ± SE, *; p-value < 0.05 vs. Clod-CL; P#; p-value < 0.05 vs. Lipo.

4. More severe sepsis-CLP with macrophage depletion, an impact of tissue inflammation

    a. Responsiveness of kidney in sepsis-CLP with macrophage depletion

Pathology of the kidney after macrophage depletion with and without sepsis demonstrated that macrophage-depleted combined with sepsis-CLP has the highest kidney damage as strong interstitial inflammatory cells, glomerular atrophy, degeneration, tubular necrosis, and vacuolation of renal tubules (Figure 18A), whereas macrophage-depleted control and sepsis without macrophage-depleted groups exhibited mild tissue inflammation as proximal and distal tubular necrosis and sloughing of tubular epithelial cells when compared with mice treated with liposome control, acted as the normal histological structures of the glomerulus, proximal convoluted tubules, and distal convoluted tubules.

Figure 18 Histological of kidney

Histological analysis using H&E staining of the kidney at a magnification of 200× (A), (n = 5/group). Lipo; liposome control, Clod; macrophage-depleted; Lipo-CLP; sepsis without macrophage-depleted; and Clod-CLP; sepsis with macrophage-depleted.

In terms of kidney cytokine production, macrophage-depleted combined with sepsis mice were significantly the highest in both pro- and anti-inflammatory cytokine productions. Moreover, sepsis without macrophage-depleted and liposome control groups showed that kidney IL-10 cytokine was significantly higher than in the macrophage-depleted without sepsis group (Figure 19A-C).
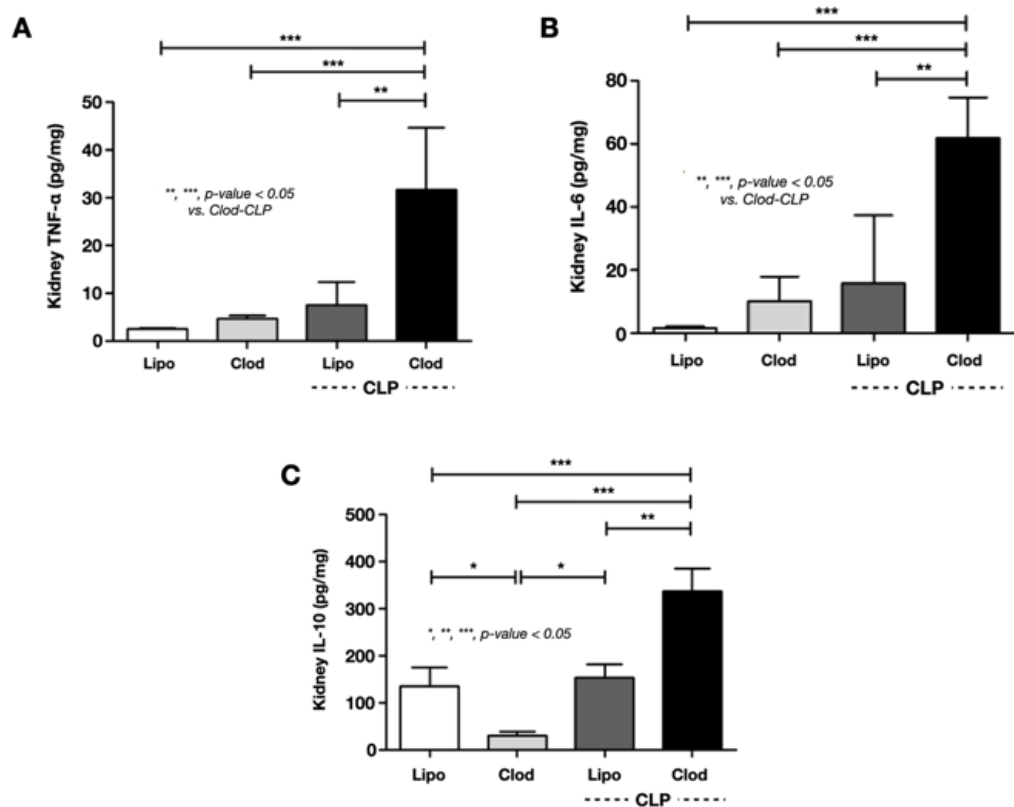
Figure 19 Production of kidney cytokines

Production of kidney cytokines containing TNF-α levels (A), IL-6 levels (B), and IL-10 levels (C), (n = 10/group). Lipo; liposome control, Clod; macrophage-depleted control; Lipo-CLP; sepsis without macrophage-depleted; and Clod-CLP; sepsis with macrophage-depleted. The data are shown as the mean ± SE, *, **, and ***; p-value < 0.05.

b. **Responsiveness of liver in sepsis-CLP with macrophage depletion**

The macrophage-depleted sepsis mice showed severe liver damage as more infiltration of inflammatory cells and necrotic cells (Figure 20A), whereas the macrophage-depleted control and sepsis without macrophage-depleted mice presented moderate hepatic centrilobular mononuclear cell infiltrations and foci of necrosis of the liver cells using liver liposome control mice acted as the normal structure of hepatocytes, sinusoids, and nucleus, which surround the central vein.
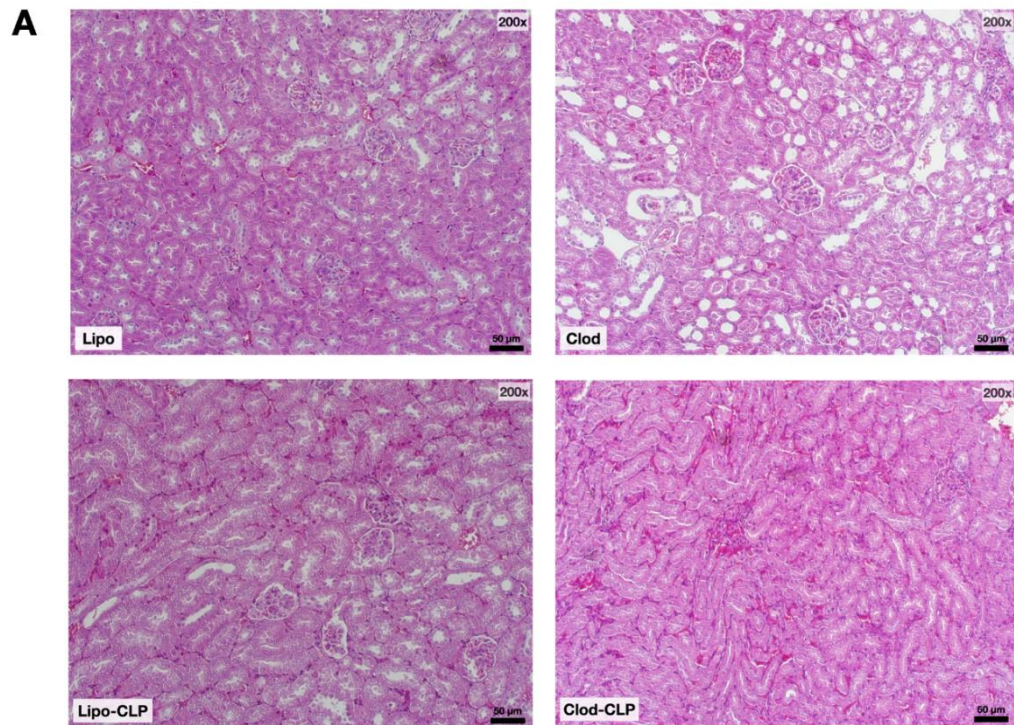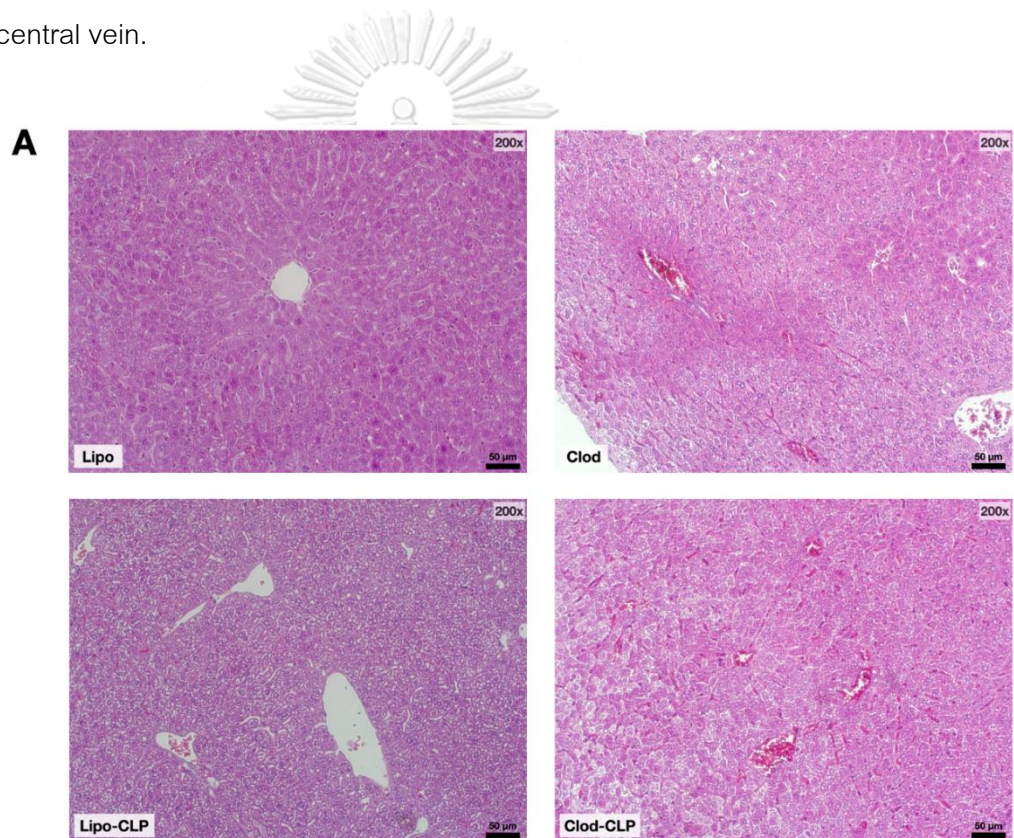

Figure 20 Histological of liver

Histological analysis using H&E staining of the liver at a magnification of 200× (A), (n = 5/group). Lipo; liposome control, Clod; macrophage-depleted; Lipo-CLP; sepsis without macrophage-depleted; and Clod-CLP; sepsis with macrophage-depleted.

Furthermore, the liver cytokines indicated that sepsis with macrophage-depleted has significantly the highest quantification of TNF-α and IL-6, in contrast to IL-10 cytokine. Liver TNF-α levels in the macrophage-depleted control showed significant inflammation more than in the liposome control, but no significant difference with the sepsis without the macrophage-depleted group. While liver IL-10 showed no differences among groups (Figure 21A-C).
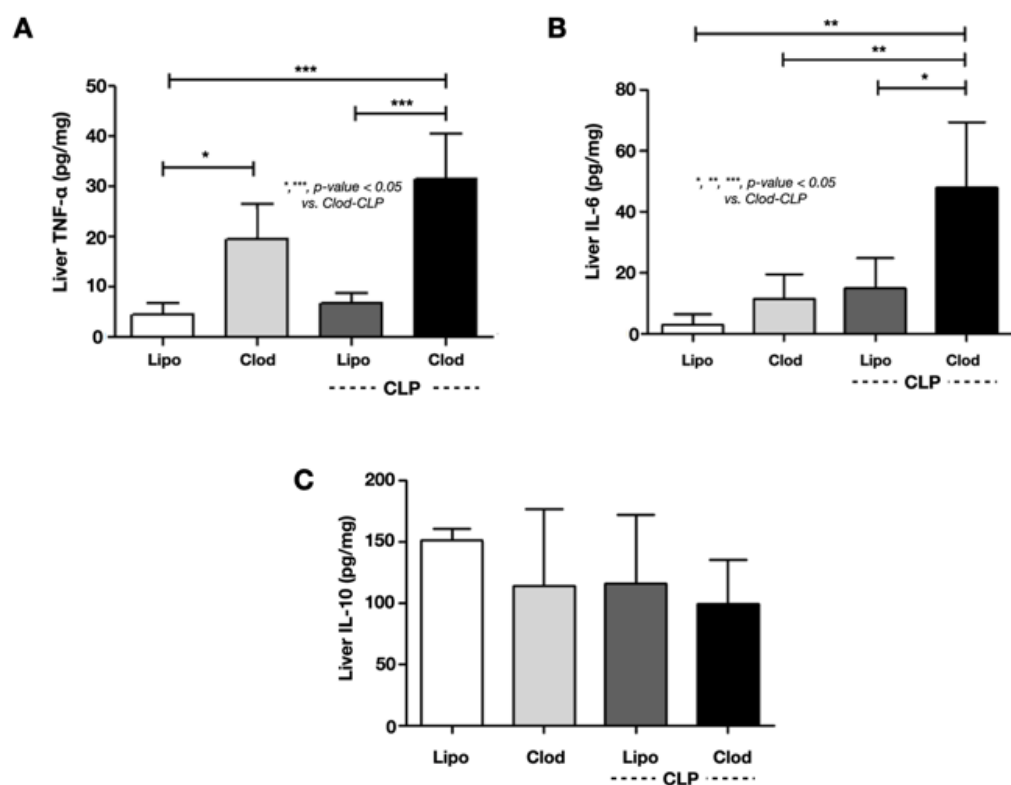
Figure 21 Characteristics of liver cytokines

The characteristics of liver cytokines analysis after macrophage depletion and performed CLP surgery. Liver TNF-α levels (A), Liver IL-6 levels (B), and Liver IL-10 levels (C), *(n = 10/group)*. Lipo; liposome control, Clod; macrophage-depleted control; Lipo-CLP; sepsis without macrophage-depleted; and Clod-CLP; sepsis with macrophage-depleted. The data are shown as the mean ± SE, *, **, and ***; p-value < 0.05 vs. Clod-CLP.*

c. **Pathology of ascending colon in sepsis-CLP with macrophage depletion**

The progression was more severe in the macrophage-depleted sepsis group, demonstrating mucosal degradation, the highest inflammatory cell infiltration, thickening of the intestinal wall, and ulceration (Figure 22A). Then, clodronate-liposome administration together with enhanced sepsis showed more inflammation that might be resulted from the reduction in peripheral blood monocytes, but not other leukocytes or erythrocytes, which causing of more severe sepsis as shown by immune cell infiltrations, abnormal cell structure, and necrosis. In addition, macrophage-depleted control and sepsis without macrophage-depleted mice exhibited few immune cell infiltrations at the laminar propria.
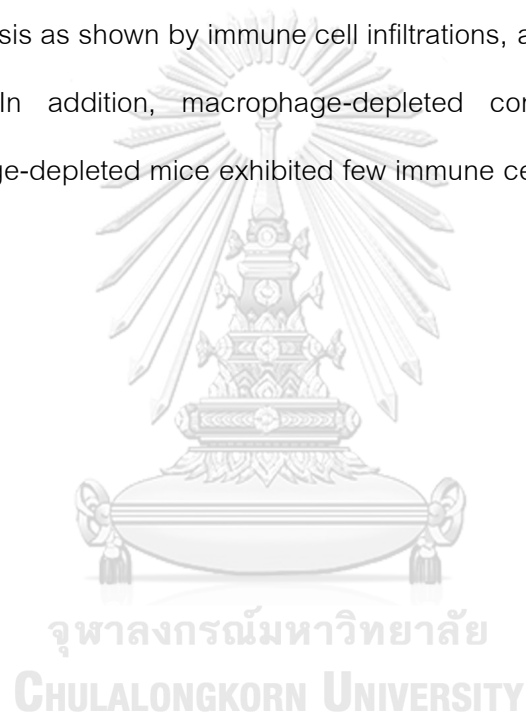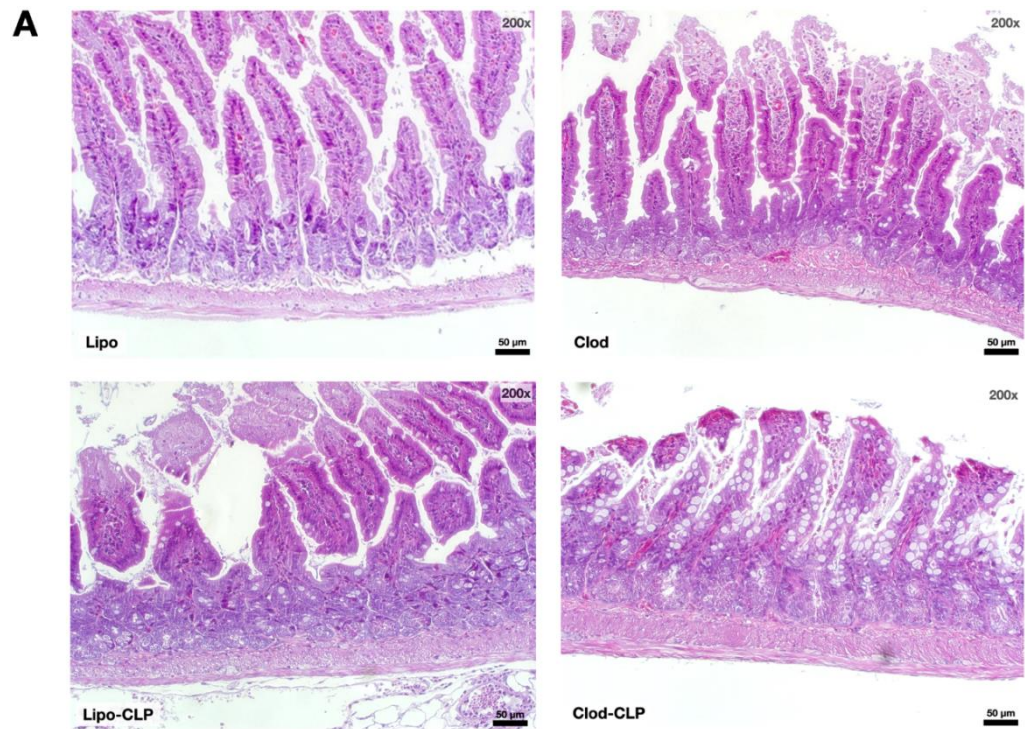
Figure 22 Histopathological of ascending colon

Histopathological examination using H&E staining of the ascending colon at a magnification of 200× (A), (n = 5/group). Lipo; liposome control, Clod; macrophage-depleted; Lipo-CLP; sepsis without macrophage-depleted; and Clod-CLP; sepsis with macrophage-depleted.

5. The association between sepsis-CLP in mice with macrophage depletion and gut dysbiosis

5.1 Gut mycobiome dysbiosis in macrophage depletion

Differentiation of gut mycobiome dysbiosis after macrophage depletion were evaluated by microbiome analysis using ITS sequence mouse feces as the sample. Fecal mycobiome sequences of macrophage-depleted (non-sepsis) mice presented phylum Ascomycota, order Saccharomycetales and Hypocreales (Figure 23A, B, and 24A), family Debaryomycetaceae and Stachybotryaceae, and genus *Mycothecium* spp., *Debaryomyce* spp., *Cladosporium* spp., and *Talaromyces* spp. (Figure 23C, D, and 24B-E) were significantly enhanced when compared to the other groups. Similarly, the alpha diversity (Shannon), which observed total operational taxonomic units (OTUs; the cluster of similar sequence variants of the marker gene sequence), and beta diversity (Bray-Curtis) were mostly raised in comparison to the non-macrophage depleted (both sepsis and non-sepsis) group (Figure 25A-C). These results confirmed the elevation of fecal fungal abundance in macrophage-depleted mice, which was clearly different from control as the separated 2 groups of data in beta diversity analysis, especially for the Ascomycota group (a group that includes *Candida* spp.) and observed OTUs and fecal culture (Figure 15C and D). While gut mycobiome was significantly decreased by enhanced sepsis in macrophage-depleted mice compared with macrophage-depleted control.
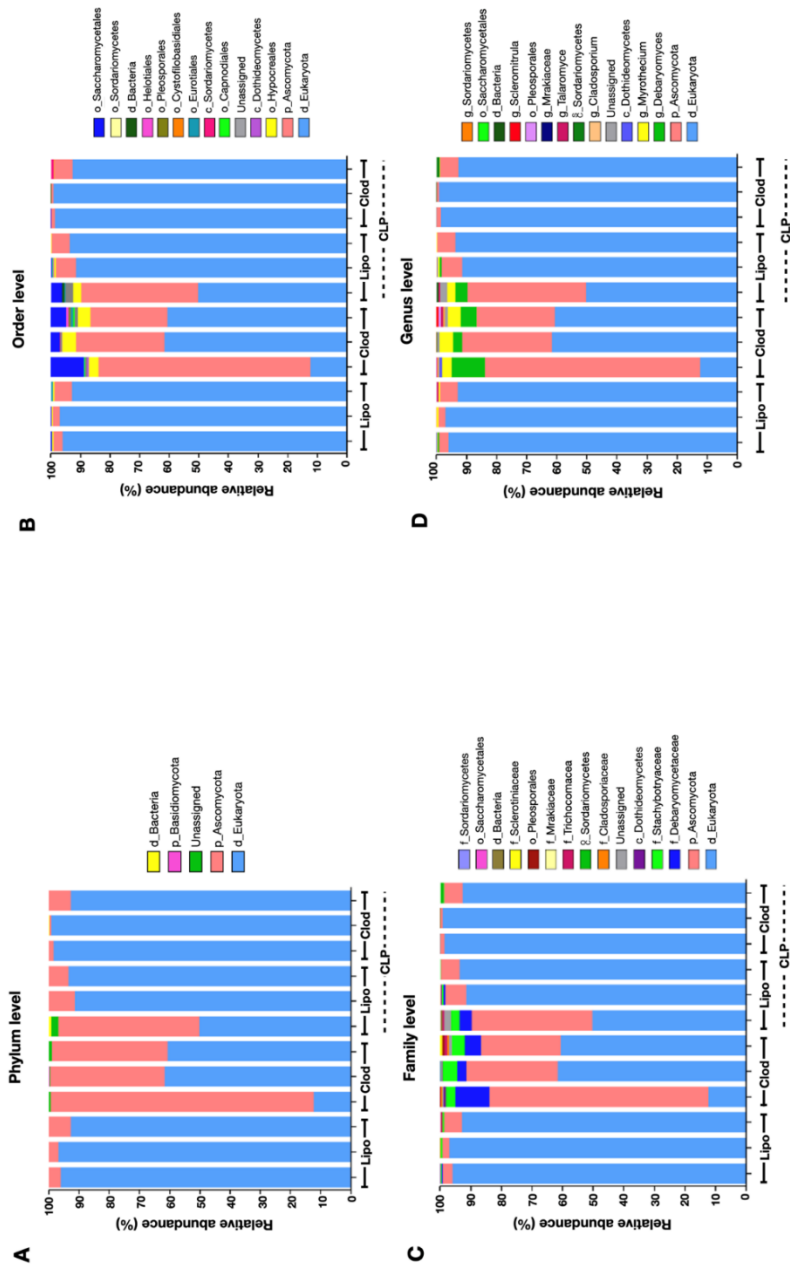
Figure 23 The fungal microbiome (mycobiome) analysis

Mycobiome analysis from feces of mice with liposome control and clodronate-liposome administration with or without sepsis as indicated by the relative abundance in the phylum (A), order (B), family (C), and genus (D) levels were demonstrated, *(n = 3/group)*. Lipo; liposome control, Clod; macrophage-depleted control; Lipo-CLP; sepsis without macrophage-depleted; and Clod-CLP; sepsis with macrophage-depleted.

Figure 24 The relative abundance of mycobiome analysis

The relative abundance of phylum Ascomycota (A), *Myrothecium* spp. (B), *Debraryomyces* spp. (C), *Cladosporium spp.* (D), and *Talaromyces* spp. (E) were demonstrated, (n = 3/group). Lipo; liposome control, Clod; macrophage-depleted control; Lipo-CLP; sepsis without macrophage-depleted; and Clod-CLP; sepsis with macrophage-depleted. The data are shown as the mean ± SE, *; *p-value < 0.05.*
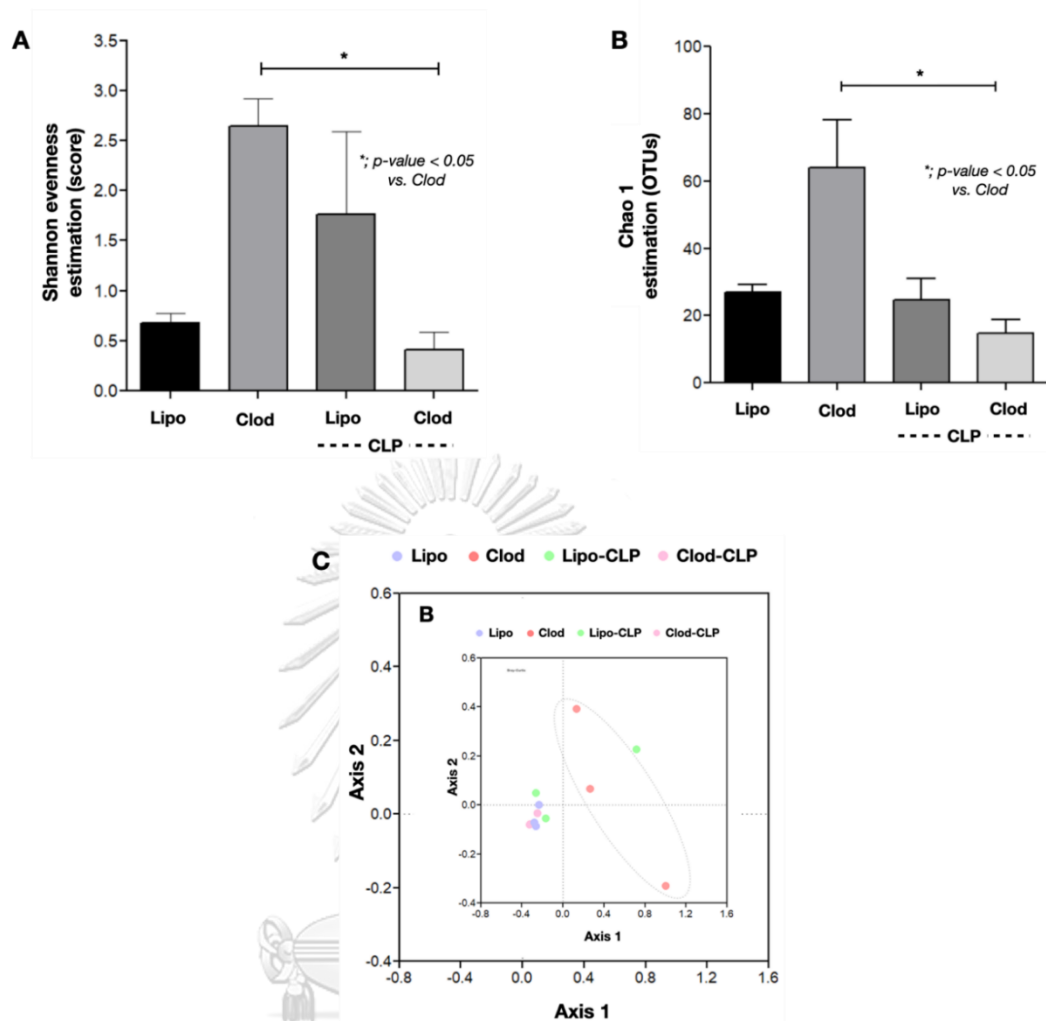
Figure 25 The fungal alpha and beta diversity

Mycobiome analysis from feces of mice with liposome control and clodronate-liposome administration with or without sepsis as indicated by alpha diversity (Shannon) (A), observed total operational taxonomic units (Chao 1) (OTUs) (B), and beta diversity (Bray Curtis) (C) were demonstrated, (n = 3/group). Lipo; liposome control, Clod; macrophage-depleted control; Lipo-CLP; sepsis without macrophage-depleted; and Clod-CLP; sepsis with macrophage-depleted. The data are shown as the mean ± SE, *; *p-value < 0.05.*

5.2 Gut bacteriome dysbiosis in macrophage depletion

In terms of sepsis with macrophage-depleted mice, fecal bacteriome sequences including phylum Proteobacteria, which associates with pathogenic bacteria, significantly increased, whereas phylum Firmicutes, which is the dominant fecal bacteria in healthy mice, were significantly decreased. While the abundance of phylum Bacteroidota was not different in the macrophage-depleted sepsis mice when compared with sepsis without macrophage-depleted mice (Figure 26A-D). Comparison of with and without sepsis diagrams shown in Figure 26 indicated that sepsis-CLP mice mostly composed of the greater of pathogenic bacteria, including *Enterobacter* spp., *Klebsiella* spp., and *Escherichia-Shigella* spp. (Proteobacteria) (Figure 27A-E). Although there were no differences in the alpha and beta diversity between CLP animals that had macrophage depletion, sepsis without macrophage-depleted mice was a significant difference from liposome control mice (Figure 27F-H).
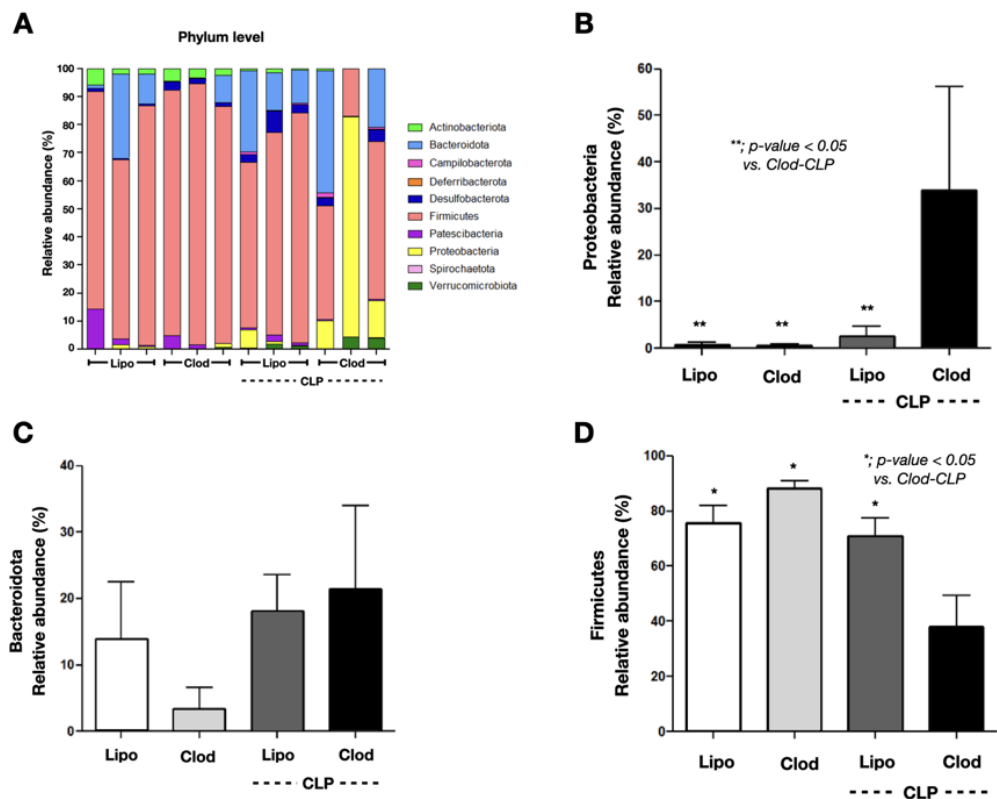
Figure 26 Bacteriome analysis

Bacteriome analysis from feces showed the relative abundance in phylum (A), the abundance of Proteobacteria (B), Bacteroidota (C), and Firmicutes (D), (n = 3/group). Lipo; liposome control, Clod; macrophage-depleted control; Lipo-CLP; sepsis without macrophage-depleted; and Clod-CLP; sepsis with macrophage-depleted. The data are shown as the mean ± SE, *; *p-value < 0.0*
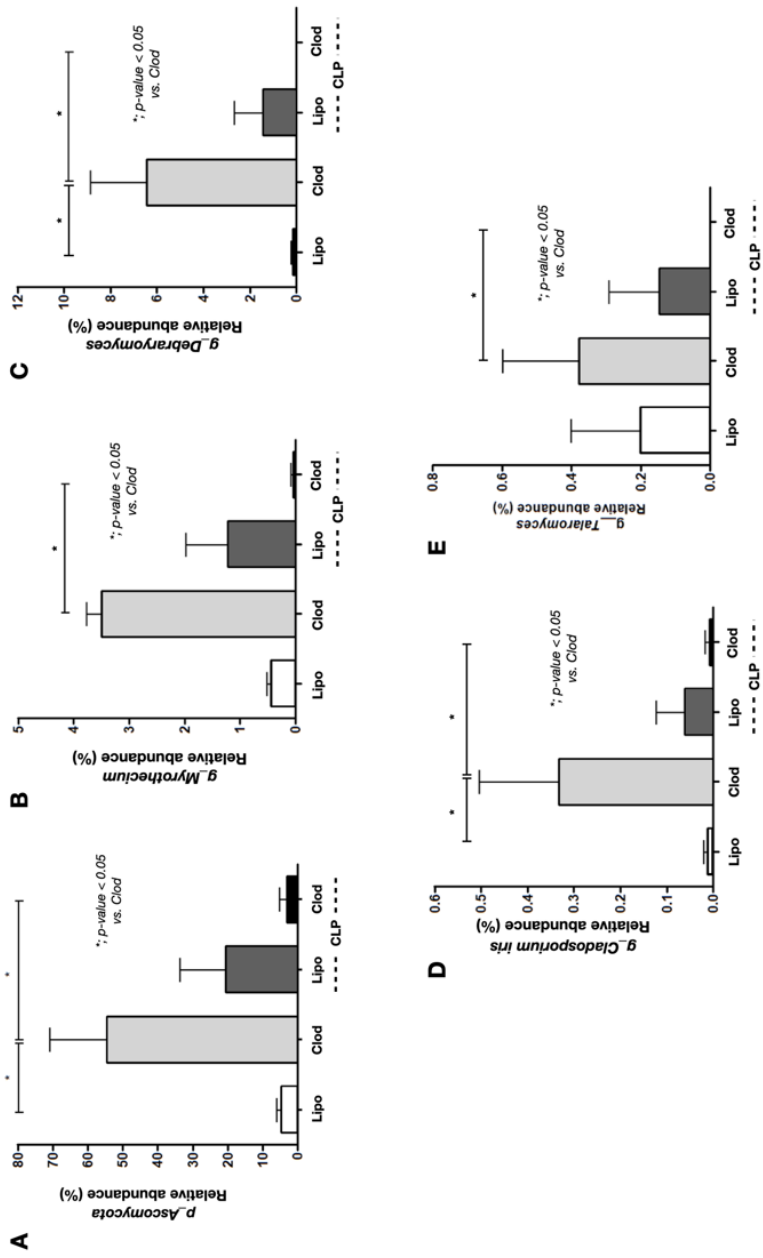
Figure 27 The relative abundance of bacteriome analysis

The bacteriome analysis as indicated by the relative abundance in the order (A) and family levels (B), *Escherichia/Shigella* (C), *Lactobacillus* spp. (D), *Roseburia* spp. (E), alpha diversity (Shannon and Chao) (F and G), and beta diversity (Bray Curtis) (H), (n = 3/group). Lipo; liposome control, Clod; macrophage-depleted control; Lipo-CLP; sepsis without macrophage-depleted; and Clod-CLP; sepsis with macrophage-depleted. The data are shown as the mean ± SE, *; *p-value < 0.05*.

6. An impact of gut fungi on overgrowth of some bacteria and the activation of enterocytes, an influence of gut fungi on sepsis severity

6.1 The interaction between gut fungi and the overgrowth of some bacteria

To investigate the gut fungi affected to the overgrowth of gut bacteria, the heat-kill lysate of isolated *C. pintolopesii*, the *Candida* yeast cells isolated from blood cultured in macrophage-depleted control mice, and heat-kill lysate of *C. albicans* ATCC 90028, and *C. albicans* (human blood) acted as the control, were co-incubated with or without live isolated bacteria from blood in macrophage-depleted mice, including *K. pneumoniae* (Kleb)*, E. faecalis* (Entero), *and A. radioresistens* (Acineto). The colony counting results demonstrated that heat-kill lysate of all *Candida* yeast cells significantly increased bacteria overgrowth in a dose-dependent manner, especially co-incubation at the multiplicity of infection (MOI) of 0.01 of live bacteria together with the highest heat-kill lysate *C. pintolopesii* (Figure 28A-C), *C. albicans* ATCC90028 (Figure 29A-C), and *C. albicans* isolated from human blood (Figure 30A-C). However, only the heat-kill lysate of *C. albicans* ATCC90028 co-incubated with *A. radioresistens* has not significantly increased the bacterial population. As (1→3)-β-D-Glucan (BG) is a significant component of the fungal cell wall that could promote the growth of some bacteria and glucan-digestible bacteria were identified, and BG of *Candida* spp. in the gut may be a source for bacterial fermentation. To investigate whether BG as representative fungal molecules can induce bacterial abundance, a purified BG in different doses, including 0.1 and 1 mg/mL was co-incubated with isolated bacteria at 37°C for 24 h demonstrating that BG significantly induce bacterial abundance (Figure 31A-C).
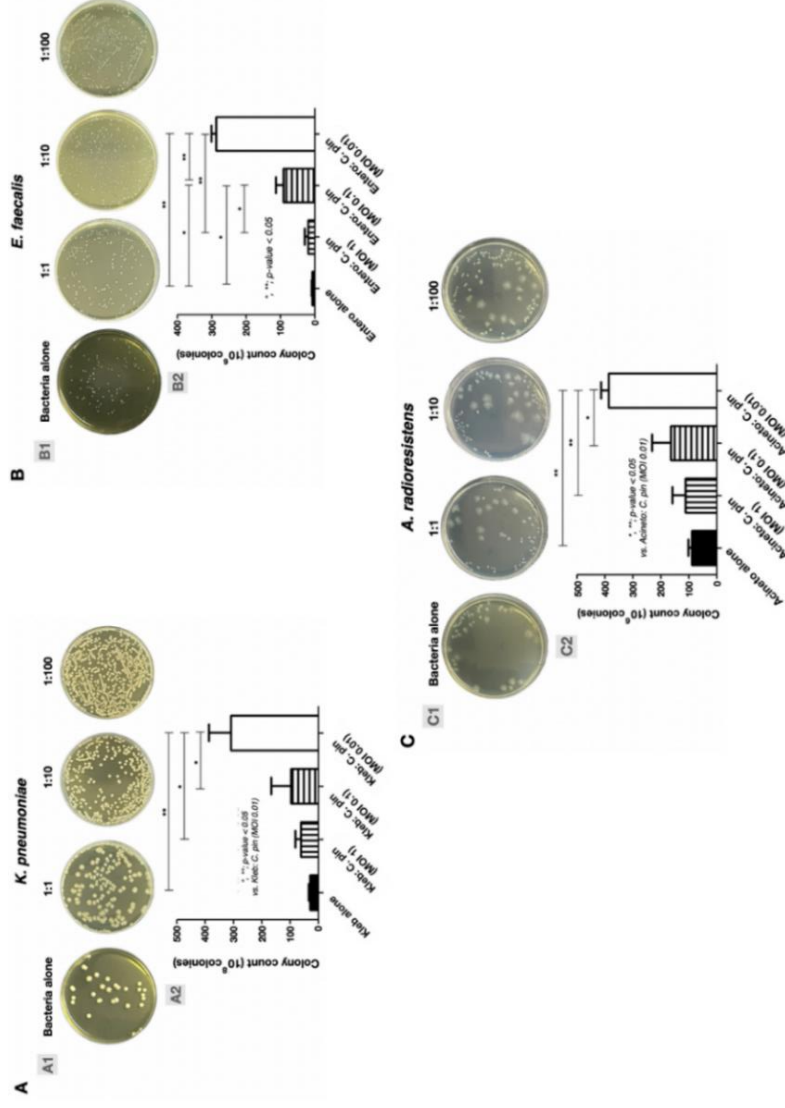
Figure 28 Characteristics of heat-kill lysate C. pintolopesii-induced bacteria overgrowth

Heat-kill lysate yeast was co-incubated with *K. pneumoniae* (A), *E. faecalis* (B), and *A. radioresistens* (C), (n = 9/group).

Kleb; *K. pneumoniae*, Entero; *E. faecalis*, Acineto; *A. radioresistens*, and C. pin; *C. pintolopesii*. The data are shown as the

mean ± SE, *, **; *p-value < 0.05 vs. bacterial in difference ratio.*
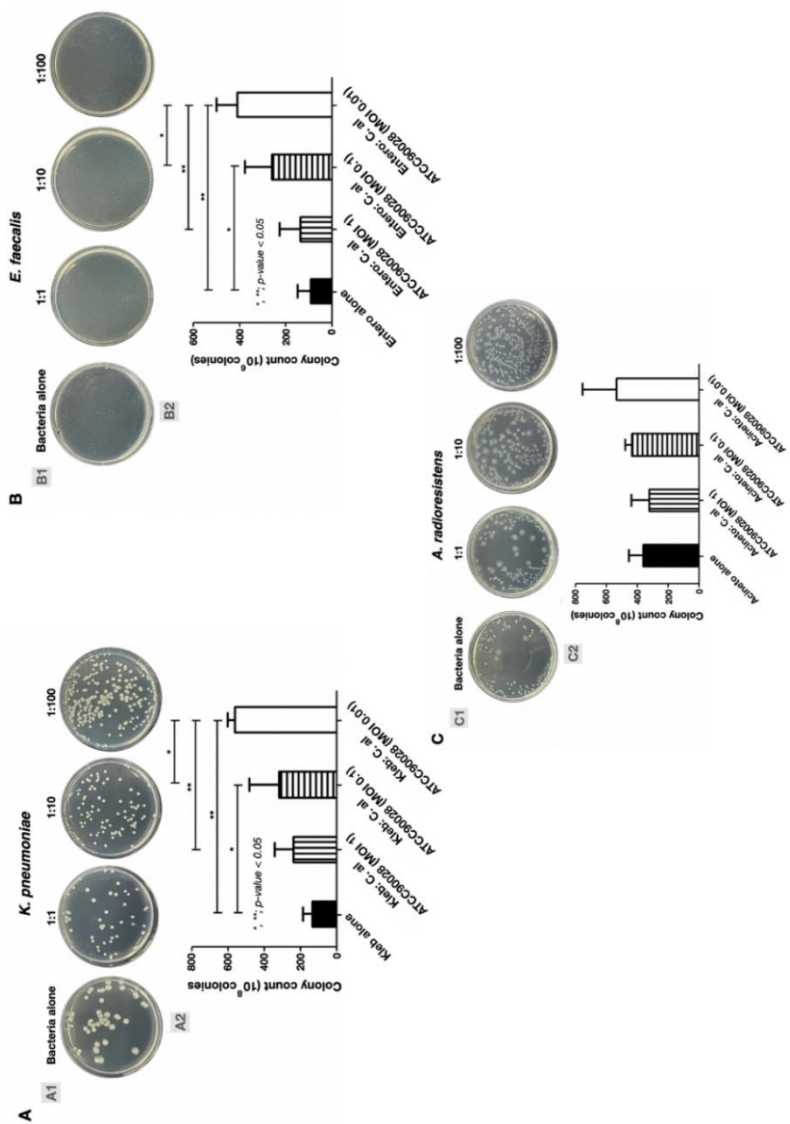
Figure 29 Characteristics of heat-kill lysate C. albicans ATCC90028 induced bacteria overgrowth

Heat-kill lysate yeast was co-incubated with *K. pneumoniae* (A), *E. faecalis* (B), and *A. radioresistens* (C), (n = 9/group).

Kleb; *K. pneumoniae*, Entero; *E. faecalis*, Acineto; *A. radioresistens*, and C. al ATCC90028; *C. albicans* ATCC90028. The

data are shown as the mean ± SE, *, **; *p-value < 0.05 vs. bacterial in difference ratio.*
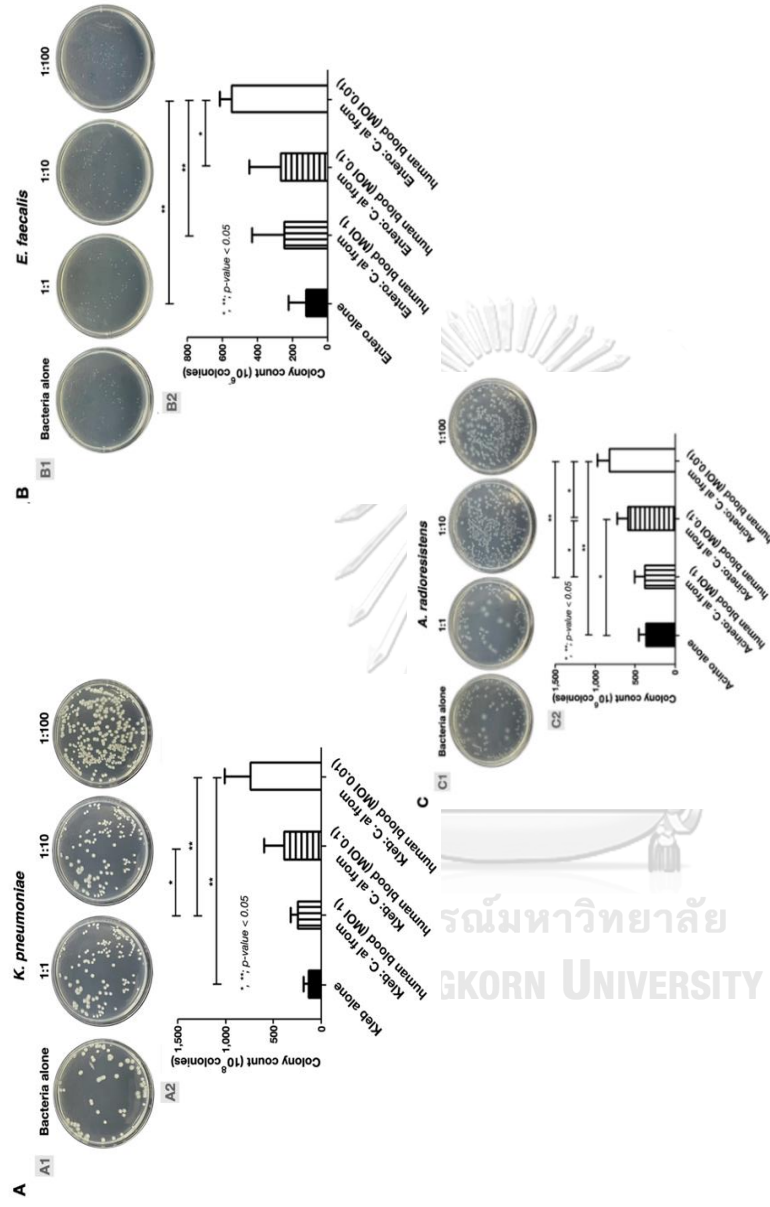
Figure 30 Characteristics of heat-kill lysate C. albicans isolated from human blood-induced bacteria overgrowth

Heat-kill lysate yeast was co-incubated together with live *K. pneumoniae* (A), *E. faecalis* (B), and *A. radioresistens* (C), (n =

9/group). Kleb; *K. pneumoniae*, Entero; *E. faecalis*, Acineto; *A. radioresistens*, and C. al from human blood; *C. albicans* which

isolated from human blood. The data are shown as the mean ± SE, *, **, *p-value < 0.05 vs. bacterial in difference ratio.*
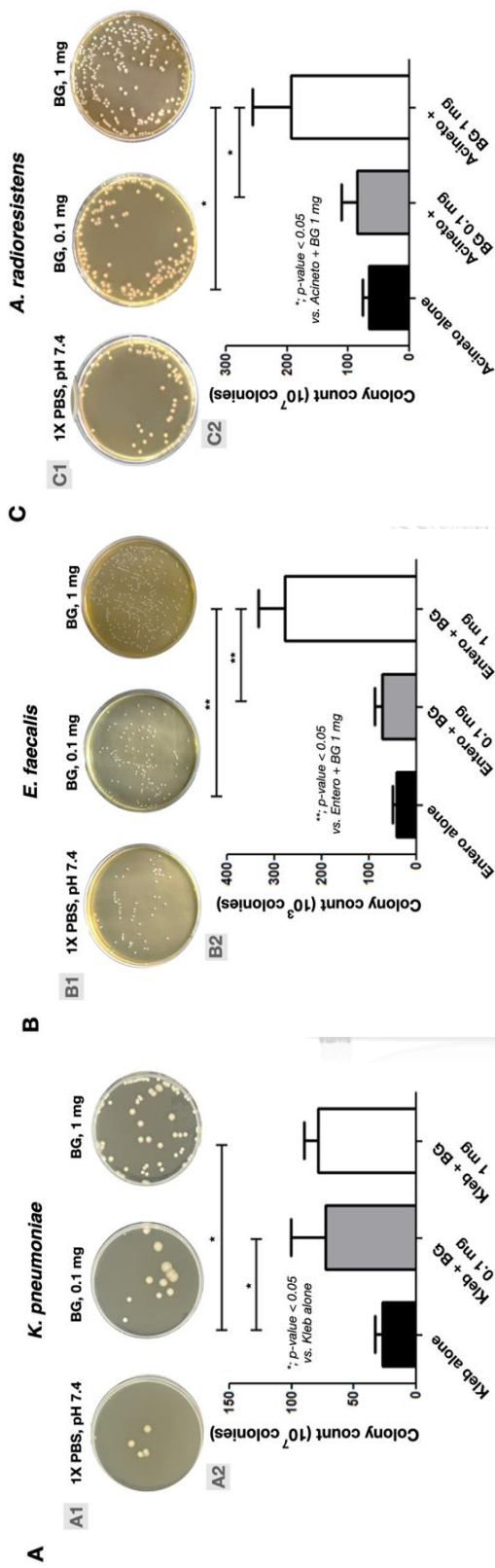
Figure 31 Characteristics of purified BG-induced bacteria overgrowth

BG were co-incubated together with live *K. pneumoniae* (A), *E. faecalis* (B), and *A. radioresistens* (C), (n = 9 /group).

The data are shown as the mean ± SE, *, **; *p-value < 0.05 vs. bacterial in difference ratio.*

6.1 Responsiveness of enterocytes against gut fungi and bacterial components

Candida spp. and BG powder not only influence bacterial abundance but also induced enterocytes and other immune cell responses. The Caco-2 enterocyte cells were co-incubated with heat-kill lysate fungi, including *C. pintolopesii*, *C. albicans* ATCC90028, and *C. albicans* with or without heat-kill lysate isolated bacteria, including *K. pneumoniae, E. faecalis,* and *A. radioresistens*, which used purified BG as the one of the positive molecules. The results showed the highest IL-8 cytokine production in the combination of heat-kill lysate *A. radioresistens* along with each *Candida*, whereas, the heat-kill lysate of yeast cells together with heat-kill lysate *K. pneumoniae* showed IL-8 cytokine production was higher than heat-kill lysate *Klebsiella* alone, but no significant difference between groups (Figure 32A-D).
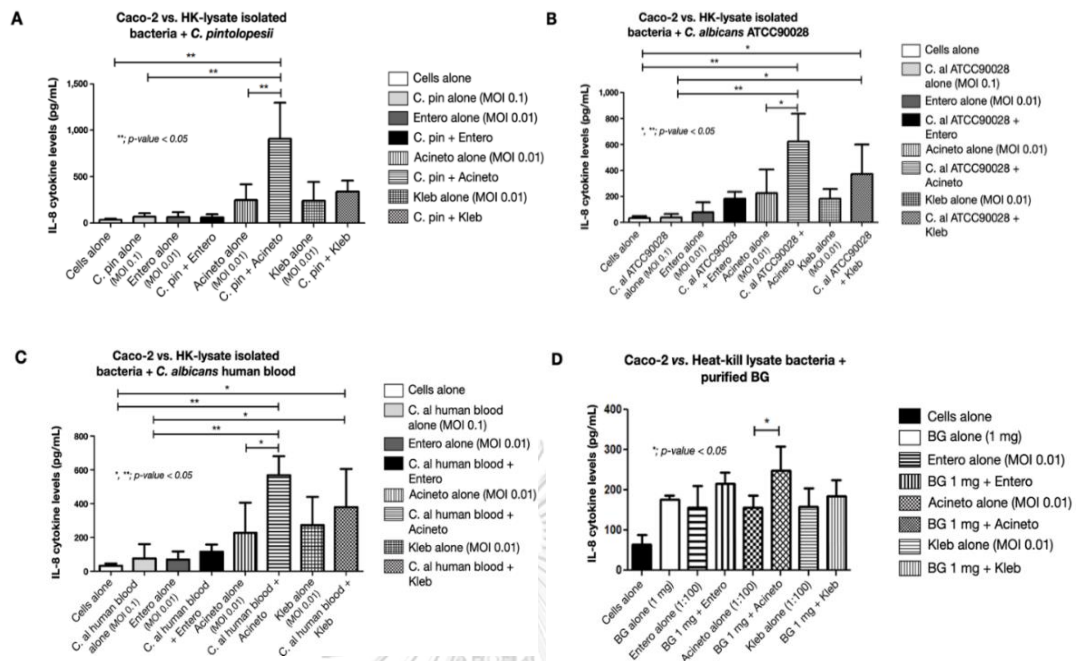
Figure 32 The levels of IL-8 cytokine in different conditions

Heat-kill lysate *C. pintolopesii* (A), heat-kill lysate *C. albicans ATCC90028* (B), heat-kill lysate *C. albicans* which isolated from human blood (C), and (1⟶3)-β-D-Glucan (BG) powder (D) were co-incubated with or without heat-kill lysate isolated bacteria, (n=9/group). The data are shown as the mean ± SE, *, **; p-value < 0.05.

CHAPTER VI
DISCUSSION

1. Increased fungi have impaired gut permeability in macrophage-depleted mice facilitated sepsis severity, a two-hit sepsis model due to fungemia and bacteremia.

The increased sepsis severity in macrophage-depleted mice containing sepsis was caused by an increase in the number of gut fungi, revealing the role of gut fungi and macrophages in sepsis. Clodronate-liposome treatment is one of the most effective methods that efficiently reduced intestinal macrophages, liver macrophages, and peripheral blood monocytes (52, 124). Therefore, macrophage dysfunction can lead to an inability to an appropriate immune response and implicated in various disease processes. In terms of macrophage depletion along with gut leakage, the imbalance of microorganisms occurred resulting in the differentiation of gut mycobiome and bacteriome, respectively, which affects to an increased severity. The intestinal macrophage dysfunction performed fungemia and the abundance of pathogenic Ascomycota fungi but not pathogenic bacteria (Proteobacteria), indicating that depleted macrophages are not able to control the gut fungi. However, in non-sepsis macrophage-depleted animals, increased fecal Ascomycota with decreased Firmicutes (a group of helpful bacteria on gut integrity) (98, 125) triggered gut dysbiosis severe enough to cause gut permeability defect (gut leakage) (126), which may partly be caused by enterocyte injury by fungi (for example, germ tube formation from *Candida*) (127). The fungemia and bacteremia in non-sepsis macrophage-depleted mice might be the first hit injury that worsens sepsis, similar to other two-hit sepsis models (128), as macrophage-depleted as the "first hit" together with sepsis-CLP as a "second hit" was more severe than in normal

mice. Despite the well-known knowledge that chronic intestinal inflammation encourages the growth of gut fungi because commensal bacterial competition is reduced, sepsis-CLP did not increase fecal fungal loads (perhaps because of too short duration). Even though the fecal contents of bacteria and fungi in macrophage-depleted animals with non-CLP versus CLP were similar by culture and detected OTUs, gut leakage in CLP mice was more severe than in sham mice, possibly because of the intestinal hypoxia and gut pathogens after sepsis (129, 130). In terms, gut dysbiosis is not only the reduction in microbial diversity and a combination of the loss of beneficial bacteria, but is also associated with pathogenic in host, for example metabolic dysfunction and gut inflammation (131, 132). As in this study, the fecal microbiome in sepsis without macrophage-depleted mice was similar to pathogenic bacteria, especially Enterobacteriaceae, in comparison with the control group, alpha diversity (a measure of microbiome diversity applicable to a single sample) and immune response was significantly higher.

In addition, previous report suggests neutrophils are significantly increased and recruited into organ tissue, during macrophage-depleted by clodronate-liposome administration (133). In short, neutrophils are the highest number of white blood cells in the human body, represent professional phagocytes of the innate immune system, and are crucial for preventing bacterial and fungal infections, such as *Candida* spp. and *Aspergillus* spp. is the most common species infecting a human (134). In this study, neutrophils should be activated by Ascomycota, especially *C. pintolopesii*, in macrophage-depleted mice. These phagocytic hunters go in the direction of invasive fungi, then secreting antimicrobial peptides, cytokines, and chemokines to recruit and activate other immune cells at the site of infections, and they also produce reactive oxygen species (ROS), such as elastase (NE) and myeloperoxidase (MPO) to destroy DNA structure of fungi. In case fungi produce

hyphae form (extracellular fungi) to invade tissue, neutrophils can produce neutrophil extracellular traps (NETs) to destroy and capture microorganisms. NETs capture a wide range of microorganisms, including bacteria, fungi, and parasites. It composes decondensed chromatin, antimicrobial proteins, including NE and MPO, and histones (135, 136). Then, macrophage-depleted induces gut dysbiosis and increased fecal and blood fungi might enhance more immune response and more severe sepsis than normal mice.

2. Some high-virulence bacterial strains in the gut were made to proliferate more quickly by fecal fungus, which facilitated bacteremia and made sepsis worse in macrophage-depleted mice.

The relevance of macrophages in the regulation of pathogenic bacteria has already been mentioned, the facilitated growth of some bacteria in gut dysbiosis, such as the growth of *P. aeruginosa* with the presence of *Candida* spp. in the gut (137). The capacity of some gut bacteria to digest BG, a key component of the fungal cell wall, might be the cause of the specific preferred proliferation in gut bacteria (137), whereas prokaryotic polyphosphates in some bacteria increase infection severity by reducing the anti-microbial activity of macrophages (138). In non-sepsis and sepsis mice with macrophage depletion, *E. faecalis*, the commensal bacteria (139), and Gram-negative pathogenic bacteria, constituted the majority of the bacteremia. Gram-negative bacteria in sepsis-CLP caused death and organ damage, suggesting the differential in bacterial virulence (104), while *E. faecalis* in sham animals only slightly elevated serum cytokines without causing organ damage. Despite commensal organisms, such as *E. faecalis*, being important for host-immune maturation and gut-barrier maintenance, they also activate immune response and inflammation during gut leakage (140). In spite of the similarities in

isolated strains of Gram-negative bacteria across sepsis-CLP animals with and without macrophage depletion, macrophage-depleted mice had significantly higher levels of pathogenic bacteria in their blood (blood culture) and feces (microbiome study). In contrast, the identified *C. pintolopesii* from mouse blood, Ascomycota (a category of *Candida* spp.) were the most prevalent fecal fungi in macrophage-depleted animals (non-sepsis and sepsis). These data indicated that macrophage depletion promotes *Candida* growth which can enhance a higher abundance of bacteria, *E. faecalis*, and Proteobacteria in non-sepsis and sepsis mice models, respectively (Figure 33A-D). It is possible that in non-sepsis mice, gut *Candida* promotes commensal bacteria, *E. faecalis*, whereas, in sepsis, gut inflammation causes the formation of pathogenic bacteria that are enhanced by gut *Candida* spp. The fact is that sepsis, even from non-gastrointestinal infections, increases gut-pathogenic bacteria and leaky gut (141, 142), in part due to stress-induced gut dysbiosis (143, 144). Because some bacteria from macrophage-depleted mice might be augmented by fungi (fungal digesters) (145), isolated bacteria from the blood of macrophage-depleted CLP mice were further tested. Accordingly, the abundances of the isolated *E. faecalis*, *K. pneumoniae*, and *A. radioresistens* in culture were enhanced by fungal lysate or $(1 \rightarrow 3)$-β-D-glucan (BG; a major molecule of the fungal cell wall), suggesting assistance of gut fungi on bacterial growth possibly due to the fungal digestion abilities (146). As a result, Proteobacteria can produce β-glucans and β-1,3-glucanase that leading to the enhancement of *Enterococcus* spp. growth in the culture media which is supplemented with β-glucans. Additional research is necessary to learn more about the mechanisms of these relationships. Additionally, this study only classified bacterial growth in aerobic conditions and little amount of blood culture, but not the

optimum condition for small populations of bacteria and anaerobic bacteria might be cannot grow. Future study might be important.

Furthermore, fungal sepsis shares common mechanisms with bacterial sepsis, but in contrast, bacteria are fast-growing Gram-negative microbiota in the feces that grew gradually up to 24 h after sepsis was induced, then it gradually decreased to the control level after 72 h (3, 147). As shown after inducing sepsis, fecal fungi decreased while pathogenic bacteria, especially Proteobacteria increased in macrophage-depleted and induce sepsis-CLP mice. However, this study determines microorganisms only at the endpoint, so the bacterial and fungal populations at difference time points should be investigate in the future.

3. **Mice lacking macrophages have increased levels of gut fungi, which influence enterocytes causing local and systemic inflammation, respectively.**

It has been previously observed that oral administration of fungus increases the level of BG translocate in the gut, which increases the severity of sepsis via increasing systemic inflammation (148-150). In this study, macrophage depletion led to the spontaneous elevation of fecal fungi in mice, specifically *C. pintolopesii* (the previously known non-albicans *Candida* in mouse guts) (151), which selectively enhanced some bacterial strains (causing gut dysbiosis) and caused gut translocation of LPS, important outer membrane components of gram-negative bacteria, and BG. Similar to a heat-kill lysate of isolated bacteria together with BG additively increased enterocyte-mediated inflammation compared with a heat-kill lysate of isolated bacteria, fungi, or BG alone which worsened sepsis more inflammation. The co-stimulation of TLR-4 and Dectin-1 in comparison to other cells may help explain why the presence of BG along with LPS in the gut may boost pro-inflammatory responses of enterocytes as compared to activation by each molecule

alone (148, 150). Indeed, the combination between BG and LPS administered intravenously causes a greater induction of serum cytokines than either molecule administered alone (101), demonstrating the additive effect of BG upon LPS responses in many mice models (4, 152). The prominent enterocyte inflammation may result in gut barrier breakdown and an increase in LPS and BG in the portal vein (97), which stimulates several cell types in the liver, including the hepatic sinusoidal endothelial cells and Kupffer cells (the first cell populations to come into contact with portal vein-derived molecules from the gut) (153), resulting in the elevated serum cytokines (but not enough to elevate liver enzyme). There is a need for more research on the reactions of the liver to gut barrier defects.

Moreover, extreme macrophage suppression from the developing macrophage interference in numerous disorders (cancers, autoimmune diseases, and sepsis) may increase the fecal fungus and worsen the severity of sepsis. When macrophage inhibition is taking place, several biomarkers (serum BG or fecal fungus) may be helpful. In addition, macrophage transfer therapy or adoptive therapy might be an interesting method, such as the transfer of M1 macrophage to control microorganisms infection and/or M2 macrophage to improve inflammation. More research is essential.
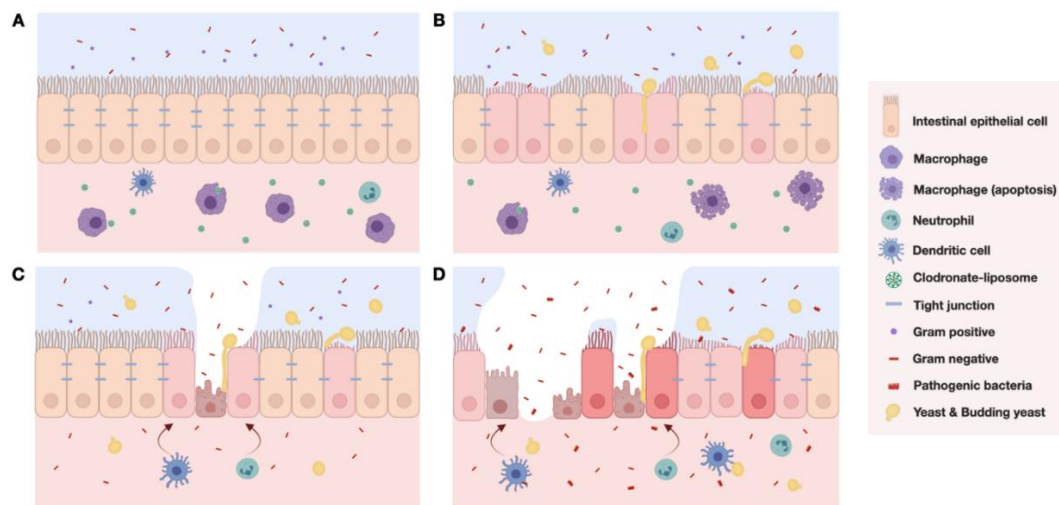
Figure 33 Diagram of macrophage depletion enhances sepsis severity

The contributing theory demonstrates a balance between immune responses, especially macrophage function, versus intestinal microbes in normal mice (A). Clodronate-liposome administration induces macrophage depletion (apoptosis) and causes an overgrowth of gut fungi (*C. pintolopesii*), (B). Clodronate-liposome administered mice without CLP performed macrophage depletion causes fungal overgrowth and enhances bacteria in the gut causing a mild degree of gut permeability defect through enterocyte tight junction damage or enterocyte cell death (C). Macrophage-depleted with CLP-sepsis demonstrated that sepsis induces the overgrowth of pathogenic bacteria (sepsis-induced gut dysbiosis), especially Gram-negative bacteria (Proteobacteria), and gut fungi which facilitates the growth of some other strains of pathogenic bacteria results in a more severe gut leakage, bacteremia of the high virulence microbes and severe sepsis (D). Diagram was created by BioRender software (https://app.biorender.com/illustrations) on November 14[th.], 2021.

CHAPTER VII
CONCLUSION

This study evaluated the sepsis severity with or without macrophage dysfunction in mice. The sepsis with macrophage-depleted mice shows the highest sepsis severity with the lowest survival rate and body weight, whereas higher gut leakage, gut translocation (fungemia as *C. pintolopesii* and bacteremia, such as *K. pneumoniae*, *A. radioresistens*, and *E. faecalis*), organ injuries (kidney and liver), serum and tissue inflammatory cytokines, and histopathology with immune cell infiltrations when compared with sepsis without macrophage-depleted mice. In addition, macrophage depletion can enhance fecal Ascomycota and pathogenic bacteria, especially Proteobacteria while a decrease in Firmicutes, suggesting that macrophage depletion enhances the progression of sepsis. Furthermore, *in vitro* studies, investigate the interactions of pathogenic microorganisms. The heat-kill lysate fungi, which are isolated from macrophage-depleted blood, and purified BG powder show significantly increased bacterial abundance in comparison with bacteria alone. Because some Proteobacteria can produce β-1,3-glucanase, there might be the assistance of gut fungi on the growth of some bacteria (the ability to digest fungal molecules). In addition, fungal molecules combine with bacterial molecules enhance more inflammatory cytokine production from enterocytes as additive effect, compared with fungal or bacterial molecules alone. In conclusion, macrophage depletion enhanced fecal *Candida* and fecal pathogenic bacteria overgrowth, intestinal barrier damage, and gut translocation of bacteria and fungi that additively worsened sepsis severity. The monitoring of fungal abundance during macrophage dysfunction is interesting. More research on these issues would be beneficial.

This thesis was cited from "Macrophage depletion alters bacterial gut microbiota partly through fungal overgrowth in feces that worsens cecal ligation and puncture sepsis mice", which has been published in the journal of Scientific Reports; Volume *12*(1):9345 (154).

จุฬาลงกรณ์มหาวิทยาลัย
CHULALONGKORN UNIVERSITY

APPENDIX A
MATERIALS AND EQUIPMENT

Materials

0.22 µm Surfactant-free cellulose acetate membrane filters (Minisart, Germany), Lot No. 220762-052-A

0.25% Trypsin in 1mM EDTA (Hyclone, USA), Lot No. 2062476

0.4% Trypan blue solution (Hyclone, USA), Lot No. 2169134

95% alcohol (Liquor distillery organization excise department, Thailand), Lot No. 255336

Absolute alcohol (Merck, Germany), Lot No. K48802114713

Alanine Transaminase (ALT) Blood Test kit (BioAssay, USA), Lot No. A1210-22-100T

Anti-Arginase1 (Irvine, California, USA), Cas No. #17-3697-82

Anti-F4/80 (Abcam, Cambridge, UK), Lot No. ab150077

Beta-mercaptone (Sigma-Aldrich, Germany), Cas No. 60-24-2

Blood agar (Oxoid, UK), Lot No. 221221(O1)

Bovine serum albumin (BSA) (Sigma-Aldrich, USA), Cas No. 9048-46-8

Chloroform (Sigma-Aldrich, Germany), Cas No. 67-66-3

Clodronate-liposome (Encapsula Nanoscience, USA), Lot No. CLD8901-07312020

Cryovial (Nunc, Denmark), Lot No. 210314-539

Dimethyl sulfoxide (DMSO) (Sigma-Aldrich, USA), Cas No. 67-68-5

Disodium hydrogen phosphate (Na_2HPO_4) (Ajax finechem Pty Ltd, Australia), Cas No. 7558-79-4

Dulbecco's Modified Eagle Medium (DMEM) (Hyclone, USA), Lot No. 2186844

EDTA (Merck, Germany), Cat No. 17892

Eosin (Merck, Germany), Cat No. 109844

Fetal bovine serum (Hyclone, USA), Cat No. 12203C

Fluorescein isothiocyanate dextran (FITC-dextran) (Sigma-Aldrich, USA), Lot No. BCCB7859

Glycerol (Merck, Germany), Cas No. 56-81-5

Hematoxylin (Merck, Germany), Cas No. 517-28-2

HEPES (Hyclone, USA), Cas No. 7365-45-9

HRP conjugated goat anti-mouse isotype-specific antibodies (BioLegend, USA), Lot No. 232582-000

Human IL-8 ELISA kits (Invitrogen, USA), Lot No. 227748-000

Iso-propanol (QRëC, New Zealand), Lot No. PR141-1-4000

Isoamyl (QRëC, New Zealand), Cas No. 123-51-3

Mouse TNF-**α**, IL-6, IL-10 ELISA kits (Invitrogen, USA), Lot No. 20933000, 206666000, and 282663-000, respectively.

Phenol (Amresco, USA), Lot No. 27066433

Potassium Chloride (KCl) (Merck, Germany, Cas No. 7447-40-7

Potassium dihydrogen phosphate (KH_2PO_4) (Sigma-Aldrich, Germany), Cas No. 7778-77-0

Sabouraud Dextrose Agar (SDA) (Oxoid, UK), Lot No. 0000533576

Sabouraud dextrose broth (SDB) (Oxoid, UK), Lot No. 0000525419

Serum creatinine kit (BioAssay, USA), Cat No. ABIN577684

Sodium Chloride (NaCl) (Sigma-Aldrich, USA), Lot No. R161V0

Sodium dodecyl sulfate (SDS) (Sigma-Aldrich, Germany), Cas No. 151-21-3

Sodium Pyruvate (Hyclone, USA), Cat No. 11360070

Streptomycin/Penicillin G (Hyclone, USA), Cat No. 15140122

Sulfuric acid (H_2SO_4) (Sigma-Aldrich, Germany), Cas No. 7664-93-9

SYBR™ Green PCR Master Mix (Thermo Fisher Scientific, USA), Cat No. 4309155

TMB substrate Set (BioLegend, USA), Lot No. 232582-000

Tris (Sigma-Aldrich, Germany), Lot No. 1A0420AMS10341

Tryptic Soy Broth (TSB) (HiMedia, India), Cat No. M290-500G

Tween 20 (Merck, Germany), Cat No. 003005

Equipment

-20°C Freezer (Sanyo, Japan)

-80°C Freezer (Sanyo, Japan)

96-Well Flat-bottom tissue culture plates (Nunclon D, Denmark), Lot No. B7.8H20-30066

Auto pipette; P-2.5, P-20, P-100, P-200, and P-1000 (Gilson, France).

Autoclave (Hirayama, Japan)

Barrier tips; 10 µL, 20 µL, 100 µL, 200 µL, and 1,000 µL (Neptune, Mexico), Lot No. BT-20-B, BT-200-B, and BT-1000-B, respectively.

Biological safety cabinet (Astec-Microflow, Bioquell UK Ltd, UK)

CO_2 incubator (BINDER GmbH, Germany)

Confocal microscope (Olympus, Japan)

Conical centrifuge tubes; 15 mL, 50 mL (Nunc, USA)

CytoSpin Chamber (Thermo Fisher Scientific, USA)

Eppendorf Master Cycler Gradient Thermal Cycler (Germany)

Heat box (Scientific Industries Inc., USA)

Hemacytometer (Bright-line) (BOECO, Germany)

Hot plate (Stuart, Germany)

Incubator (Memmert GmbH, Germany)

Inverted microscope (Olympus, Japan)

Micropipette (Gilson, France)

Multi-channel pipette (Socorex, Switzerland)

NanoDropTM 1000 Spectrophotometer (Thermo Fisher Scientific, USA)

pH meter (Thermo Fisher Scientific, USA)

Refrigerated centrifuge (Sanyo, Japan)

Safety cabinet (Augustin, Thailand)

Serological pipettes; 5 mL, 10 mL, and 25 mL (Corning, USA), Lot No. F150001 and

G020001

Sonicator (Sonics Vibra Cell, USA)

Spectrophotometer (Thermo Fisher Scientific, USA)

Sterile nylon Silke (HAVELS, USA), Lot No. 1701009

Sterile surgical blade (HAVELS, USA), Lot No. 200509A

Surgical Needle (HAVELS, USA), Lot No. 21L12

Syringe; 1 mL and 5 mL (Nipro, Thailand), Lot No. 20110616

Tissue culture flask; 25 cm^2, 75 cm^2 (Nunc, Denmark), Lot No. 422203

UV transilluminator (Bio-Rad, USA)

Vertical laminar flow workstation (Microflow, UK)

Water bath (Memmert GmbH, Germany)

Software and programs

Biorender

Endnote 20

G-power

GraphPad Prism 6.0

Keynote

Microsoft Office

APPENDIX B

MOLECULAR ANALYSIS

1. DNA extraction

   1.1 Reagents

   Lysis solution; 20 mM NaCl, 20 mM EDTA, 40 mM Tris-HCl pH 8.0, 0.5%
   SDS, and 0.5% Beta-mercaptone

5 M NaCl	20 mL
0.5 M EDTA	20 mL
1 M Tris	20 mL
10% SDS	25 mL
Beta-mercaptone	2.5 mL (Should be added to the solution

   prior to use)

Distilled water	412.5 mL

   *Proteinase K; 20 mg/mL in DW

   *Saturated NaCl (approximately 6 M)

   1.2 Protocol

   1. Mouse feces or microorganisms were lysed in 500 µL of lysis buffer at
      65°C for 3 h. Then, 20 µL of proteinase K (20 mg/mL) was added.
      (Optional; add 250 µL of Saturated NaCl, shake well for 10 sec, and
      incubate on ice for 15 min)

   2. The sample was broken via bead beater for 3-5 min and centrifuged at
      4°C, 10,000 rpm for 10 min.

3. The supernatant was transferred into a new tube, then 500 µL of Phenol: Chloroform: Isoamyl [25:24:1], incubated on ice for 5 min. The sample was centrifuged at 4°C, 10,000 rpm for 10 min.

4. The supernatant was collected into a new tube, added 500 µL of Chloroform: Isoamyl [24:1], and incubated on ice for 5 min. The sample was centrifuged at 4°C, 10,000 rpm for 10 min.

5. The clear DNA in the supernatant was transferred into a new tube and clod isopropanol was added immediately. The sample was incubated on ice for 1 h or overnight in a -20°C Freezer.

6. The sample was centrifuged at 4°C, 10,000 rpm for 10 min, discard supernatant, and washed with 500 µL of 75% ethanol alcohol, then centrifuged again.

7. Absolute alcohol was added to the pellet for final washing, plate DNA pellet air dry for 20 min.

8. PCR water was added to dilute the pelleted DNA and kept in a -80°C Freezer until use.

2. **Real-time PCR for determining bacteria genes**

   2.1 **Real-time PCR mixture preparation**

   Calculation and aliquot PCR master mix as follows table in 1.5 mL microcentrifuge tube.

PCR master mix	μL/sample
SYBR™ Green PCR Master Mix	5
Forward primer	0.5
Reveres primer	0.5
PCR water	2
	8 μL/sample
DNA sample	2

   Primers; Bacteria, 515F, Forward primer; 5'-GTGCCAGCMGCCGCGGTAA-3'

   Bacteria, 806R, Reveres primer; 5'-GGACTACHVGGGTWTCTAAT-3'

   2.2 **Real-time PCR condition**

   The Thermal cycle was adjusted as in the table.

Step	Temperature (°C)	Time	Cycle
1	95	10 min	
2	95	15 sec	
3	60	1 min	40 cycles
4	72	30 sec	
5	72	1 min	
6	4	Forever	

APPENDIX C
THE HISTOLOGY STAINING

1. **Hematoxylin and Eosin staining (H&E)**

    1.1 Slides were put into a xylene jar to de-paraffin, 3 jars, for 10 min per jar.

    1.2 The slide was put into a 95% alcohol jar, 3 jars, for 20 min per jar. Then, the slide was soaked with water running for 3 min (beware of slide drying).

    1.3 During the staining steps, the slide was added into a hematoxylin jar for 3 min, then washed with running water for 3 min. The slide was dipped in 95% alcohol, 10 times.

    1.4 The slide was added into an eosin jar for 3 min and dipped in 95% alcohol, 10 times. After that slide was dipped in absolute alcohol 10 times and dipped in a xylene jar, 10 times.

2. **Immunohistochemistry staining**

    2.1 Before beginning the staining technique, it is necessary to rehydrate the tissue. Rinse the slides with deionized water.

    2.2 Using a barrier pen, encircle the tissue with a hydrophobic barrier.

    2.3 In order to stop endogenous peroxidase activity, incubate the sample for 5–15 min with 1-3 drops of peroxidase-blocking reagent (3% H_2O_2 in water or methanol).

    2.4 After rinsing, gently wash the sample in a wash buffer for 5 min.

    2.5 The section was blocked with 1-3 drops of serum-blocking reagent for 15 min to decrease non-specific hydrophobic interactions between the primary antibodies and the tissue. Before moving on to the next step, the slides were

drained, and removed any extra obstructing reagent using a damp cloth. Never rinsed.

2.6 The avidin-blocking reagent was added 1-3 drops on the sample for 15 min to prevent binding to endogenous biotin. Slides were drained and removed any extra wash buffer before rinsing the sample.

2.7 The sample should be incubated with 1-3 drops of biotin-blocking reagent for 15 min in order to prevent further binding to the avidin used in step 6 from occurring. Drain the slides after rinsing with wash buffer and removing any extra wash buffer with a clean cloth.

2.8 The incubation buffer was used to incubate the sample with the primary antibody. It is advised to incubate overnight at 2-8°C. This incubation procedure lowers non-specific background staining while enabling the best possible specific binding of antibodies to tissue targets. Then, the sample was washed with a buffer after rinsing.

2.9 The biotinylated secondary antibody was applied to the sample for 30–60 min. Then, the sample was rinsed with wash buffer 3 times for 15 min on each slide.

2.10 High Sensitivity Streptavidin-HRP conjugate (HSS-HRP) was added to incubate the sample for 30 min. After that, rinsed and washed 3 times in the wash buffer for 2 min on each slide.

2.11 The required working volume of DAB/AEC Chromogen Solution that 100-200 μL is required to cover the entire tissue section on a single slide. Add 1-5 drops of DAB/AEC Chromogen Solution to cover the entire tissue section and incubate for 3-20 min. The sample was rinsed and washed 3 times in the wash buffer for 2 min. Then, drained the slides after rinsing them with deionized water.

2.12 For better tissue morphology visualization, stained tissue can be mounted either without nuclear counterstaining or with nuclear counterstain hematoxylin. Cover stained tissue with a coverslip of the proper size.

3. Immunofluorescence staining

3.1 Tissue preparation; the sectioned tissue was added on a slide.

3.2 Fixation; 100% chilled methanol at -20°C was added to the sample slide for 10 min.

3.3 Permeabilization; the sample was permeabilized with 0.1–0.05% Triton X-100 in 1X PBS, pH 7.4 (containing 100 mM glycine) for 20 min at room temperature. After permeabilization rinses the coverslips with 1X PBS at least three times.
*Permeabilization is used when staining for internal antigens.

3.4 Blocking; block for an h at room temperature with 2-5% animal serum, BSA, or milk diluted in 1X PBS, pH 7.4.

3.5 Incubating with primary antibody; The slide sample was incubated with diluted primary antibody (1:) in 1% blocking buffer for 1 h at room temperature. Then, the slide was washed with a washing buffer 3 times.

3.6 Incubating with secondary antibody; The slide sample was incubated with diluted secondary antibody (1:) in 1% blocking buffer for 1 h at room temperature. Then, the slide was washed with a washing buffer 3 times.

3.7 The slide was stained with DAPI (1:10,000) for 10 m then rinse with water.

3.8 Mounting; the slide was mounted with a mounting buffer, then leave the slides to dry overnight.

APPENDIX D
CACO-2 CELL CULTURE

1. Media preparation

    1.1 DMEM completed medium

DMEM serum-free media (high glucose)	100.0 mL
FBS	20.0 mL
HEPES	1.0 mL
Sodium Pyruvate	1.0 mL
PenG/Step	1.0 mL

    *DMEM completed medium was kept at 4 °C before use.

2. Thawing frozen cells and cell culture

    2.1 The cryovial containing the Caco-2 frozen cells was removed from liquid nitrogen storage and immediately place into a 37°C water bath.

    *Gently swirl the vial in the 37°C water bath until there is just a tiny quantity of ice left in the vial, and quickly defrost the cells (1 min).

    2.2 The vial was placed inside a hood with laminar airflow. Wipe the vial's outside with 70% ethanol before opening them.

    2.3 Caco-2 cell was added into the pre-warmed completed DMEM medium for Caco-2 into the centrifuge tube containing the thawed cells. Then, the cell suspension was centrifuged at 1,500 rpm, 4°C for 5 min.

    2.4 The cell pellet was collected, gently resuspend the cells in a complete growth medium.

3. **Freezing cells**

Cells should be in the log phase.

3.1 Freezing media preparation; 10% DMSO was added into in-activated FBS.

3.2 The cells were centrifuged at 1,500 rpm, 4°C for 5 min to pellet cells. Using a pipette, remove the supernatant down to the smallest volume without disturbing the cells. Then, the viable cell number should be counted before cryopreserving.

3.3 Caco-2 cell was aliquoted into cryogenic storage vials. Place vials on wet ice or in a 4°C refrigerator, and start the freezing procedure within 5 min.

3.4 All vials were placed in an insulated box and placed in a freezer that is between -70°C and -90°C before being moved to liquid nitrogen storage.
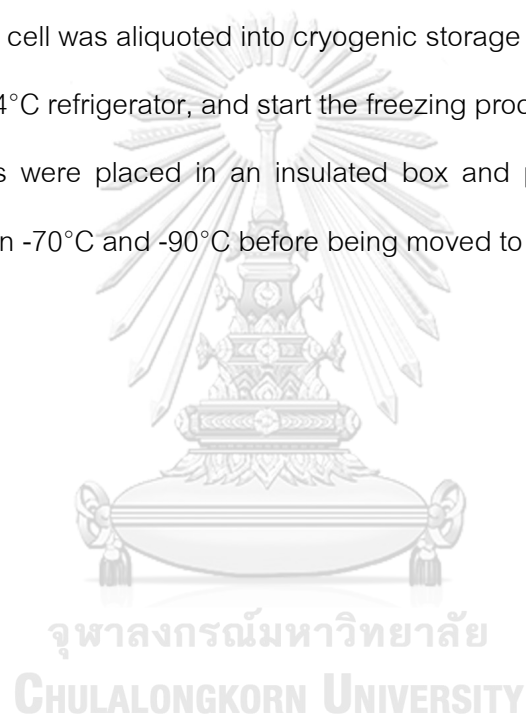
APPENDIX E
CULTURE MEDIA

1. **Sabouraud Dextose Agar (SDA)**, Lot No. 0000533576

Pancreatic digest of casein	5.0 g
Peptic digest of animal tissue	5.0 g
Dextrose	40.0 g
Agar	15. 0 g
Distilled water	1,000 mL

    *SDA was sterilized by autoclave at 121°C for 15 min and all plates were kept at 4°C before use.

2. **Sabouraud Dextose Broth (SB)**, Lot No. 0000525419

Dehydrated SB	30.0 g
Distilled water	1,000 mL

    *SB was sterilized by autoclave at 121°C for 15 min and kept at 4°C before use.

3. **Blood agar**, Lot No. 221221(O1)

Dehydrated TSB	30.0 g
Agar	15.0 g
Distilled water	1,000 mL

    *The media was sterilized by autoclave at 121°C for 15 min, then 50 mL of sheep blood was added into a warm medium (50-60°C), and all plates were kept at 4°C before use.

4. **Tryptic Soy Agar (TSA)**, Cat No. M290-500G

      Dehydrated TSB   30.0 g

      Agar   15.0 g

      Distilled water   1,000 mL

      *TSA was sterilized by autoclave at 121°C for 15 min and all plates were kept at 4°C before use.

5. **Tryptic Soy Broth (TSB)**, Cat No. M290-500G

      Dehydrated TSB   30.0 g

      Distilled water   1,000 mL

      *TSB was sterilized by autoclave at 121°C for 15 min and kept at 4°C before use.

APPENDIX F
REAGENTS FOR ELISA ASSAY

Human IL-8 ELISA kits (Invitrogen, USA), Lot No. 227748-000, mouse TNF-α (Invitrogen, USA), Lot No. 20933000, mouse IL-6 (Invitrogen, USA), Lot No. 206666000, and mouse IL-10 (Invitrogen, USA), Lot No. 282663-000 ELISA kits (Invitrogen, USA) were used to determine cytokine levels.

1. 10X Phosphate buffer saline (10X PBS), pH 7.4

NaCl	80.0 g
KCl	2.0 g
KH_2PO_4	1.4 g
Na_2HPO_4	9.1 g
Distilled water	1,000 mL

*10X PBS was sterilized by autoclave at 121°C for 15 min and kept at room temperature before use.

2. Washing buffer (1X PBS, pH 7.4-Tween20)

Sterile 10X PBS	100 mL
Sterile distilled water	900 mL
Tween20	0.05 mL

3. 1X Coating buffer (100 reactions)

10X coating buffer	1.0 mL
Distilled water	9.0 mL

*Or using 1X PBS, pH 7.4 as a coating buffer.

4. Capture antibody (1:250) (100 reactions)

    Capture antibody   40 µL

    1X Coating buffer   9.960 mL

5. 1X ELISPOT/Diluent (100 reactions)

    5X ELISPOT   4.0 mL

    1X Coating buffer   16.0 mL

    1X ELISPOT should be kept on ice before use.

6. Standard cytokines (100 reactions)

6.1 Mouse TNF-**α**; 500-7.8 pg/mL of the standard samples were prepared, and the standard samples were diluted with 1X ELISPOT in 2-fold dilutions for 8 points standard curve.

6.2 Mouse IL-6; 500 pg/mL top standard was prepared, and the standard samples were diluted with 1X ELISPOT in 2-fold dilutions for 8 concentrations.

6.3 Mouse IL-10; 2,000 pg/mL top standard was prepared, and the standard samples were diluted with 1X ELISPOT in 2-fold dilutions for 8 concentrations.

6.4 Human IL8; 2,000-15.625 pg/mL standard samples were prepared, and the standard samples were diluted with 1X ELISPOT in 2-fold dilutions.

    *All standard samples should be prepared freshly before use.

7. Detection antibody (1:250) (100 reactions)

    Detection antibody   40 µL

    1X ELISPOT   9.960 mL

8. Avidin-HRP solution (1:250) (100 reactions)

     Avidin-HRP   40 µL

     1X ELISPOT   9.960 mL

9. TMB substrate (100 reactions)

     TMB reagent (100 µL/well)   10.0 mL

     *TMB should be kept in the dark and avoided light during use.
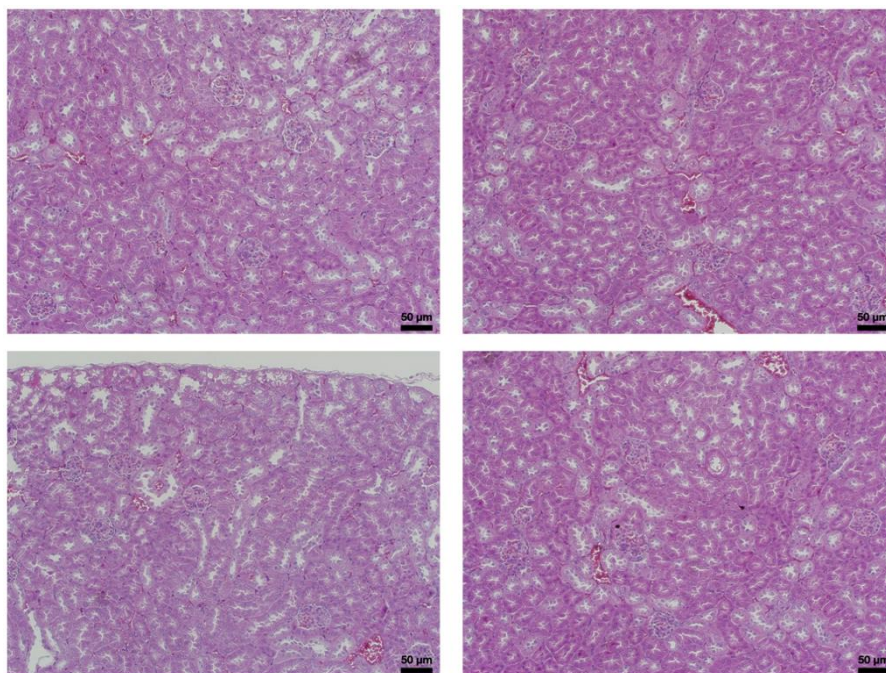

*All cytokines were determined by ELISA assay (Invitrogen, USA).
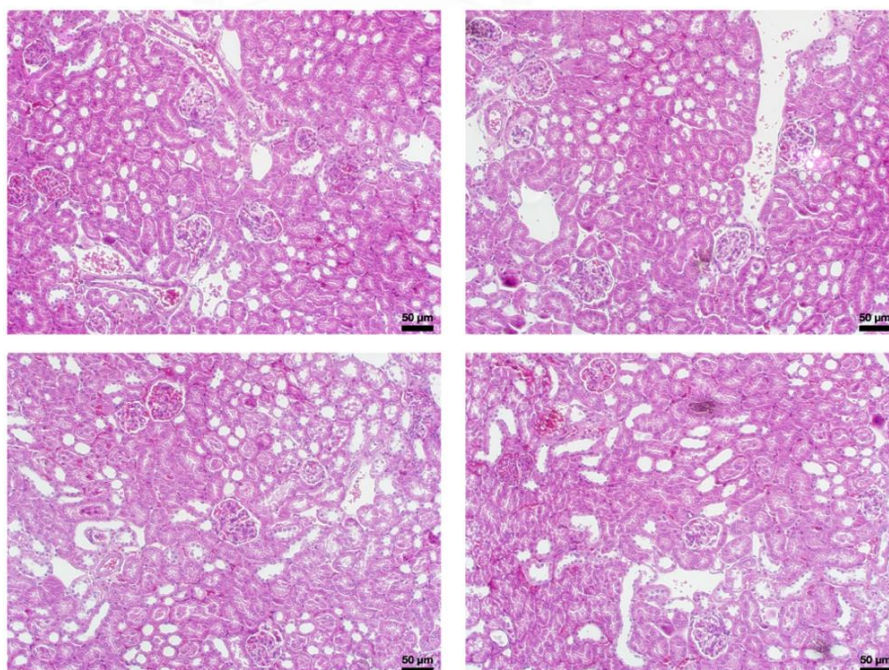
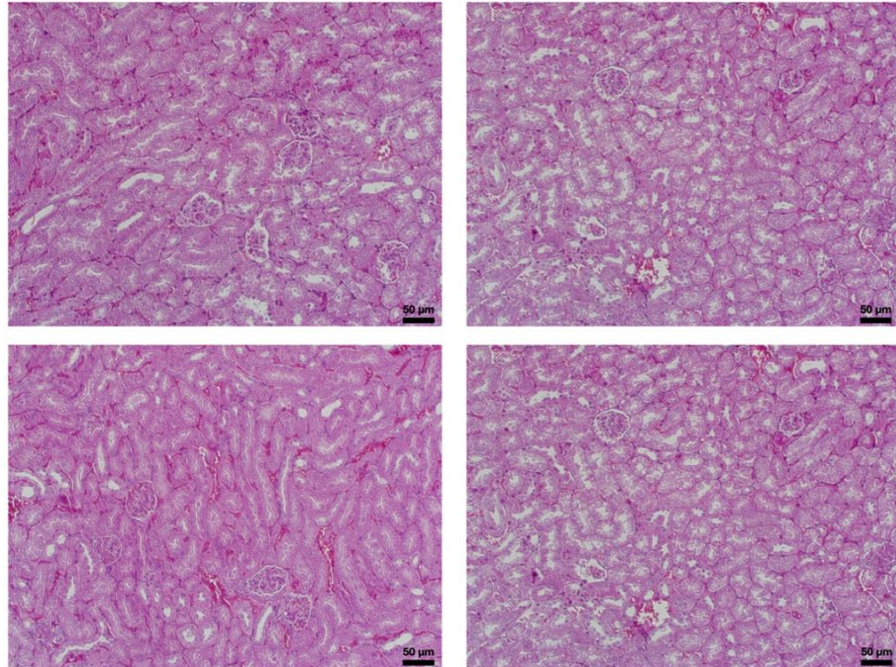# APPENDIX G

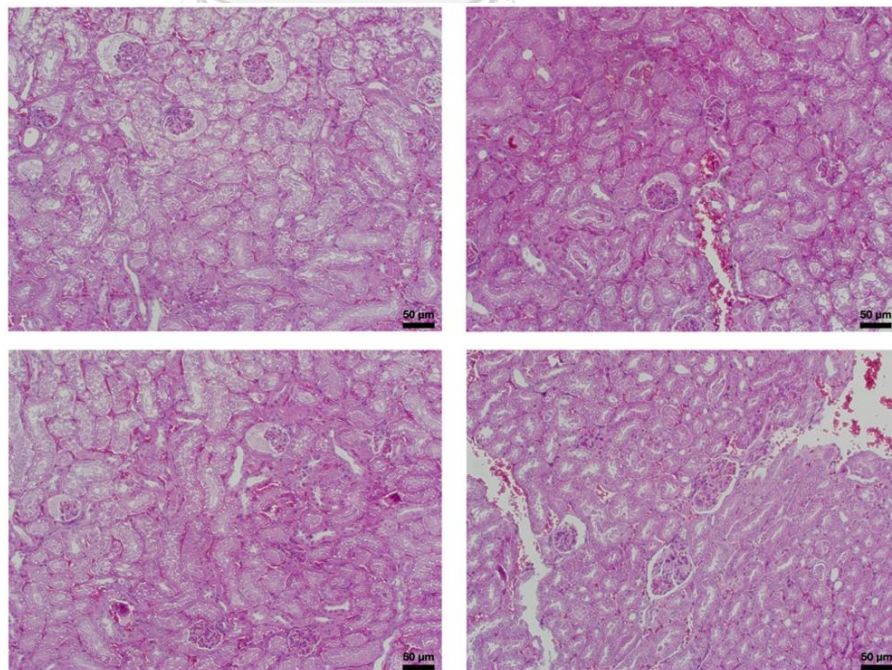# HISTOPATHOLOGICAL RESULTS

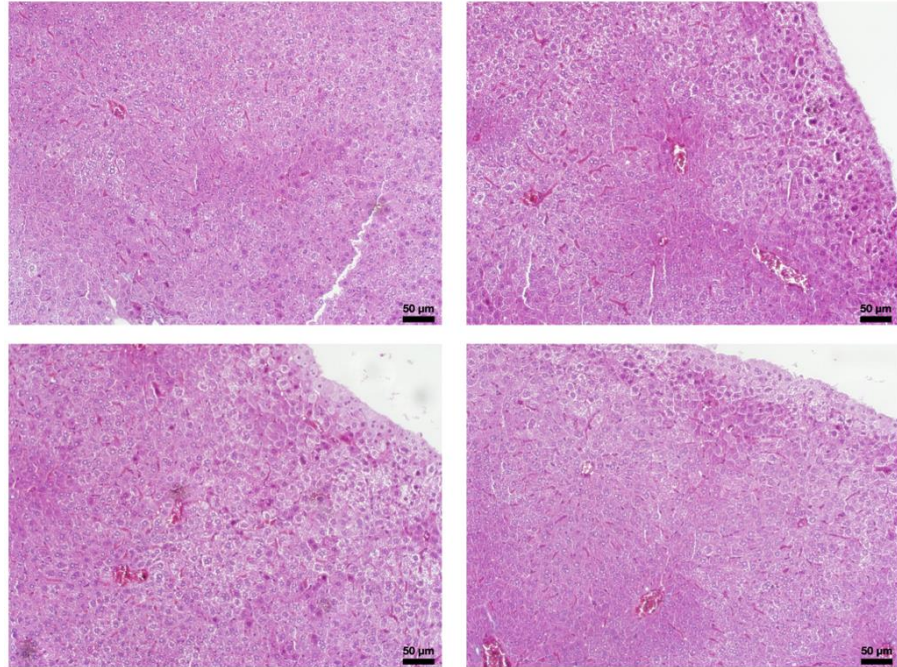- Kidney: Liposome control

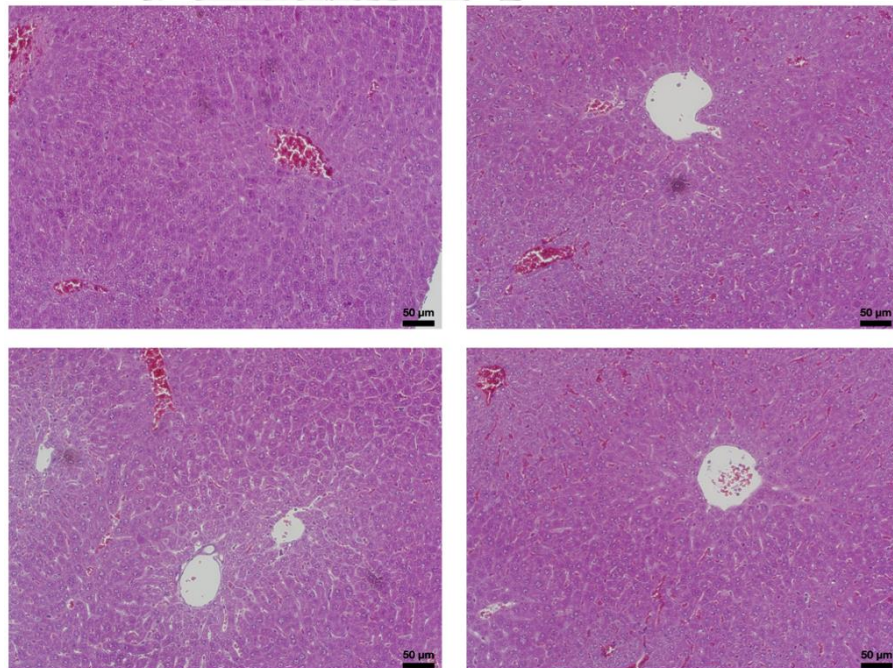- Kidney: Clodronate alone

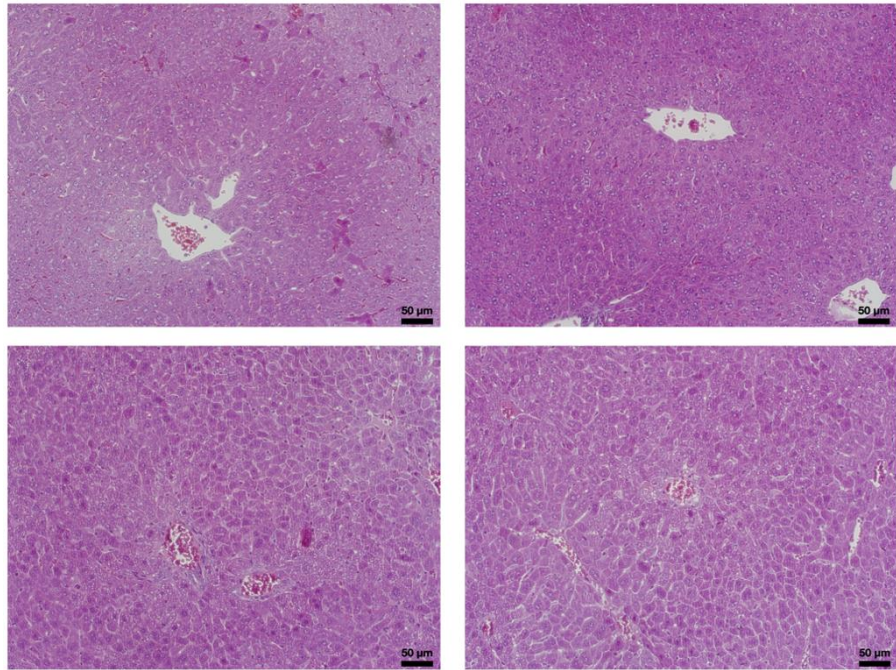- Kidney: Liposome + CLP

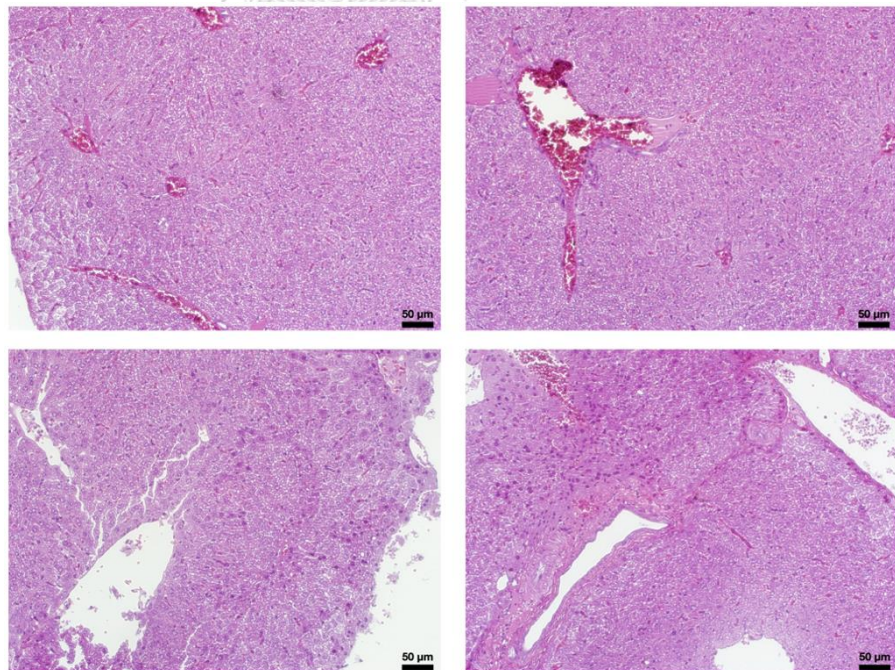- Kidney: Clodronate + CLP

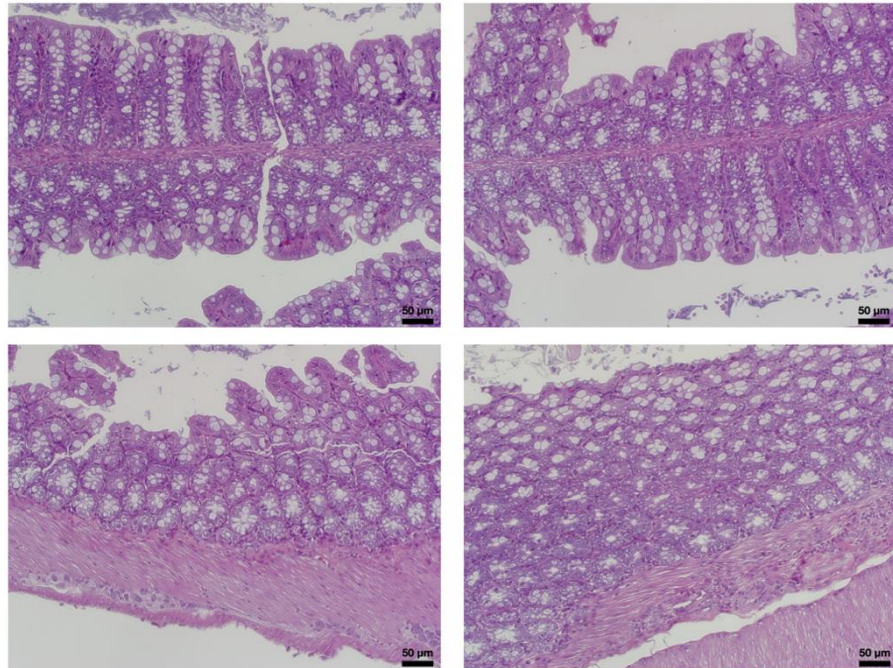- Liver: Liposome control

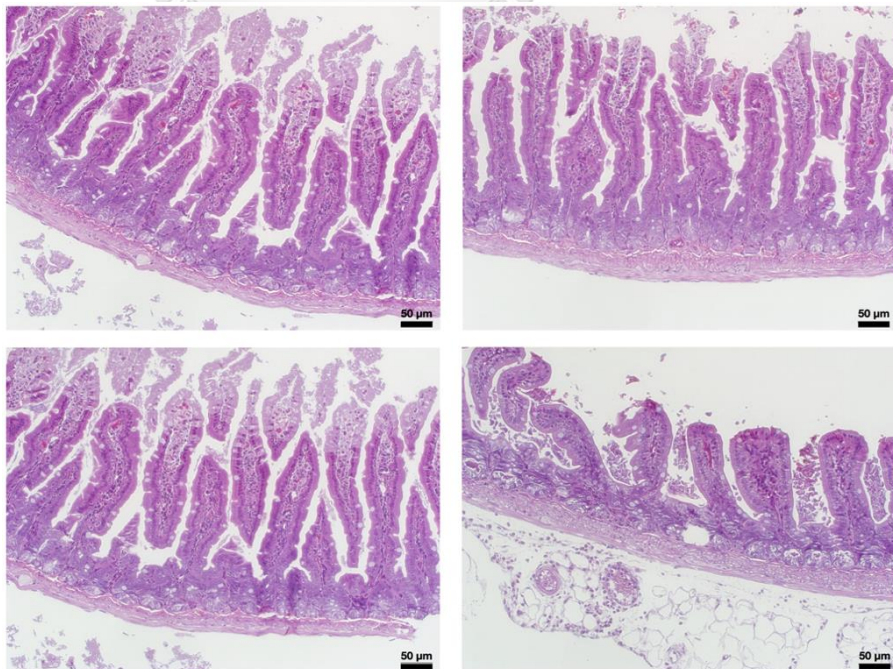- Liver: Clodronate alone
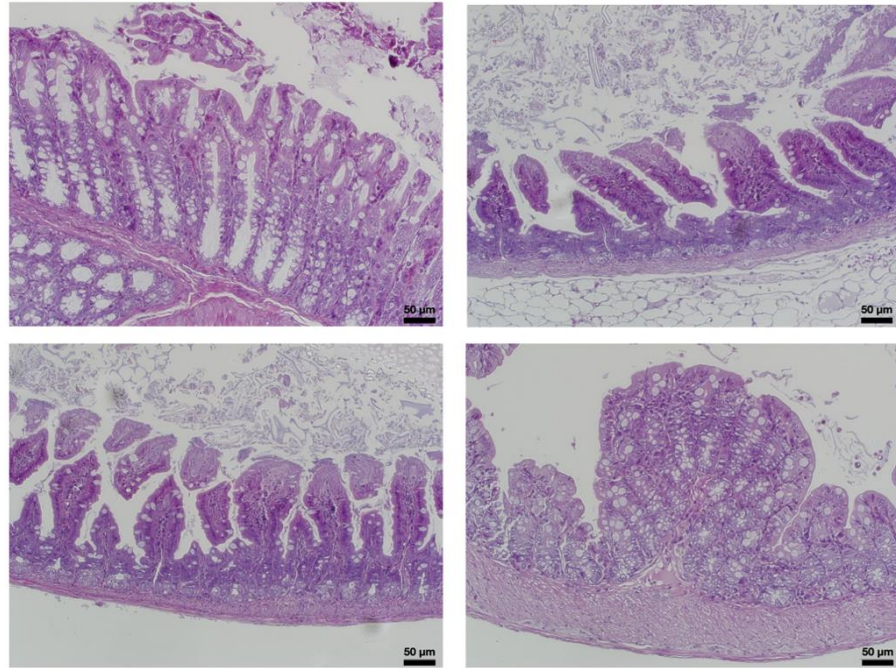
- Liver: Liposome + CLP

- Liver: Clodronate + CLP
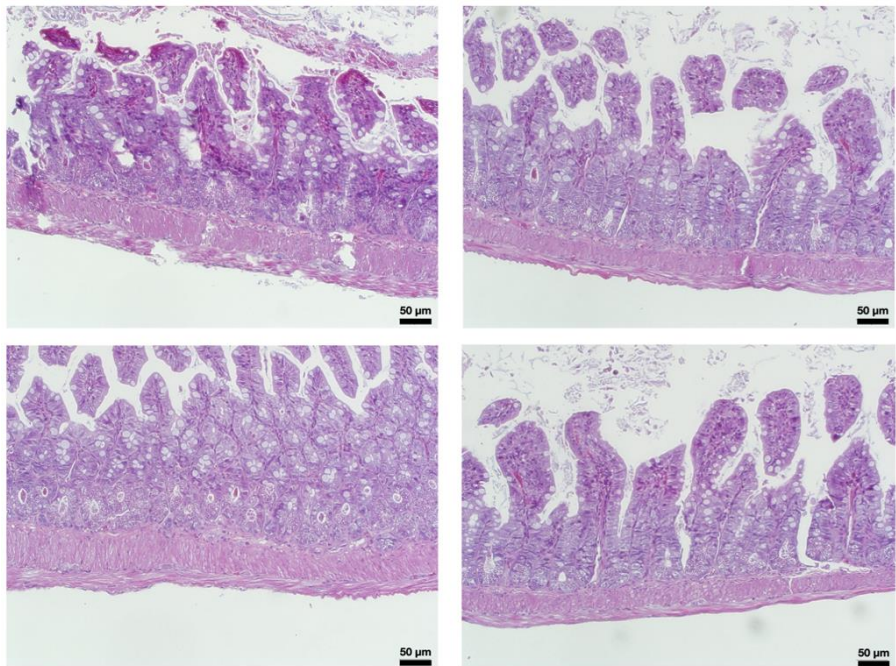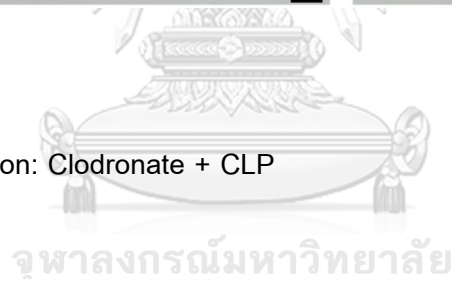
- Ascending colon: Liposome control

- Ascending colon: Clodronate alone

- Ascending colon: Liposome + CLP

- Ascending colon: Clodronate + CLP

REFERENCES

1.   Boulange CL, Neves AL, Chilloux J, Nicholson JK, Dumas ME. Impact of the gut microbiota on inflammation, obesity, and metabolic disease. Genome Med. 2016;8(1):42.

2.   Gyawali B, Ramakrishna K, Dhamoon AS. Sepsis: The evolution in definition, pathophysiology, and management. SAGE Open Med. 2019;7:2050312119835043.

3.   Dolin HH, Papadimos TJ, Chen X, Pan ZK. Characterization of Pathogenic Sepsis Etiologies and Patient Profiles: A Novel Approach to Triage and Treatment. Microbiol Insights. 2019;12:1178636118825081.

4.   Panpetch W, Somboonna N, Bulan DE, Issara-Amphorn J, Worasilchai N, Finkelman M, et al. Gastrointestinal Colonization of Candida Albicans Increases Serum $(1{\rightarrow}3)$-β-D-Glucan, without Candidemia, and Worsens Cecal Ligation and Puncture Sepsis in Murine Model. Shock. 2018;49(1):62-70.

5.   Lu R, Zhang YG, Xia Y, Sun J. Imbalance of autophagy and apoptosis in intestinal epithelium lacking the vitamin D receptor. FASEB J. 2019;33(11):11845-56.

6.   Lavin Y, Mortha A, Rahman A, Merad M. Regulation of macrophage development and function in peripheral tissues. Nature Reviews Immunology. 2015;15(12):731-44.

7.   Li X, Mu G, Song C, Zhou L, He L, Jin Q, et al. Role of M2 Macrophages in Sepsis-Induced Acute Kidney Injury. Shock. 2018;50(2):233-9.

8.   McWhorter FY, Wang T, Nguyen P, Chung T, Liu WF. Modulation of macrophage phenotype by cell shape. Proc Natl Acad Sci U S A. 2013;110(43):17253-8.

9.   Xing RL, Zhao LR, Wang PM. Bisphosphonates therapy for osteoarthritis: a meta-analysis of randomized controlled trials. Springerplus. 2016;5(1):1704.

10.   Saviola G, Abdi-Ali L, Povino MR, Campostrini L, Sacco S, Dalle Carbonare L, et al. Intramuscular clodronate in erosive osteoarthritis of the hand is effective on pain and reduces serum COMP: a randomized pilot trial-The ER.O.D.E. study (ERosive Osteoarthritis and Disodium-clodronate Evaluation). Clin Rheumatol. 2017;36(10):2343-50.

11.   Moreno SG. Depleting Macrophages In Vivo with Clodronate-Liposomes. Methods Mol Biol. 2018;1784:259-62.

12.   Kameka AM, Haddadi S, Jamaldeen FJ, Moinul P, He XT, Nawazdeen FH, et al. Clodronate treatment significantly depletes macrophages in chickens. Can J Vet Res. 2014;78(4):274-82.

13.   Weisser SB, van Rooijen N, Sly LM. Depletion and reconstitution of macrophages in mice. J Vis Exp. 2012(66):4105.

14.   Yan A, Zhang Y, Lin J, Song L, Wang X, Liu Z. Partial Depletion of Peripheral M1 Macrophages Reverses Motor Deficits in MPTP-Treated Mouse by Suppressing Neuroinflammation and Dopaminergic Neurodegeneration. Front Aging Neurosci. 2018;10:160.

15.   Hurst M, Noble S. Clodronate: a review of its use in breast cancer. Drugs Aging. 1999;15(2):143-67.

16.   Zeisberger SM, Odermatt B, Marty C, Zehnder-Fjällman AHM, Ballmer-Hofer K, Schwendener RA. Clodronate-liposome-mediated depletion of tumour-associated macrophages: a new and highly effective antiangiogenic therapy approach. British Journal of Cancer. 2006;95(3):272-81.

17.   Navegantes KC, de Souza Gomes R, Pereira PAT, Czaikoski PG, Azevedo CHM, Monteiro MC. Immune modulation of some autoimmune diseases: the critical role of macrophages and neutrophils in the innate and adaptive immunity. J Transl Med. 2017;15(1):36.

18.   Roszer T. Understanding the Biology of Self-Renewing Macrophages. Cells. 2018;7(8).

19.   Davies LC, Taylor PR. Tissue-resident macrophages: then and now. Immunology. 2015;144(4):541-8.

20.   Schmid MC, Varner JA. Myeloid cells in tumor inflammation. Vasc Cell. 2012;4(1):14.

21.   Liddiard K, Rosas M, Davies LC, Jones SA, Taylor PR. Macrophage heterogeneity and acute inflammation. Eur J Immunol. 2011;41(9):2503-8.

22.   Sindrilaru A, Peters T, Wieschalka S, Baican C, Baican A, Peter H, et al. An unrestrained proinflammatory M1 macrophage population induced by iron impairs wound

healing in humans and mice. The Journal of Clinical Investigation. 2011;121(3):985-97.

23. Allison AC, Ferluga J, Prydz H, Schorlemmer HU. The role of macrophage activation in chronic inflammation. Agents Actions. 1978;8(1-2):27-35.

24. Kasraie S, Werfel T. Role of Macrophages in the Pathogenesis of Atopic Dermatitis. Mediators of Inflammation. 2013;2013:942375.

25. Bohlson SS, O'Conner SD, Hulsebus HJ, Ho MM, Fraser DA. Complement, c1q, and c1q-related molecules regulate macrophage polarization. Front Immunol. 2014;5:402.

26. Orkin SH, Zon LI. Hematopoiesis: an evolving paradigm for stem cell biology. Cell. 2008;132(4):631-44.

27. Murray PJ, Allen JE, Biswas SK, Fisher EA, Gilroy DW, Goerdt S, et al. Macrophage activation and polarization: nomenclature and experimental guidelines. Immunity. 2014;41(1):14-20.

28. Martinez FO, Gordon S. The M1 and M2 paradigm of macrophage activation: time for reassessment. F1000Prime Rep. 2014;6:13.

29. Guilliams M, Ginhoux F, Jakubzick C, Naik SH, Onai N, Schraml BU, et al. Dendritic cells, monocytes and macrophages: a unified nomenclature based on ontogeny. Nat Rev Immunol. 2014;14(8):571-8.

30. Dale DC, Boxer L, Liles WC. The phagocytes: neutrophils and monocytes. Blood. 2008;112(4):935-45.

31. Chinetti-Gbaguidi G, Colin S, Staels B. Macrophage subsets in atherosclerosis. Nat Rev Cardiol. 2015;12(1):10-7.

32. Liu YC, Zou XB, Chai YF, Yao YM. Macrophage polarization in inflammatory diseases. Int J Biol Sci. 2014;10(5):520-9.

33. Furlan R, Cuomo C, Martino G. Animal models of multiple sclerosis. Methods Mol Biol. 2009;549:157-73.

34. Jablonski KA, Amici SA, Webb LM, Ruiz-Rosado Jde D, Popovich PG, Partida-Sanchez S, et al. Novel Markers to Delineate Murine M1 and M2 Macrophages. PLoS One. 2015;10(12):e0145342.

35. Mantovani A, Sica A, Sozzani S, Allavena P, Vecchi A, Locati M. The chemokine

system in diverse forms of macrophage activation and polarization. Trends Immunol. 2004;25(12):677-86.

36. Kraakman MJ, Murphy AJ, Jandeleit-Dahm K, Kammoun HL. Macrophage polarization in obesity and type 2 diabetes: weighing down our understanding of macrophage function? Front Immunol. 2014;5:470.

37. Gordon S, Taylor PR. Monocyte and macrophage heterogeneity. Nat Rev Immunol. 2005;5(12):953-64.

38. David S, Kroner A. Repertoire of microglial and macrophage responses after spinal cord injury. Nat Rev Neurosci. 2011;12(7):388-99.

39. Anderson CF, Mosser DM. A novel phenotype for an activated macrophage: the type 2 activated macrophage. J Leukoc Biol. 2002;72(1):101-6.

40. Junttila IS, Mizukami K, Dickensheets H, Meier-Schellersheim M, Yamane H, Donnelly RP, et al. Tuning sensitivity to IL-4 and IL-13: differential expression of IL-4Ralpha, IL-13Ralpha1, and gammac regulates relative cytokine sensitivity. J Exp Med. 2008;205(11):2595-608.

41. Hao NB, Lü MH, Fan YH, Cao YL, Zhang ZR, Yang SM. Macrophages in tumor microenvironments and the progression of tumors. Clin Dev Immunol. 2012;2012:948098.

42. Frediani B, Bertoldi I. Clodronate: New directions of use. Clinical Cases in Mineral and Bone Metabolism. 2015;12:97-108.

43. McLellan J. Science-in-brief: Bisphosphonate use in the racehorse: Safe or unsafe? Equine Vet J. 2017;49(4):404-7.

44. Russell RG. Bisphosphonates: mode of action and pharmacology. Pediatrics. 2007;119 Suppl 2:S150-62.

45. Kelly C, Jefferies C, Cryan SA. Targeted liposomal drug delivery to monocytes and macrophages. J Drug Deliv. 2011;2011:727241.

46. Ponzoni M, Pastorino F, Di Paolo D, Perri P, Brignole C. Targeting Macrophages as a Potential Therapeutic Intervention: Impact on Inflammatory Diseases and Cancer. Int J Mol Sci. 2018;19(7).

47. Epstein-Barash H, Gutman D, Markovsky E, Mishan-Eisenberg G, Koroukhov N,

Szebeni J, et al. Physicochemical parameters affecting liposomal bisphosphonates bioactivity for restenosis therapy: internalization, cell inhibition, activation of cytokines and complement, and mechanism of cell death. J Control Release. 2010;146(2):182-95.

48.   Chono S, Tanino T, Seki T, Morimoto K. Influence of particle size on drug delivery to rat alveolar macrophages following pulmonary administration of ciprofloxacin incorporated into liposomes. J Drug Target. 2006;14(8):557-66.

49.   Crépin S, Laroche ML, Sarry B, Merle L. Osteonecrosis of the jaw induced by clodronate, an alkylbiphosphonate: case report and literature review. Eur J Clin Pharmacol. 2010;66(6):547-54.

50.   Muratore M, Quarta E, Grimaldi A, Calcagnile F, Quarta L. Clinical utility of clodronate in the prevention and management of osteoporosis in patients intolerant of oral bisphosphonates. Drug Des Devel Ther. 2011;5:445-54.

51.   Liu X-G, Chen P-J, Zhao L-L, Zeng Z-G, Xiao W-H. Macrophages depletion impairs skeletal muscle regeneration by regulating inflammation and oxidative stress levels. Sheng li xue bao : [Acta physiologica Sinica]. 2018;70:23-32.

52.   Bader JE, Enos RT, Velázquez KT, Carson MS, Nagarkatti M, Nagarkatti PS, et al. Macrophage depletion using clodronate liposomes decreases tumorigenesis and alters gut microbiota in the AOM/DSS mouse model of colon cancer. Am J Physiol Gastrointest Liver Physiol. 2018;314(1):G22-g31.

53.   Michalski MN, Zweifler LE, Sinder BP, Koh AJ, Yamashita J, Roca H, et al. Clodronate-Loaded Liposome Treatment Has Site-Specific Skeletal Effects. J Dent Res. 2019;98(4):459-67.

54.   Belizário JE, Napolitano M. Human microbiomes and their roles in dysbiosis, common diseases, and novel therapeutic approaches. Frontiers in Microbiology. 2015;6(1050).

55.   Segata N, Haake SK, Mannon P, Lemon KP, Waldron L, Gevers D, et al. Composition of the adult digestive tract bacterial microbiome based on seven mouth surfaces, tonsils, throat and stool samples. Genome Biol. 2012;13(6):R42.

56.   Manichanh C, Rigottier-Gois L, Bonnaud E, Gloux K, Pelletier E, Frangeul L, et al.

Reduced diversity of faecal microbiota in Crohn's disease revealed by a metagenomic approach. Gut. 2006;55(2):205-11.

57.	Martinez JE, Kahana DD, Ghuman S, Wilson HP, Wilson J, Kim SCJ, et al. Unhealthy Lifestyle and Gut Dysbiosis: A Better Understanding of the Effects of Poor Diet and Nicotine on the Intestinal Microbiome. Front Endocrinol (Lausanne). 2021;12:667066.

58.	Safadi JM, Quinton AMG, Lennox BR, Burnet PWJ, Minichino A. Gut dysbiosis in severe mental illness and chronic fatigue: a novel trans-diagnostic construct? A systematic review and meta-analysis. Molecular Psychiatry. 2022;27(1):141-53.

59.	Wick EC, Sears CL. Bacteroides spp. and diarrhea. Curr Opin Infect Dis. 2010;23(5):470-4.

60.	Starr J. Clostridium difficile associated diarrhoea: diagnosis and treatment. Bmj. 2005;331(7515):498-501.

61.	Cremon C, Stanghellini V, Pallotti F, Fogacci E, Bellacosa L, Morselli-Labate AM, et al. Salmonella gastroenteritis during childhood is a risk factor for irritable bowel syndrome in adulthood. Gastroenterology. 2014;147(1):69-77.

62.	Vanya M, Szili K, Meszaros E, Laluska B, Lajos G. Acute diarrhoea caused by Salmonella enterica subsp. enterica serovar Give infections in male prisoners: a case report. Reviews and Research in Medical Microbiology. 2016;27(2).

63.	Mylonakis E, Ryan ET, Calderwood SB. Clostridium difficile–Associated Diarrhea: A Review. Archives of Internal Medicine. 2001;161(4):525-33.

64.	O'Brien AD, Gentry MK, Thompson MR, Doctor BP, Gemski P, Formal SB. Shigellosis and Escherichia coli diarrhea: relative importance of invasive and toxigenic mechanisms. Am J Clin Nutr. 1979;32(1):229-33.

65.	Marchelletta RR, Gareau MG, Okamoto S, Guiney DG, Barrett KE, Fierer J. Salmonella-induced Diarrhea Occurs in the Absence of IL-8 Receptor (CXCR2)-Dependent Neutrophilic Inflammation. J Infect Dis. 2015;212(1):128-36.

66.	Gallardo F, Gascón J, Ruiz J, Corachan M, Jimenez de Anta M, Vila J. Campylobacter jejuni as a cause of traveler's diarrhea: clinical features and antimicrobial susceptibility. J Travel Med. 1998;5(1):23-6.

67.   Zhang J, Ni Y, Qian L, Fang Q, Zheng T, Zhang M, et al. Decreased Abundance of Akkermansia muciniphila Leads to the Impairment of Insulin Secretion and Glucose Homeostasis in Lean Type 2 Diabetes. Adv Sci (Weinh). 2021;8(16):e2100536.

68.   Gu ZY, Pei WL, Zhang Y, Zhu J, Li L, Zhang Z. Akkermansia muciniphila in inflammatory bowel disease and colorectal cancer. Chin Med J (Engl). 2021;134(23):2841-3.

69.   Million M, Maraninchi M, Henry M, Armougom F, Richet H, Carrieri P, et al. Obesity-associated gut microbiota is enriched in Lactobacillus reuteri and depleted in Bifidobacterium animalis and Methanobrevibacter smithii. Int J Obes (Lond). 2012;36(6):817-25.

70.   Ghosh S, van Heel D, Playford RJ. Probiotics in inflammatory bowel disease: is it all gut flora modulation? Gut. 2004;53(5):620-2.

71.   Bozkurt HS, Kara B. A new treatment for ulcerative colitis: Intracolonic Bifidobacterium and xyloglucan application. European Journal of Inflammation. 2020;18:2058739220942626.

72.   Ahmed I, Roy BC, Khan SA, Septer S, Umar S. Microbiome, Metabolome and Inflammatory Bowel Disease. Microorganisms. 2016;4(2).

73.   Verdam FJ, Fuentes S, de Jonge C, Zoetendal EG, Erbil R, Greve JW, et al. Human intestinal microbiota composition is associated with local and systemic inflammation in obesity. Obesity (Silver Spring). 2013;21(12):E607-15.

74.   Fan X, Jin Y, Chen G, Ma X, Zhang L. Gut Microbiota Dysbiosis Drives the Development of Colorectal Cancer. Digestion. 2021;102(4):508-15.

75.   Swidsinski A, Weber J, Loening-Baucke V, Hale LP, Lochs H. Spatial organization and composition of the mucosal flora in patients with inflammatory bowel disease. J Clin Microbiol. 2005;43(7):3380-9.

76.   Skinner C, Thompson AJ, Thursz MR, Marchesi JR, Vergis N. Intestinal permeability and bacterial translocation in patients with liver disease, focusing on alcoholic aetiology: methods of assessment and therapeutic intervention. Therap Adv Gastroenterol. 2020;13:1756284820942616.

77. van Nood E, Vrieze A, Nieuwdorp M, Fuentes S, Zoetendal EG, de Vos WM, et al. Duodenal infusion of donor feces for recurrent Clostridium difficile. N Engl J Med. 2013;368(5):407-15.

78. Kastl AJ, Terry NA, Wu GD, Albenberg LG. The Structure and Function of the Human Small Intestinal Microbiota: Current Understanding and Future Directions. Cellular and Molecular Gastroenterology and Hepatology. 2020;9(1):33-45.

79. Vaishnavi C. Translocation of gut flora and its role in sepsis. Indian J Med Microbiol. 2013;31(4):334-42.

80. Belkaid Y, Hand TW. Role of the microbiota in immunity and inflammation. Cell. 2014;157(1):121-41.

81. Okumura R, Takeda K. Roles of intestinal epithelial cells in the maintenance of gut homeostasis. Exp Mol Med. 2017;49(5):e338.

82. Pakbin B, Brück WM, Rossen JWA. Virulence Factors of Enteric Pathogenic Escherichia coli: A Review. Int J Mol Sci. 2021;22(18).

83. Richardson JP, Brown R, Kichik N, Lee S, Priest E, Mogavero S, et al. Candidalysins Are a New Family of Cytolytic Fungal Peptide Toxins. mBio. 2022;13(1):e0351021.

84. Coskun M. Intestinal epithelium in inflammatory bowel disease. Front Med (Lausanne). 2014;1:24.

85. Iwasaki A, Medzhitov R. Toll-like receptor control of the adaptive immune responses. Nat Immunol. 2004;5(10):987-95.

86. Singh AK, Jiang Y. Lipopolysaccharide (LPS) induced activation of the immune system in control rats and rats chronically exposed to a low level of the organothiophosphate insecticide, acephate. Toxicology and Industrial Health. 2003;19(2-6):93-108.

87. Raetz CR, Whitfield C. Lipopolysaccharide endotoxins. Annu Rev Biochem. 2002;71:635-700.

88. Park BS, Song DH, Kim HM, Choi BS, Lee H, Lee JO. The structural basis of lipopolysaccharide recognition by the TLR4-MD-2 complex. Nature. 2009;458(7242):1191-

5.

89.   Delaloye J, Calandra T. Invasive candidiasis as a cause of sepsis in the critically ill patient. Virulence. 2014;5(1):161-9.

90.   Estrada A, Yun CH, Van Kessel A, Li B, Hauta S, Laarveld B. Immunomodulatory activities of oat beta-glucan in vitro and in vivo. Microbiol Immunol. 1997;41(12):991-8.

91.   El Khoury D, Cuda C, Luhovyy BL, Anderson GH. Beta glucan: health benefits in obesity and metabolic syndrome. J Nutr Metab. 2012;2012:851362.

92.   Novak M, Vetvicka V. Beta-glucans, history, and the present: immunomodulatory aspects and mechanisms of action. J Immunotoxicol. 2008;5(1):47-57.

93.   Underhill DM, Rossnagle E, Lowell CA, Simmons RM. Dectin-1 activates Syk tyrosine kinase in a dynamic subset of macrophages for reactive oxygen production. Blood. 2005;106(7):2543-50.

94.   Herre J, Marshall AS, Caron E, Edwards AD, Williams DL, Schweighoffer E, et al. Dectin-1 uses novel mechanisms for yeast phagocytosis in macrophages. Blood. 2004;104(13):4038-45.

95.   Saijo S, Fujikado N, Furuta T, Chung SH, Kotaki H, Seki K, et al. Dectin-1 is required for host defense against Pneumocystis carinii but not against Candida albicans. Nat Immunol. 2007;8(1):39-46.

96.   Goodridge HS, Wolf AJ, Underhill DM. Beta-glucan recognition by the innate immune system. Immunol Rev. 2009;230(1):38-50.

97.   Amornphimoltham P, Yuen PST, Star RA, Leelahavanichkul A. Gut Leakage of Fungal-Derived Inflammatory Mediators: Part of a Gut-Liver-Kidney Axis in Bacterial Sepsis. Dig Dis Sci. 2019;64(9):2416-28.

98.   Ondee T, Pongpirul K, Visitchanakun P, Saisorn W, Kanacharoen S, Wongsaroj L, et al. Lactobacillus acidophilus LA5 improves saturated fat-induced obesity mouse model through the enhanced intestinal Akkermansia muciniphila. Sci Rep. 2021;11(1):6367.

99.   Issara-Amphorn J, Surawut S, Worasilchai N, Thim-uam A, Finkelman M, Chindamporn A, et al. The Synergy of Endotoxin and (1→3)-β-D-Glucan, from Gut Translocation, Worsens Sepsis Severity in a Lupus Model of Fc Gamma Receptor IIb-

Deficient Mice. Journal of Innate Immunity. 2018;10(3):189-201.

100.   Ferwerda G, Meyer-Wentrup F, Kullberg BJ, Netea MG, Adema GJ. Dectin-1 synergizes with TLR2 and TLR4 for cytokine production in human primary monocytes and macrophages. Cell Microbiol. 2008;10(10):2058-66.

101.   Hiengrach P, Visitchanakun P, Finkelman MA, Chancharoenthana W, Leelahavanichkul A. More Prominent Inflammatory Response to Pachyman than to Whole-Glucan Particle and Oat-β-Glucans in Dextran Sulfate-Induced Mucositis Mice and Mouse Injection through Proinflammatory Macrophages. Int J Mol Sci. 2022;23(7).

102.   Karnatovskaia LV, Festic E. Sepsis: a review for the neurohospitalist. Neurohospitalist. 2012;2(4):144-53.

103.   Ramachandran G. Gram-positive and gram-negative bacterial toxins in sepsis: a brief review. Virulence. 2014;5(1):213-8.

104.   Abe R, Oda S, Sadahiro T, Nakamura M, Hirayama Y, Tateishi Y, et al. Gram-negative bacteremia induces greater magnitude of inflammatory response than Gram-positive bacteremia. Critical Care. 2010;14(2):R27.

105.   Umemura Y, Ogura H, Takuma K, Fujishima S, Abe T, Kushimoto S, et al. Current spectrum of causative pathogens in sepsis: A prospective nationwide cohort study in Japan. International Journal of Infectious Diseases. 2021;103:343-51.

106.   Ferrer R, Martin-Loeches I, Phillips G, Osborn TM, Townsend S, Dellinger RP, et al. Empiric antibiotic treatment reduces mortality in severe sepsis and septic shock from the first hour: results from a guideline-based performance improvement program. Crit Care Med. 2014;42(8):1749-55.

107.   Arina P, Singer M. Pathophysiology of sepsis. Curr Opin Anaesthesiol. 2021;34(2):77-84.

108.   Panpetch W, Sawaswong V, Chanchaem P, Ondee T, Dang CP, Payungporn S, et al. Candida Administration Worsens Cecal Ligation and Puncture-Induced Sepsis in Obese Mice Through Gut Dysbiosis Enhanced Systemic Inflammation, Impact of Pathogen-Associated Molecules From Gut Translocation and Saturated Fatty Acid. Front Immunol. 2020;11:561652.

109.	Hunter P. Sepsis under siege: a new understanding of sepsis might lead to the development of therapies to treat septic shock. EMBO Rep. 2006;7(7):667-9.

110.	Vincent JL. The Clinical Challenge of Sepsis Identification and Monitoring. PLoS Med. 2016;13(5):e1002022.

111.	Hotchkiss RS, Moldawer LL, Opal SM, Reinhart K, Turnbull IR, Vincent JL. Sepsis and septic shock. Nat Rev Dis Primers. 2016;2:16045.

112.	Chaudhry H, Zhou J, Zhong Y, Ali MM, McGuire F, Nagarkatti PS, et al. Role of cytokines as a double-edged sword in sepsis. In Vivo. 2013;27(6):669-84.

113.	Evans TJ. CHAPTER 19 - The Role of Macrophages in Septic Shock. Immunobiology. 1996;195(4):655-9.

114.	Chen X, Liu Y, Gao Y, Shou S, Chai Y. The roles of macrophage polarization in the host immune response to sepsis. Int Immunopharmacol. 2021;96:107791.

115.	Cheng Y, Marion TN, Cao X, Wang W, Cao Y. Park 7: A Novel Therapeutic Target for Macrophages in Sepsis-Induced Immunosuppression. Front Immunol. 2018;9:2632.

116.	Kotas ME, Matthay MA. Mesenchymal stromal cells and macrophages in sepsis: new insights. Eur Respir J. 2018;51(4).

117.	Saqib U, Sarkar S, Suk K, Mohammad O, Baig MS, Savai R. Phytochemicals as modulators of M1-M2 macrophages in inflammation. Oncotarget. 2018;9(25):17937-50.

118.	Yao Y, Xu XH, Jin L. Macrophage Polarization in Physiological and Pathological Pregnancy. Front Immunol. 2019;10:792.

119.	Watanabe N, Suzuki Y, Inokuchi S, Inoue S. Sepsis induces incomplete M2 phenotype polarization in peritoneal exudate cells in mice. J Intensive Care. 2016;4:6.

120.	Liu Z, Li N, Fang H, Chen X, Guo Y, Gong S, et al. Enteric dysbiosis is associated with sepsis in patients. FASEB J. 2019;33(11):12299-310.

121.	Lobatón T, Bessissow T, De Hertogh G, Lemmens B, Maedler C, Van Assche G, et al. The Modified Mayo Endoscopic Score (MMES): A New Index for the Assessment of Extension and Severity of Endoscopic Activity in Ulcerative Colitis Patients. Journal of Crohn's and Colitis. 2015;9(10):846-52.

122.	Arfken AM, Frey JF, Summers KL. Temporal Dynamics of the Gut Bacteriome and

Mycobiome in the Weanling Pig. Microorganisms. 2020;8(6).

123.   Sambrook J, Russell DW. Purification of nucleic acids by extraction with phenol:chloroform. CSH Protoc. 2006;2006(1).

124.   Bader JE, Enos RT, Velázquez KT, Carson MS, Sougiannis AT, McGuinness OP, et al. Repeated clodronate-liposome treatment results in neutrophilia and is not effective in limiting obesity-linked metabolic impairments. Am J Physiol Endocrinol Metab. 2019;316(3):E358-e72.

125.   Sae-Khow K, Charoensappakit A, Visitchanakun P, Saisorn W, Svasti S, Fucharoen S, et al. Pathogen-Associated Molecules from Gut Translocation Enhance Severity of Cecal Ligation and Puncture Sepsis in Iron-Overload β-Thalassemia Mice. J Inflamm Res. 2020;13:719-35.

126.   Panpetch W, Hiengrach P, Nilgate S, Tumwasorn S, Somboonna N, Wilantho A, et al. Additional Candida albicans administration enhances the severity of dextran sulfate solution induced colitis mouse model through leaky gut-enhanced systemic inflammation and gut-dysbiosis but attenuated by Lactobacillus rhamnosus L34. Gut Microbes. 2020;11(3):465-80.

127.   Allert S, Förster TM, Svensson CM, Richardson JP, Pawlik T, Hebecker B, et al. Candida albicans-Induced Epithelial Damage Mediates Translocation through Intestinal Barriers. mBio. 2018;9(3).

128.   Restagno D, Venet F, Paquet C, Freyburger L, Allaouchiche B, Monneret G, et al. Mice Survival and Plasmatic Cytokine Secretion in a "Two Hit" Model of Sepsis Depend on Intratracheal Pseudomonas Aeruginosa Bacterial Load. PLoS One. 2016;11(8):e0162109.

129.   Visitchanakun P, Saisorn W, Wongphoom J, Chatthanathon P, Somboonna N, Svasti S, et al. Gut leakage enhances sepsis susceptibility in iron-overloaded β-thalassemia mice through macrophage hyperinflammatory responses. Am J Physiol Gastrointest Liver Physiol. 2020;318(5):G966-g79.

130.   Haussner F, Chakraborty S, Halbgebauer R, Huber-Lang M. Challenge to the Intestinal Mucosa During Sepsis. Front Immunol. 2019;10:891.

131.   Belizário JE, Faintuch J. Microbiome and Gut Dysbiosis. Exp Suppl. 2018;109:459-

76.

132.   Carding S, Verbeke K, Vipond DT, Corfe BM, Owen LJ. Dysbiosis of the gut microbiota in disease. Microb Ecol Health Dis. 2015;26:26191.

133.   Lee HH, Aslanyan L, Vidyasagar A, Brennan MB, Tauber MS, Carrillo-Sepulveda MA, et al. Depletion of Alveolar Macrophages Increases Pulmonary Neutrophil Infiltration, Tissue Damage, and Sepsis in a Murine Model of Acinetobacter baumannii Pneumonia. Infect Immun. 2020;88(7).

134.   Ermert D, Zychlinsky A, Urban C. Fungal and bacterial killing by neutrophils. Methods Mol Biol. 2009;470:293-312.

135.   Urban CF, Nett JE. Neutrophil extracellular traps in fungal infection. Semin Cell Dev Biol. 2019;89:47-57.

136.   Desai JV, Lionakis MS. The role of neutrophils in host defense against invasive fungal infections. Curr Clin Microbiol Rep. 2018;5(3):181-9.

137.   Hiengrach P, Panpetch W, Worasilchai N, Chindamporn A, Tumwasorn S, Jaroonwitchawan T, et al. Administration of Candida Albicans to Dextran Sulfate Solution Treated Mice Causes Intestinal Dysbiosis, Emergence and Dissemination of Intestinal Pseudomonas Aeruginosa and Lethal Sepsis. Shock. 2020;53(2):189-98.

138.   Roewe J, Stavrides G, Strueve M, Sharma A, Marini F, Mann A, et al. Bacterial polyphosphates interfere with the innate host defense to infection. Nat Commun. 2020;11(1):4035.

139.   Silva N, Igrejas G, Gonçalves A, Poeta P. Commensal gut bacteria: distribution of Enterococcus species and prevalence of Escherichia coli phylogenetic groups in animals and humans in Portugal. Annals of Microbiology. 2012;62(2):449-59.

140.   Panpetch W, Kullapanich C, Dang CP, Visitchanakun P, Saisorn W, Wongphoom J, et al. Candida Administration Worsens Uremia-Induced Gut Leakage in Bilateral Nephrectomy Mice, an Impact of Gut Fungi and Organismal Molecules in Uremia. mSystems. 2021;6(1).

141.   Sencio V, Machado MG, Trottein F. The lung-gut axis during viral respiratory infections: the impact of gut dysbiosis on secondary disease outcomes. Mucosal Immunol.

2021;14(2):296-304.

142.   Wolff NS, Jacobs MC, Wiersinga WJ, Hugenholtz F. Pulmonary and intestinal microbiota dynamics during Gram-negative pneumonia-derived sepsis. Intensive Care Med Exp. 2021;9(1):35.

143.   Sun Y, Li L, Xie R, Wang B, Jiang K, Cao H. Stress Triggers Flare of Inflammatory Bowel Disease in Children and Adults. Front Pediatr. 2019;7:432.

144.   Geng S, Yang L, Cheng F, Zhang Z, Li J, Liu W, et al. Gut Microbiota Are Associated With Psychological Stress-Induced Defections in Intestinal and Blood-Brain Barriers. Front Microbiol. 2019;10:3067.

145.   Wu Q, Dou X, Wang Q, Guan Z, Cai Y, Liao X. Isolation of β-1,3-Glucanase-Producing Microorganisms from Poria cocos Cultivation Soil via Molecular Biology. Molecules. 2018;23(7).

146.   Robledo-Mahón T, Martín MA, Gutiérrez MC, Toledo M, González I, Aranda E, et al. Sewage sludge composting under semi-permeable film at full-scale: Evaluation of odour emissions and relationships between microbiological activities and physico-chemical variables. Environ Res. 2019;177:108624.

147.   Liberatore AMA, Menchaca-Diaz JL, Silva RM, Taki MY, Silva MR, Francisco J, et al. Sepsis provokes host's microbiota overgrowth of commensal Gram-negative bacteria and subsequent induction of bacterial translocation in rats. Critical Care. 2007;11(3):P23.

148.   Issara-Amphorn J, Surawut S, Worasilchai N, Thim-Uam A, Finkelman M, Chindamporn A, et al. The Synergy of Endotoxin and (1→3)-β-D-Glucan, from Gut Translocation, Worsens Sepsis Severity in a Lupus Model of Fc Gamma Receptor IIb-Deficient Mice. J Innate Immun. 2018;10(3):189-201.

149.   Panpetch W, Somboonna N, Bulan DE, Issara-Amphorn J, Finkelman M, Worasilchai N, et al. Oral administration of live- or heat-killed Candida albicans worsened cecal ligation and puncture sepsis in a murine model possibly due to an increased serum (1→3)-β-D-glucan. PLoS One. 2017;12(7):e0181439.

150.   Saithong S, Saisorn W, Visitchanakun P, Sae-Khow K, Chiewchengchol D, Leelahavanichkul A. A Synergy Between Endotoxin and (1→3)-Beta-D-Glucan Enhanced

133

Neutrophil Extracellular Traps in Candida Administered Dextran Sulfate Solution Induced Colitis in FcGRIIB-/- Lupus Mice, an Impact of Intestinal Fungi in Lupus. J Inflamm Res. 2021;14:2333-52.

151.   Segal E, Frenkel M. Experimental In Vivo Models of Candidiasis. Journal of Fungi. 2018;4(1):21.

152.   Leelahavanichkul A, Worasilchai N, Wannalerdsakun S, Jutivorakool K, Somparn P, Issara-Amphorn J, et al. Gastrointestinal Leakage Detected by Serum $(1\rightarrow3)$-β-D-Glucan in Mouse Models and a Pilot Study in Patients with Sepsis. Shock. 2016;46(5):506-18.

153.   Knolle PA, Löser E, Protzer U, Duchmann R, Schmitt E, zum Büschenfelde KH, et al. Regulation of endotoxin-induced IL-6 production in liver sinusoidal endothelial cells and Kupffer cells by IL-10. Clin Exp Immunol. 1997;107(3):555-61.

154.   Hiengrach P, Panpetch W, Chindamporn A, Leelahavanichkul A. Macrophage depletion alters bacterial gut microbiota partly through fungal overgrowth in feces that worsens cecal ligation and puncture sepsis mice. Scientific Reports. 2022;12(1):9345.

VITA

NAME	Pratsanee Hiengrach
DATE OF BIRTH	29 December 1993
PLACE OF BIRTH	Sakon Nakhon
INSTITUTIONS ATTENDED	2012-2016: B.Sc. (Biomedical Sciences), Faculty of Allied Health Sciences, Burapha University (BUU), Chon Buri, Thailand.
	2015-2018: M.Sc. (Medical Microbiology), Division of Mycology, Department of Microbiology, Faculty of Medicine, Chulalongkorn University, Bangkok, Thailand.
HOME ADDRESS	595/70 The MOST Itsaraphap, Phran Nok Road, Khwaeng Ban Chang Lo, Khet Bangkok Noi, Krung Thep Maha Nakhon 10700
PUBLICATION	1. Hiengrach P, Panpetch W, Chindamporn A, Leelahavanichkul A. 2022. Helicobacter pylori, Protected from Antibiotics and Stresses Inside Candida albicans Vacuoles, Cause Gastritis in Mice. Int J Mol Sci 23.
	2. Hiengrach P, Panpetch W, Chindamporn A, Leelahavanichkul A. 2022. Macrophage depletion alters bacterial gut microbiota partly through fungal overgrowth in feces that worsens cecal ligation and puncture sepsis mice. Sci Rep 12:9345.
	3. Hiengrach P, Visitchanakun P, Tongchairawewat P, Tangsirisatian P, Jungteerapanich T, Ritprajak P, Wannigama DL, Tangtanatakul P, Leelahavanichkul A. 2022. Sepsis Encephalopathy Is Partly Mediated by miR370-3p-

Induced Mitochondrial Injury but Attenuated by BAM15 in Cecal Ligation and Puncture Sepsis Male Mice. Int J Mol Sci 23.

4. Hiengrach P, Visitchanakun P, Finkelman MA, Chancharoenthana W, Leelahavanichkul A. 2022. More Prominent Inflammatory Response to Pachyman than to Whole-Glucan Particle and Oat-beta-Glucans in Dextran Sulfate-Induced Mucositis Mice and Mouse Injection through Proinflammatory Macrophages. Int J Mol Sci 23.

5. Hiengrach P, Panpetch W, Worasilchai N, Chindamporn A, Tumwasorn S, Jaroonwitchawan T, Wilantho A, Chatthanathon P, Somboonna N, Leelahavanichkul A. 2020. Administration of Candida albicans to Dextran Sulfate Solution Treated Mice Causes Intestinal Dysbiosis, Emergence, and Dissemination of Intestinal Pseudomonas aeruginosa and Lethal Sepsis. Shock 53:189-198.

จุฬาลงกรณ์มหาวิทยาลัย
CHULALONGKORN UNIVERSITY